Technical Report 75
DECEMBER, 1950

Explosions in Ice

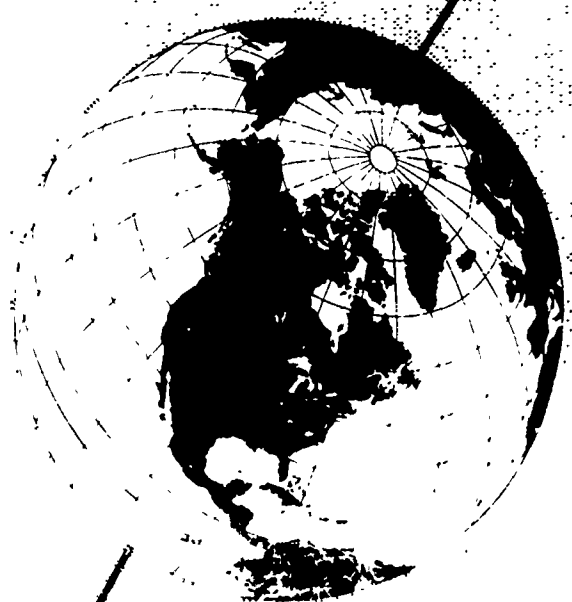

U. S. ARMY
SNOW ICE AND PERMAFROST
RESEARCH ESTABLISHMENT
Corps of Engineers

Technical Report 75

DECEMBER, 1960

Explosions in Ice

by Clifton W. Livingston

U. S. ARMY SNOW ICE AND PERMAFROST
RESEARCH ESTABLISHMENT
Corps of Engineers
Wilmette, Illinois

PREFACE

This is a final report of work on SIPRE* Project 22.4-10. Explosions in ice, performed under Contract DA-11-190-ENG-27 with Barodynamics, Inc. The field work was conducted as Corps of Engineers Project 26 of the 1957 Greenland Research Program. The purpose of the investigation is to supplement data from explosions in frozen ground and acquire information for the development of criteria for the destruction and protection of structures in or on ice.

The design and planning of this project were accomplished under the direction of the Frozen Ground Applied Research Branch, Snow Ice and Permafrost Research Establishment. The work was sponsored jointly by U. S. Army SIPRE, WES, and ERDL. U. S. Army Engineer Arctic Task Force provided operational support, construction equipment, and personnel. U. S. Army Waterways Experiment Station furnished and operated the instrumentation equipment for airblast and under-ice shock measurements. Field work, supervision, and analysis were conducted by Barodynamics, Inc.

This report has been reviewed and approved for publication by the Office of the Chief of Engineers, U.S. Army.

W. L. NUNGESSER
Colonel, Corps of Engineers
Director

Manuscript received 16 March 1960
Department of the Army Project 8-66-02-400

* Redesignated U. S. Army Cold Regions Research and Engineering Laboratory, 1 February 1961.

CONTENTS

	Page
Preface	ii
Summary	v
General plan of the tests	1
Objectives and scope	1
Procedure	2
Test site	2
Physical properties of the ice	2
Ablation and its effect upon operations	5
Auger drilling	6
Blasting procedure	6
Proposed colored columns and trenches	7
Excavation, field analysis, and crater surveys	9
Instrumentation	10
Seismic measurements	13
Compilation of the data	14
Symbols and nomenclature	14
Empirical evaluation of venting phenomena	15
Introduction	15
Flyrock travel height	17
The apparent crater	22
Crater evaluation theory	22
Method of evaluating the data	22
Determining critical depth and optimum depth	24
Evaluation procedure	25
Critical depth and the strain energy factor	27
Optimum depth and the materials behavior index	29
True crater evaluation	29
Variation of V/W of the true crater with Δ	29
Energy utilization number, A	33
Depth of the true crater, K_h	33
Crater shape factor, K_s	33
True crater radius, K_r	37
Air and under-ice shock	37
Under-ice pressure records	37
Near-surface airblast and under-ice pressure	39
Direct under-ice shock	39
Air-induced under-ice shock	41
Near-surface air blast pressure	41
Seismic measurements	41
Effect of charge depth at constant weight	41
Effect of charge weight at critical depth	48
Seismic velocity vs charge-to-pressure gage shock velocity	49
References	50

Appendix

Data sheets A: Blast hole and apparent crater data
Data sheets B: True crater measurements and energy utilization factors
Data sheets C: Crater coefficients
Data sheets D: Seismic data
Figures A1-23. Shock data

CONTENTS (cont'd)

Page

ILLUSTRATIONS

Figure

1. Index map, Thule area ---- viii
2. Test site looking southwest from mile 2½ on ramp road ---- 1
3. Banding in the ice along wall of test pit ---- 1
4. Ambient air and subsurface ice temperature ---- 3
5. Headquarters building at test site ----
6. Subsurface temperature gradient ---- 5
7. Auger drill rig ---- 6
8. Cutting heads redesigned to chip ice ---- 6
9. Plastic sphere containing explosive ---- 7
10. Blasts in ice ---- 8
11. Air and contact blasts ---- 9
12. Doming of the ice surface at near critical depth ---- 9
13. Fracture pattern, blasts between critical and optimum depths 9
14. Refreezing of the ice near the explosion cavity ---- 10
15. Fracture pattern at wall of vertical trench near an explosion in ice ---- 10
16. Air and under-ice shock gages ---- 12
17. Gage calibration ---- 12
18. Miller recording unit ---- 12
19. Final check of airblast gage slant distances ---- 12
20. Preparation for contact burst instrumentation ---- 12
21. Portable, high resolution, SIE reflection seismograph ---- 12
22. Placing geophones to measure vibration ---- 13
23. Crater and camouflet nomenclature ---- 16
24-27. N-scaled flyrock travel height ---- 18
28-31. Apparent crater V/W vs Δ ---- 19
32-35. N-scaled apparent crater radius ---- 20
36-39. N-scaled apparent crater depth ---- 21
40-43. V/W vs Δ ---- 30
44-47. Energy utilization number ---- 32
48-51. N-scaled true crater depth ---- 34
52-55. Crater shape factor ---- 35
56-59. N-scaled true crater radius ---- 36
60. Under-ice pressure records ---- 38
61. Typical near surface, air blast and under-ice pressure records ---- 38
62-66. Blast pressures ---- 40
67-72. Typical seismic records ---- 42
73-75. Isometric - under-ice V vs Δ and $R/\sqrt[3]{W}$ ---- 45
76-77. Longitudinal wave velocity ---- 48

TABLES

Table

I. Physical properties of ice, Thule ramp ---- 4
II. Properties of the test explosives ---- 7
III. Dimensions of explosives spheres ---- 7
IV. Shock-gage scaled slant distances ---- 13
V. Instrumented contact and near surface blasts ---- 14
VI. Explosions in glacier ice ---- 28

SUMMARY

Twenty-four instrumented and 106 uninstrumented blasts ranging in weight from 2.5 to 40 lb of four types of explosives were detonated above, in contact with, and at various depths below the ice surface. The tests were conducted at the edge of the Greenland Ice Cap, near Camp Tuto, during the summer of 1957. Under-ice direct shock pressure, air-induced under-ice shock pressure, and airblast pressure from shallow under-ice bursts, contact bursts, and near-contact bursts were measured. The apparent crater and the true crater were measured, and the mechanics of the fracture process were studied. The height to which the flyrock was thrown was measured using motion pictures, and ground rise and venting phenomena were studied. Sixty-six seismic records were taken.

Evaluation of the data takes into account both energy partitioning and variation in behavior of the ice with the scale of the experiment. Crater measurements and flyrock travel height are reduced to dimensionless units using the critical depth $\underline{N}$ as a scaling parameter. Shock and seismic measurements are referred both to the scaled gage distance and to the depth ratio.

The height to which the ice is thrown by an explosion and dimensions of the apparent crater are greatest at low depth ratios and in the range where the breakage process is inefficient. At a given depth ratio, both the N-scaled flyrock travel height and N-scaled dimensions of the apparent crater vary with type of explosive and weight of charge.

Measurements are evaluated using: 1) equations involving a length or a damage distance, and containing coefficients measurable at critical depth; and 2) equations involving volume measurements and containing coefficients measurable at optimum depth.

The critical depth $\underline{N}$ was measured in the field separately for 2.5-, 5-, 10-, 20-, and 40-lb spherical charges of four test explosives. Results demonstrate consistently for all four explosives and for all weights tested that explosions in glacier ice deviate from cube-root scaling. The strain-energy factor $\underline{E}$, calculated from

$$N = E\sqrt[3]{W} \qquad \text{where } \underline{W} \text{ is charge weight}$$

is greater for high-energy and high-velocity explosives than for low-energy and low-velocity explosives. The maximum value of $\underline{E}$ occurs where the tangent to the log $\underline{N}$ vs log $\underline{W}$ curve has a slope of one-third. The slope of the curve is less than one-third if the weight of the charge is greater than 10 lb.

As the weight of the charge increases, the ice becomes more plastic-acting. The change is measured by the materials behavior index $\underline{B}$. Although $\underline{B}$ is a constant for a given material, weight of charge, and type of explosive, it varies both with the weight and with the type of explosive when blasting in glacier ice. A greater range in the behavior of the ice was observed when blasting with C-4 than when blasting with the other explosives.

The equation for crater volume is

$$V/W = E^3ABC.$$

As the stress distribution number $\underline{C}$ is a constant for the conditions of these tests, and $\underline{E}$ and $\underline{B}$ are constants for a given explosive and weight of charge,

SUMMARY (cont'd)

any variation in V/W, volume of true crater per pound of explosive, depends upon the energy utilization number A, which is a relative measure of the part of the total energy of the explosion that is partitioned to the fracture process at various depth ratios.

Because the energy from a contact burst is partitioned to the material and to the atmosphere in a complex manner, it is difficult to detect a change in behavior due either to the explosive or to the weight of the charge. The change in behavior becomes increasingly evident as the depth of the charge increases and energy partitioning becomes less complex. When the relations between V/W and depth ratio are compared with the relations between fly-rock travel height and depth ratio, it becomes apparent that:

1) energy utilized in deforming the ice without loss of cohesion is not available to the fracture process;

2) energy utilized to deform without loss of cohesion and to fracture the ice is not available to accelerate the isolated fragments;

3) events subsequent to the breakage process, such as the scouring action of the vented gas bubble, depend upon the manner in which energy is partitioned to the breakage process — and in turn upon all of the parameters that affect cratering in ice.

Energy utilization curves were derived mathematically from the V/W curves. A family of curves is required for each type of explosive. Maxima, minima, and points of inflection define the energy level at which a given phenomenon begins or ends, and the energy level is related mathematically to the depth ratio. For example, breakthrough of the gas bubble marks the beginning of venting phenomena and occurs where A is maximum. The energy utilization curves, together with the optimum depth ratios indicate that the beginning or ending of a given phenomenon, or series of phenomena, depends both upon the explosive and the material, and that the two are dependent rather than independent variables. As the weight of the charge and the scale of the experiment are increased, more of the total energy of the explosion is utilized by the material between the beginning of deformation and breakthrough of the gas bubble.

The depth of the crater is the sum of the depth to the center of gravity of the charge and the vertical radius of the explosion cavity. The vertical radius is larger for a contact burst than for a charge at optimum depth, larger at critical depth than at optimum depth, larger at critical depth than at optimum weight, and is affected by both charge shape and by type of explosive. Variations in crater shapes and radius with depth ratio are consistent with transition limits as defined by the energy utilization curves. They also are consistent with other parameters of the breakage process equation

$$V/W = E^{\frac{1}{3}}AB,$$

Tables, curves, and equations presented in the report make it possible, within the range of the experiments, to predict accurately any desired dimension of the true or apparent crater in glacier ice, and to calculate the height to which the ice would be thrown by an explosion. When extrapolating beyond the range of the experiments, the observed variation in E, A, and B should prove useful.

Pressure-distance relations as summarized do not take into account either the effect of charge depth, or the gage position. Additional instrumentation data are necessary before an analysis can be completed.

At scaled distances of 1.5^3W or less, the under-ice pressure pulse is similar in shape to that in water or in air; but as the distance increases, the shape changes gradually.

The form of the seismic record is affected both by the depth and by the weight of the charge. If the charge is detonated in air a short distance above the surface of the ice, both direct under-ice shock and airblast-induced under-ice shock are recorded. The airblast-induced shock is suppressed at relatively shallow depths of charge; within the range ($0 < \Delta < 1$), the amplitude of vibrations first arriving at the geophones increases as the depth of the charge increases. At critical depth, all of the energy of the explosion is partitioned to processes that precede fracturing. If the N-scaled depth charge is held constant at critical depth, and the weight of the charge of a given type of explosive is increased, the duration of high amplitude vibrations at a given scaled geophone distance increases.

In the region near the charge, the charge-to-gage shock velocity depends both upon the depth ratio of the shot and upon the place of observation. The variation of the under-ice shock velocity with charge depth, explosive type, and scaled slant distance appears to be as follows:

1) If shock gages are placed at given scaled slant distances from the charge, the under-ice shock velocity of a blast in glacier ice at a given depth of charge depends both upon the type and weight of explosive.

2) In the range where both plastic deformation and fracturing occur, the under-ice charge-to-gage shock velocity approaches a minimum if the charge is placed at the optimum depth for a given type of explosive and weight of charge.

3) At optimum depth, the under-ice charge-to-gage shock velocity increases with the scaled gage distance in the range where fracturing predominates over plastic deformation.

A variation in charge-to-gage shock velocity becomes increasingly difficult to detect as the distance to the place of observation increases. In the range where seismic measurements were made, the velocity of the longitudinal wave, as measured at the ice surface, appears to be constant at 12,000 ft/sec regardless of charge depth, charge weight, or explosives type. However, the dispersion of the data decreases and the accuracy with which the velocity can be measured increases if variations in behavior of the material with charge depth, charge weight, and explosive type are considered.

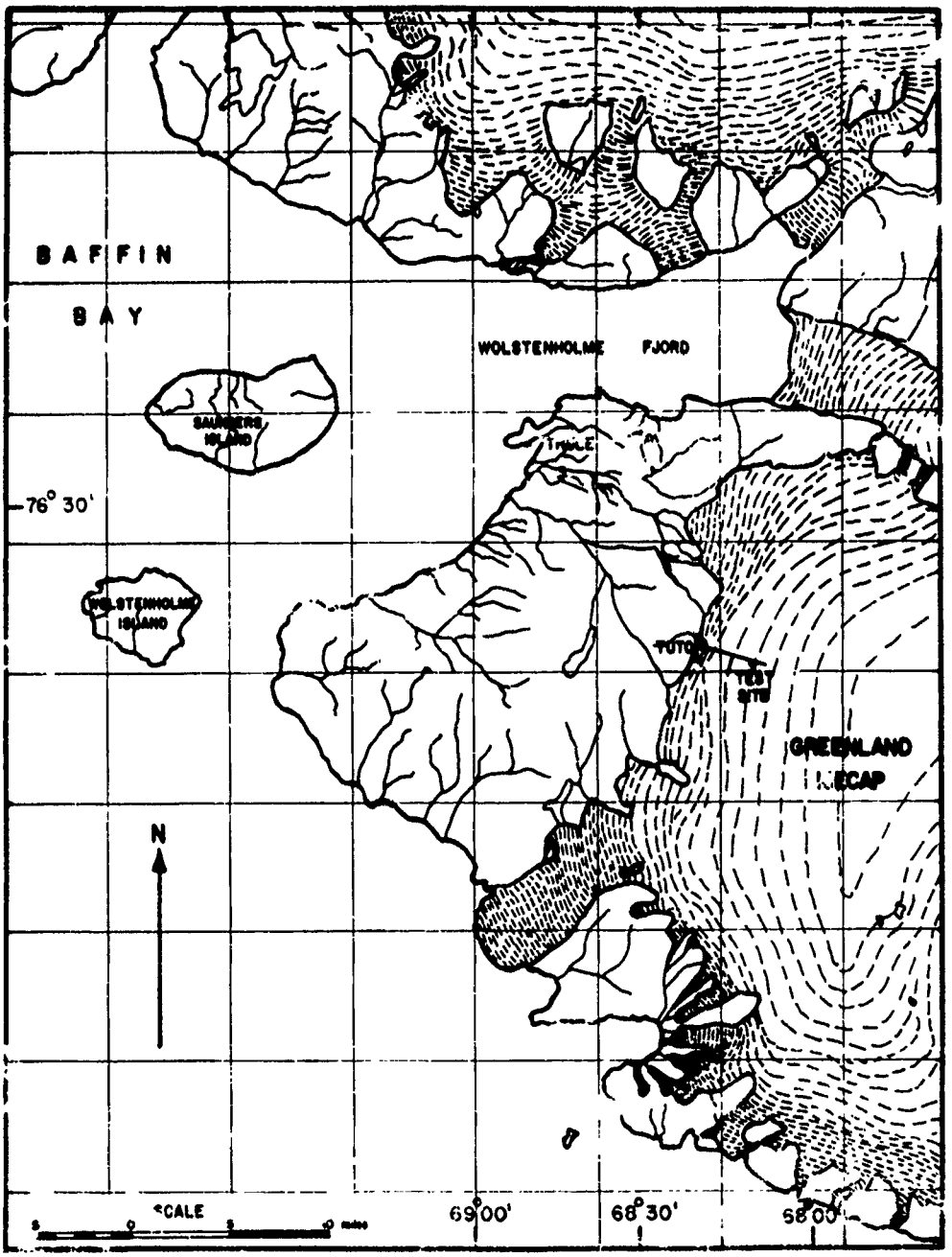

Figure 1. Index map, Thule area.

EXPLOSIONS IN ICE

by

Clifton W. Livingston

GENERAL PLAN OF THE TESTS

The tests were conducted during the summer of 1957 at a test site on glacier ice $2\frac{1}{2}$ miles from Camp Tuto near Thule, Greenland. Atlas 60 Percent Straight Gelatin, military explosive C-4, Atlas Coalite 7S, and Atlas Coalite 5S were tested. Twenty-four blasts instrumented for pressure measurements and 106 uninstrumented blasts ranging in weight from 2.5 to 40 lb of explosive were detonated in charges of spherical shape. In addition to blasts at various depths (Fig. 10) four contact blasts were detonated and at least one instrumented 10-lb charge of each explosive was detonated in air above the ice at a distance in feet equal to the cube root of the charge weight (Fig. 11).

Motion pictures were taken to determine the initial velocity of flyrock, to measure the height to which ice was thrown, and to aid in studying ground-rise phenomena. Under-ice pressures were measured and both air and under-ice pressures were measured for shallow blasts and blasts detonated above the ice surface. Seismic measurements were made at various scaled distances from the shot point

OBJECTIVES AND SCOPE

"Explosions in Ice" is a continuation of the Keweenaw Blast Tests and the Fort Churchill Blast Tests (Livingston, 1956; 1959), which were designed to obtain fundamental data on producing excavations in frozen ground, on forming trenches and foxholes for troops in arctic and sub-arctic regions, and on the design of structures in an arctic or sub-arctic environment to resist damage by explosions.

The following objectives are added to those of the Keweenaw Blast Tests and of the Fort Churchill Blast Tests:

1) to obtain numerical values of the crater coefficients, the strain-energy factor E, the energy utilization number A, and the materials behavior index B of the Livingston crater equations;

2) to investigate the significance of the strain-energy factor relative to the model laws for explosions;

3) to correlate the effects of explosions in frozen ground and in ice;

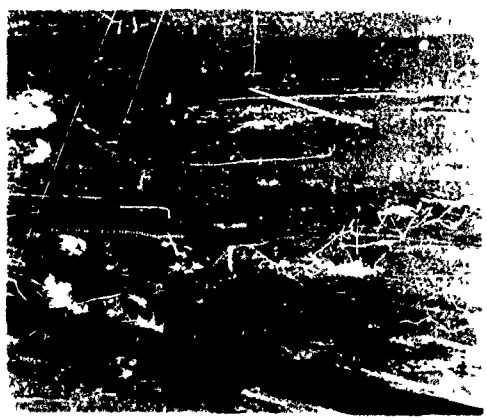

Figure 2. Test site looking southwest from mile $2\frac{1}{2}$ on the ramp road.

Figure 3. Banding in the ice along wall of test pit.

4) to determine whether the dimensions of a crater in ice — or the variables of the Livingston crater equations, which are known to be functions of the depth ratio Δ, and of the energy density within the medium — are related to peak pressure, impulse, or other pressure or seismic effects;

5) to search for fundamentals of behavior of materials of the earth's crust.

The report is restricted to:

1) a description of field and office procedures

2) a preliminary correlation of under-ice pressure measurements, crater dimensions, flyrock travel, and airblast pressure;

3) the presentation of the data.

PROCEDURE

Test site

The test site was $2\frac{1}{2}$ miles east of Camp Tuto on the Thule ramp (Fig. 1). The surface of the ice cap at the test site ranges from 2480 to 2550 ft above sea level, and slopes gently towards the edge of the ice cap.

The ice increases in thickness to 800 ft at the test site. The edge of the ice cap at Camp Tuto is buttressed against thick glacial moraine, and the ice is stagnant to a distance of roughly 3000 ft from the edge. In the vicinity of the test site, the ice moves about 8 ft/yr — 4 ft during the summer test season and 4 ft the rest of the year (personal communication, F. J. Sanger, ACFEL). Glaciology in the vicinity of Camp Tuto and the test site is described in SIPRE Report 28 (Schytt, 1955) and in SIPRE Research Report 17 (Bishop, 1957).

The site (Fig. 2) was located so that blasting did not interfere with other research operations in the vicinity. A 500-ft safety zone was left between project headquarters beside the ramp road and the near edge of the blast test area.

The site was laid out so that blasting and excavation advance up the ice ramp. Instrumented shots were placed in the center of the test strip and uninstrumented shots on both sides. Although the Thule ramp is comparatively free from large crevasses, cracks up to 2 in. wide formed during the winter and were present under the snow cover at the time of arrival of the field party. Later, a 3-ft wide crevasse was discovered at a point roughly 1000 ft southwest of the test site. The first step in laying out the test site was to determine the position and direction of the shrinkage cracks so that seismic measurements need not be taken across the openings. Strips of the ice surface were exposed with a bulldozer, and the strips were laid out so as to collect and divert melt water from the area between them. The ice surface was found to be smooth, and the predominant direction of the shrinkage cracks was nearly at right angles to the ramp road. The cracks were not straight, nor were they regularly spaced. The spacing ranged from 50 to 100 ft.

Shortly after field work began, melt water filled the cracks and soon froze. After this water had frozen, the earlier existence of a crack would be detected only by a change in color or texture of the ice. Freezing and expansion of melt water in the shrinkage cracks may explain the greater rate of movement of the ice surface in summer than during the rest of the year.

Physical properties of the ice

The glacier ice of the test site was free from dirt. Color bands roughly parallel to the ice surface were evident in trenches, in test pits, and on the walls of craters excavated during the test season. Ice containing no air bubbles (which is blue) is of higher density than ice containing abundant air bubbles (which is white). Ice crystals ranging from 3/4 to 4 in. long and from 1/8 to 1/2 in. in diameter are oriented with their long axes at right angles to the banding. Figure 3 shows the banding in the ice and the breakdown of the ice surface along crystal boundaries by melting and radiation.

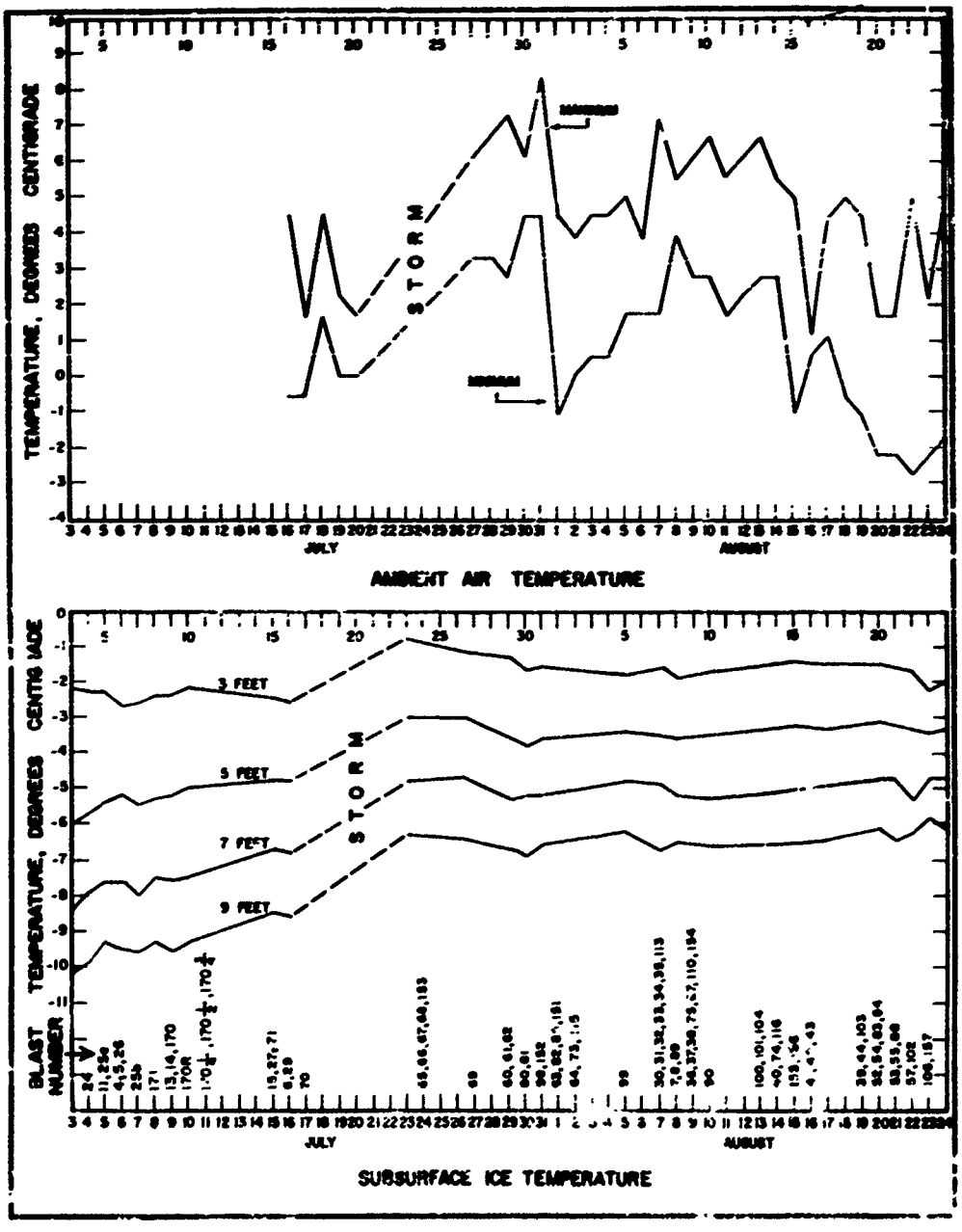

Figure 4. Ambient air and subsurface ice temperature.

Table I. Physical properties of ice at the explosions test site, Thule ramp. (From Butkovich, 1959)

	kg/cm²	psi
Crushing strength, mean vertical	35.8	509
Ring tensile strength, mean vertical at density range		
0.860 - 0.880 g/cm³	18.0	256
0.880 - 0.900 g/cm³	23.0	327
0.900 - 0.915 g/cm³	27.0	384
Flexural strength, mean failure stress at center of horizontal beam beam at depth (ft)		
0.00 - 0.70	11.6	165
3.05 - 4.33	14.0	199
6.70 - 8.03	16.8	239
	dynes/cm²	psi
Static modulus of elasticity, mean	1.3×10^{10}	0.1885×10^{6}
*Dynamic modulus of elasticity (at mean density 0.899 g/cm³ - horizontal beams)	8.7×10^{10}	1.26×10^{6}

*From Roethlisberger (1959).

Samples of the ice were tested in the under-ice laboratory at the USA SIPRE ice tunnel to determine physical properties. It was concluded from the results that the glacier ice of the test site differs appreciably from various types of ice encountered when driving the SIPRE ice tunnel. Test procedure and results are included in SIPRE Research Report 47 (Butkovich, 1959). Table I summarizes some of the physical properties of the ice, determined at a loading rate in which the stress-strain curve is linear. The tests were made at -5C, near the temperature that prevailed during the test season between 5 and 7 ft below the ice surface (Fig. 4).

Ice density varied from 0.859 to 0.914 g/cm³ at the test site. The variation depends upon the size and abundance of air bubbles in individual bands. The bubbles are irregular in shape and in some bands are as large as 7 mm in diameter.

Figure 4 summarizes the maximum and minimum ambient air temperatures as measured 3 ft above the ice surface at mile 2 on the ramp road. From a comparison of temperatures at mile 2 and mile 3 during the test season, it may be inferred that ambient air temperatures at the test site (which is roughly halfway between the two weather stations) were within ±1C of those at mile 2.

During the test season as much as 12 ft of ice melted from the surface of the ice cap adjacent to the headquarters building (Fig. 5). The extent of ablation of the ice is indicated by the difference in elevation of the surface of the ice underneath the building and the surface in the foreground. Ablation was less at other places on the test site, but the lowering of the ice surface required that the position of subsurface temperature gages be referred to a permanent bench mark. The temperatures of the ice 3, 5, 7, and 9 ft below the surface (Fig. 4) were obtained using the temperature gradient at fixed gage positions and the position of the ice surface relative to the reference bench mark.

Figure 5. Headquarters building at test site, showing ablation during the melt season. Rocks prevented building from sliding off ice pinnacle.

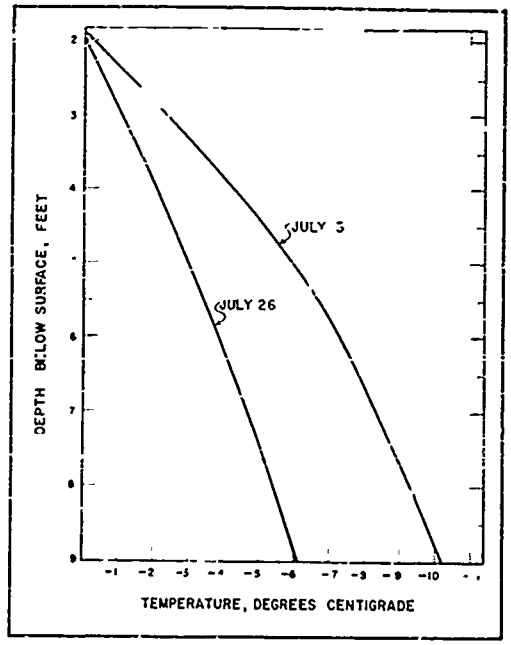

Figure 6. Subsurface temperature gradient.

Ablation and its effect upon operations

Melting began at the edge of the ice cap and proceeded up the ramp to engulf the test site. Regardless of the location picked along the ramp road for the test site, the situation would have been much the same, but melting would have occurred at a different time during the season. Melt streams, developed behind the slush zone, were impossible to control with equipment available.

Ablation of the ice surface was the cause of most difficulties experienced during the test work. Pumping became a major problem. Channels cut in the ice to drain surface water from test areas overflowed or became clogged and were buried so that transportation on foot was impossible at times. The movement of drilling and excavating equipment was seriously restricted. During the period that the slush zone advanced through the test site, all operations — drilling, blasting, excavating, measuring of craters — were seriously affected.

After a crater was mapped, it filled again with water. Pins and flags driven into the ice to mark the crater limits soon were lost because of wind, black-body radiation, or surface ablation. Snow soon drifted over the slush-filled craters. The deep excavations and the slippery sides of craters that had been abandoned created a trap for men and equipment. Areas where excavations had been made were isolated by using a bulldozer to build up snow piles, but water accumulated behind the piles and encroached upon the active working area.

Ablation of the ice surface was accompanied by warming of the upper part of the ice. Figure 6, a temperature gradient such as was used in preparing the record of sub-surface ice temperatures, shows that the upper 2 ft of ice was at the melting point. When drilling blast holes, even though surface water had been diverted from the coll-

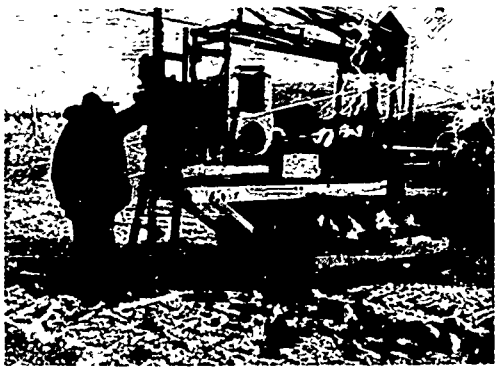

Figure 7. Auger drill rig.

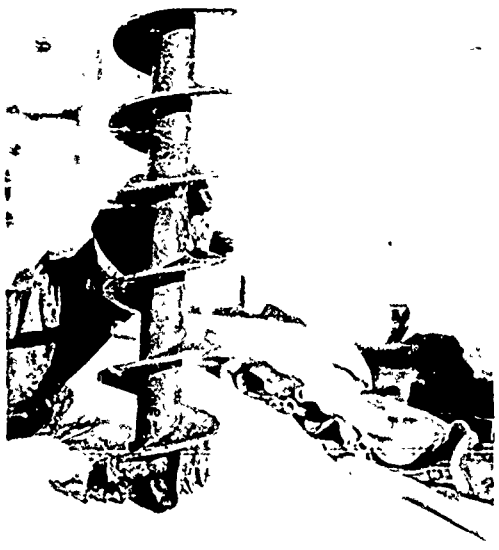

Figure 8. Cutting heads were redesigned to chip the ice.

of a drill hole, a flow might be encountered within the upper 2 ft of warm ice. Warm slush that formed on the auger flites at shallow depths was carried downward into colder ice as the hole deepened. If it became necessary to stop the rotation of the drill, the slush-covered auger flites froze instantaneously to the walls of the hole. Cuttings of slush ice sometimes formed beneath the cutting head of the auger and gradually enlarged into a ball as the hole deepened. Eventually the ball completely encased the cutting head so as to stop the drilling action and to raise both drill and caterpillar mounting.

Drill holes filled with water soon after completion and the water began to freeze from the walls of the hole inward. In the bottom of the hole, where the ice was coldest, freezing was more rapid than at shallower depths. The result was that, if too long a time elapsed between drilling and blasting, the hole became too small at the bottom to accommodate the plastic sphere containing the explosive.

The conflicting requirements that pressure gages must be frozen in the ice to obtain true pressure measurements and that blast holes must not refreeze before the placing of the charge, restricted the operating cycle.

Auger drilling

Blast holes ranging from 6 to 14 in. in diameter were drilled. The rig (Fig. 7) consists of a Joy Model 7 diamond drill with AX mechanical feed screw and auxiliary jack shaft driven from a gasoline engine and mounted on a D-4 caterpillar tractor.

As the drill had to penetrate 0C ice and enter colder ice, and because of the abundance of water on the test site during the ablation period, cutting heads of the augers were redesigned to chip rather than to slice the ice (Fig. 8).

Dry drilling, in which drill cuttings were removed by the auger flites or by a jet of compressed air, was eliminated in favor of wet drilling. Water was diverted to the drill hole from nearby melt streams, and the cuttings were floated to the surface. A 2 ft section of auger flite was used as an agitator behind the cutting head and the hole was deepened by adding AX drill rod.

Blasting procedure

Three commercial explosives and one military explosive (Table II) were tested so as to observe as large a range as practical in velocity and energy.

Table II. Properties of the test explosives.

Explo.	Classification	Energy (cal/g)	Explosion pressure (psi)	Detonation velocity* (ft/sec)	Unit wt † (in^3/lb)
C-4	Military	1235		24,000	16.9
A-60	Straight Gelatin	1249	13.018	20,000	16.[illegible]
C-7S	Ammonia Permissible	916	14,913	10,000	25.0
C-5S	Ammonia Permissible	942		5,000	27.0

* confined
† packed in spheres

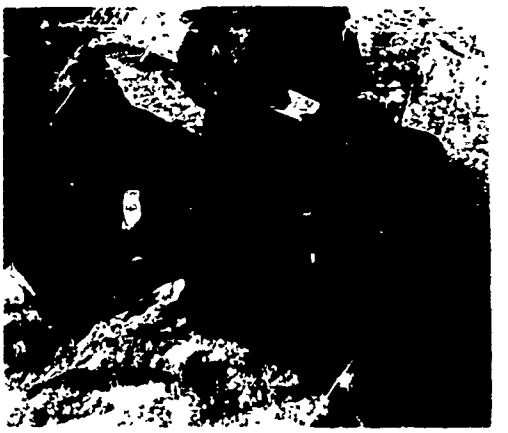

Figure 9. Plastic sphere containing explosive.

The explosives were hand packed into plastic spheres (Table III) and detonated by electric blasting caps. A booster sleeve was used also to detonate C-4. Halves of plastic spheres were taped together with electrician's tape. A copper wire was wrapped around the outside of the sphere to lower the charge into the hole and to serve as a means of determining the instant of detonation (Fig. 9). The blast hole was filled to the collar with sand stemming. Uninstrumented charges were detonated using a Southwestern Industrial Electronics blasting machine designed for reflection seismic work. Figures 10 and 11 show the relations between charge weight and depth or height of charge.

Table III. Dimensions of explosives spheres.

Explo.	Inside radius (ft)				
	2.5-lb	5.0-lb	10.0-lb	20.0-lb	40.0-lb
C-4	0.188	0.240	0.300	0.375	0.470
A-60	0.188	0.240	0.300	0.375	0.470
C-7S	0.219	0.276	0.340	0.436	0.540
C-5S	0.240	0.276	0.340	0.436	0.540

Proposed colored columns and trenches

Plans to use the colored column technique developed by USA ERDL to study deformation in the ice below the bottom of the crater had to be abandoned because of surface melting. Holes 1-3/8 in. in diameter were drilled at predetermined scaled distances from the explosive charge and filled with water soluble dye, using different colors for each column. Water flowing on the surface and within the upper 2 ft of ice

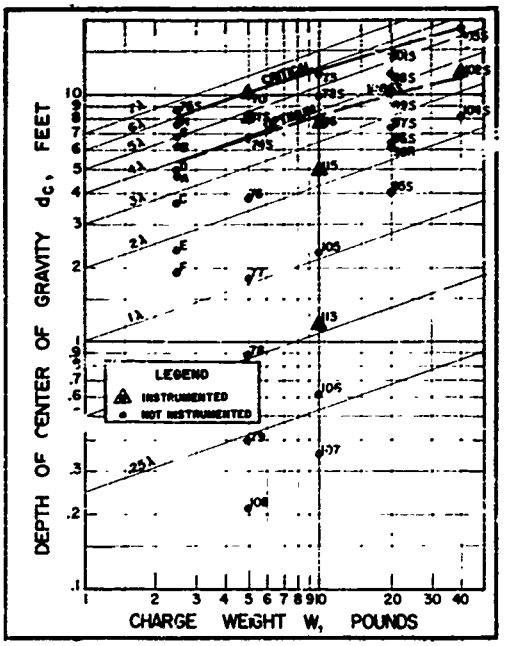

a. Atlas 60

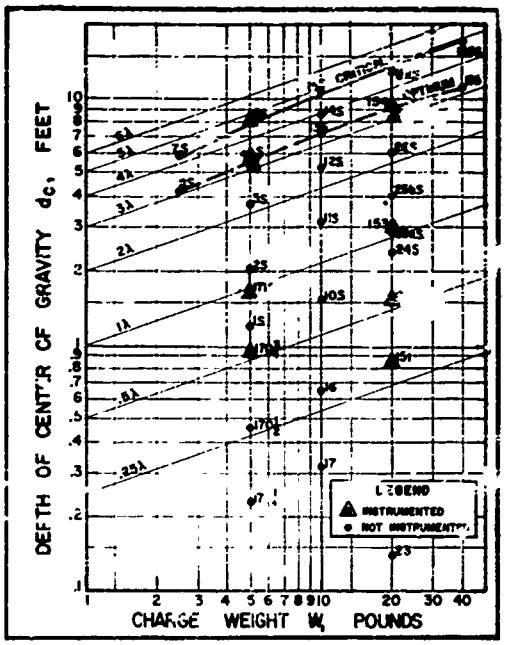

b. C-4

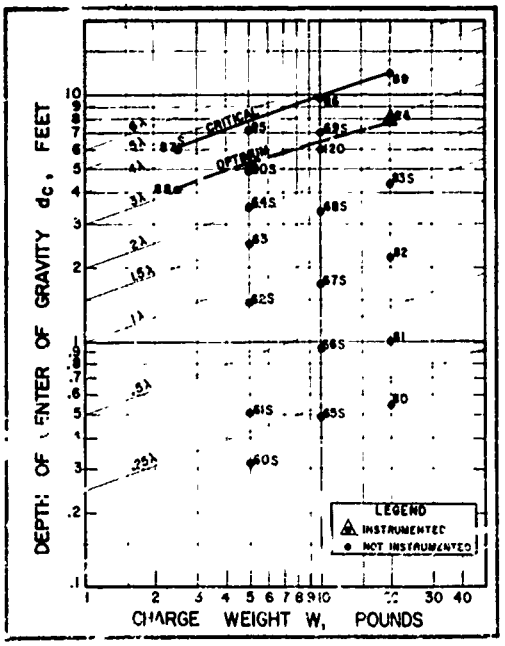

c. Coalite 7S

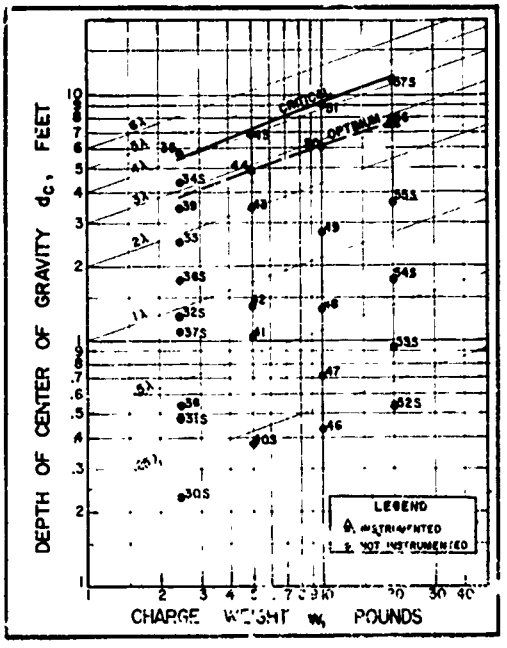

d. Coalite 5S

Figure 10. Blasts in ice. Seismic measurements were made for blasts marked "S".

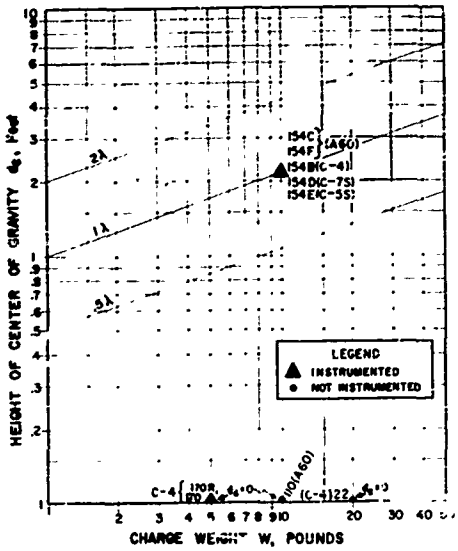

Figure 11. Air and contact blasts.

Figure 12. Doming of the ice surface at near critical depth.

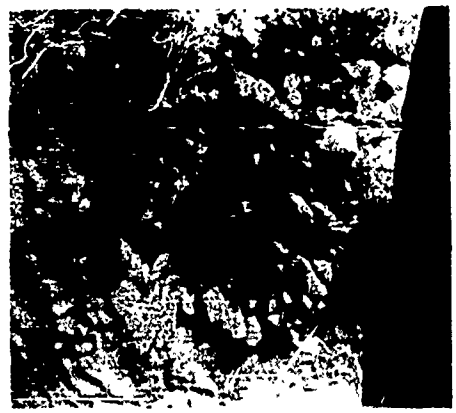

Figure 13. Fracture pattern in ice for blasts between critical and optimum depths.

washed out and removed the dye. After a hole was drilled, it filled with surface water and freezing from the walls drove the water-soluble dye inward, where eventually it froze in a column about the size of the lead in a pencil. Another difficulty during the period of rapid ablation of the ice surface was that the crater filled with water so rapidly after a blast that it was impossible to pump out the water-ice mixture with the pumps available. The amount of water on the test site was so great at times that it was impossible to keep a trench open long enough to inspect the colored columns.

It was intended also to study deformation and fracturing of the ice beyond the crater using trenches dug with a trenching machine. Unfortunately, the trenching machine was transported by ship and arrived too late to be used extensively. However, it did arrive in time to demonstrate: 1) that an explosion in ice produces a zone of shearing that extends a substantial distance beyond the crater, and 2) that a trench 18 in. wide by 8 ft deep can be advanced in ice with a conventional trenching machine at approximately 1 ft/min.

The direction of displacement along shear planes and the flat dip of the planes are the same as for thrust faults. (The hanging wall is thrust over the footwall.) The term "thrust zone" is used here to designate the zone of shearing beyond the crater. The existence of the shear planes and their orientation with respect to the explosive charge was observed in trenches in the thrust zone, but unfortunately the limits of thrusting could not be studied.

Excavation, field analysis, and crater surveys

The apparent crater was mapped in plan and cross section. The crater was then excavated either by hand or with a clamshell. The true crater was mapped using the

Figure 14. Refreezing after deformation and disaggregation of the ice near the explosion cavity

Figure 15. Fracture pattern at wall of a vertical trench near an explosion in ice.

reference points used to map the apparent crater.

A field analysis was made of each blast in an effort to obtain information useful in comparing the behavior of ice with that of other materials. Figures 12-15 illustrate phenomena that are characteristic of the behavior of ice or that differ from the behavior of frozen ground.

Figure 12 shows how the surface of the ice is domed as a result of blasts at near-critical depth. The doming is in contrast to the slabbing action characteristic of brittle substances and suggests that "secondary effects" associated with expansion of the gas bubble may be of greater importance in cratering in ice than "primary effects" associated with reflection of the shock wave.

Figure 13 illustrates the fracture pattern typical of blasts at depths ranging from critical depth to optimum depth. In brittle substances, slabs are formed parallel to the surface by reflection of the shock wave. In ice, failure occurs primarily on radial and tangential planes, and appears to be a result of displacement outwardly from the explosion cavity.

Figure 14 illustrates 1) "plastic deformation" of the ice adjacent to the explosion cavity, 2) compaction due to heat and pressure below the explosion cavity, and 3) disaggregation along crystal boundaries (which possibly may be due to energy release and expansion of the ice after the pressure declines).

Figure 15 shows damage to walls of a vertical trench in ice in the zone beyond the rim of the crater. The crater exhibited effects such as shown in Figure 13, but the fractures adjacent to the walls of the trench are of a different type. They are vertical and are oriented concentrically about the explosive charge. It seems that, if caused by reflection of the shock wave, the fractures should have formed parallel to the wall of the trench and the ends should curve in the opposite direction. If caused by thrusting, the fractures would be inclined rather than vertical.

Instrumentation

The scope of the instrumentation program was limited by difficulties encountered in the field and by time and funds available. The number of under-ice shock gages available for the tests also was limited. Early in the test program, gage and cable damage were high. The tests also were hindered by winds that at one time reached velocities in excess of 100 mph. During much of the test season it was impossible to control melt water on the test site. Melt water and wind-blown moisture contributed greatly to the difficulties of instrumentation. Near the end of the test season, the few

gages that had remained serviceable were damaged by freezing of the Epon coating that covered the gage elements.

To determine whether it was essential to freeze the gages in the ice, pressure measurements from gages frozen in the ice were compared with those from gages in water-filled holes at the same scaled distance. It was apparent that the gages should be frozen into the ice to obtain proper coupling. Also it was observed that the peak pressure in glacier ice is substantially less than in artificial ice or in water at the same scaled distance. Presumably air bubbles in the ice cause the peak pressure to be reduced. The upper 2 ft of ice contained water during the first month of testing and behaved differently than the cold ice at greater depths.

Placement and recovery of under-ice gages were difficult. Gages placed at less than 2.5 ft below the ice surface did not freeze for several days. As the ice surface continued to deteriorate by radiation and by melting along the crystal boundaries, the gage was no longer at the specified depth by the time it had frozen in. Furthermore, it was difficult to prevent moisture from entering the cable couplings because the velocity of the wind seldom was less than 20 mph. When the gages had frozen in, usually one or more circuits had shorted out. By the time the difficulty had been detected and corrected, refreezing might reduce the diameter of the blast hole so much that the charge could not be placed at the specified depth. Furthermore, the collar of the drill hole was no longer at the same elevation as when drilled.

Difficulties first encountered when recovering the gages were more exasperating than those experienced when placing them. The depth of a gage and its position with respect to the crater determined whether or not the gage was blown loose by the shot, whether the cables were sheared off, or whether gage and cable were undamaged. Gages that remained in position were recovered by hand picking, by drilling, or by a combination of hand picking, drilling, and blasting. The volume of water on the test site made it difficult to keep the crater free from water during excavation, and the presence of the cables made it impractical to excavate with a clamshell.

Most of the gage recovery difficulties were solved by using a steam jet. However, it still was impossible to follow a standard pattern when placing the gages because the depth of warm ice remained nearly constant and could not be scaled with the experiment, and, depending upon the position of the gage with respect to the crater, shearing displacement sufficient to destroy the cables occurred at various depths below the surface.

Under-ice gage layouts. Because of the difficulties, it was necessary to adopt a pattern of gage placement in which the scaled slant gage distance was held constant, rather than the scaled charge depth or the scaled gage depth. The depth of the gage was determined both by the thickness of the layer of warm ice and by the depth of the crater. It was found through experience that the radius of the true crater was in the order of 25 times the radius of the charge. One or more gages were placed at this distance. Two or more were placed inside the crater and two outside. Standard slant distances for spheres of Atlas 60 Percent Straight Gelatin and military explosive C-4 (which are of the same diameter for a given weight of explosive) are listed in Table IV. Because of continual ablation of the ice surface and the lapse of time between placing the gages and firing the shot, the gage slant distances were remeasured after the charge had been placed and differ slightly from the design distances.

Instrumentation for airblast and under-ice pressure measurements. Three types of gages (Fig. 16) were used to measure air and under-ice shock pressure. Disk-shaped or "pancake" gages with tourmaline-crystal elements 1-5/8, or 2-1/4 in. diameter were used to measure pressures in air. Underwater shock gages with tourmaline gage elements 1/4, 3/8, or 1/2 in. in diameter were used to measure under-ice shock pressure. A few under-ice shock measurements at distances greater than 50 ft were made using earth pressure gages (Fig. 16, right) manufactured by the Department of

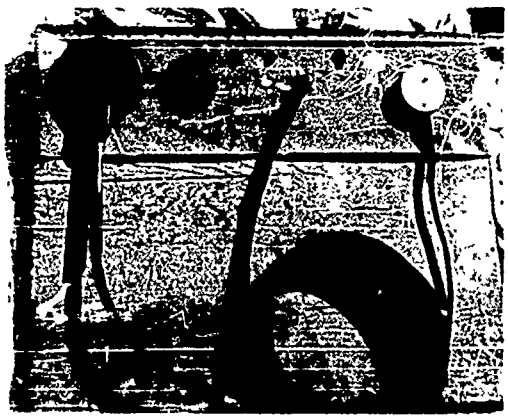

Figure 16. Air and under-ice shock gages.

Figure 17. Gage calibration.

Figure 18. Miller recording unit.

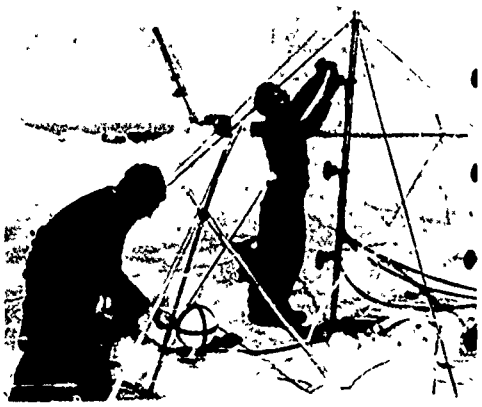

Figure 19. Final check of airblast gage slant distances.

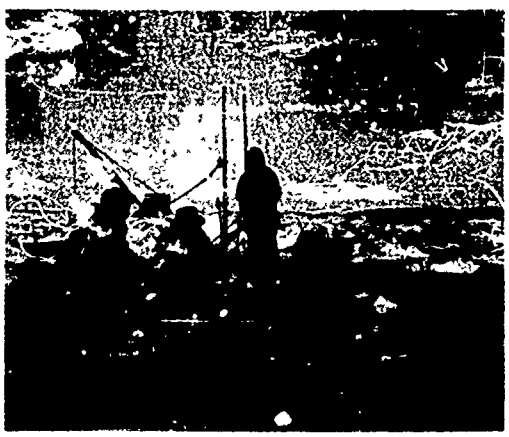

Figure 20. Preparation for contact burst instrumentation.

Figure 21. Portable, high resolution, SIE reflection seismograph.

Table IV. Shock-gage scaled slant distances. (Atlas 60 and C-4)

$f(\lambda)^*$	$f(r_o)$
1.50	11.[illegible]
2.24	16.[illegible]0
3.36	25.00
5.03	37.50
7.56	56.25

* Scaling factor λ is a distance which, in feet, is numerically equal to the cube root of the weight of charge W, in pounds.

Figure 22. Placing geophones to measure the three components of vibration.

Scientific and Industrial Research, Road Research Laboratory, Hardmondsworth, Middlesex, England. The RRL gage is 3 in. in diameter and 5/8 in. thick and is housed in an aluminum alloy. A laminated pile of four x-cut quartz crystals electrically connected in parallel is contained within the housing.

The gages were calibrated in the field using a pressure pot (Fig. 17). The calibration simulated dynamic conditions in that the voltage drop across the piezoelectric gage was measured as the calibration pressure was released instantaneously from the fluid in which the gage was immersed.

Gage signals were recorded using a Miller recording unit (Fig. 18) containing eight dual-beam cathode-ray oscilloscopes and a rotating-drum camera. Millisecond timing lines were imposed upon the records. One of the sixteen channels was used to measure zero-time, another to measure the time of ice movement, and the remaining to measure under-ice pressure or the pressure in the air.

In addition to under-ice shock measurements at positions designated in Table IV, instrumented blasts were fired at shallow depths below the surface, at the surface, and above the surface (Table V). The gage layouts are shown in the appendix (Figs. A1-23). Slant distances in air for under-ice shots were measured from ground zero (Fig. A3). Airblast gages were mounted as shown in Figures 19 and 20.

Seismic measurements

A portable, high resolution, reflection seismograph (Fig. 21) manufactured by Southwestern Industrial Electronics was available for the tests. The instrument could not be calibrated under conditions in the field; therefore, the amplitude of vibration could not be converted to absolute units of displacement. To offset this disadvantage, the arrival time and the frequency of each of the three components of vibration (Fig. 22) could be measured at each of two geophone stations at specified scaled distances from the shot point. It was possible also to measure the thickness of the ice along a profile from the edge of the ice-cap to the explosions test site.

At scaled distances less than 150λ the geophones were driven beyond their limit with the amplifier gain set at its minimum value. Geophone stations were established at standard distances of 200λ and 225λ, and most records were made using the full frequency range of 70 to 425 cps. A few measurements were taken at scaled distances of 250, 275, 300, and 325λ. A total of 66 blasts was recorded. For 6 of these blasts, pressure measurements were also made. Seismic measurements also were taken of one above-surface blast with each of the four test explosives (blasts 154b, c, d, and e).

The time of arrival of the under-ice pressure disturbance was measured by shock gages placed so as later to be within and adjacent to the crater and by seismic geophones placed at scaled distances ranging from 200λ to 325λ. Under-ice shock gages were placed at scaled distances ranging from 1.5λ to 7.5λ. The average charge-to-gage

Table V. Instrumented contact and near surface blasts.

	Scaled depth of charge $\frac{d_c}{\sqrt[3]{W}}$	Explosive	Blast no.	Measurement
	-0.25	C-4	170-1/2	Airblast
	-0.50	C-4	170-3/4	Airblast
Shallow	-1.0	C-4	171	Airblast
under-ice	-0.25	C-4	151	Airblast
blasts	-0.50	C-4	152	and under-
	-0.50	A-60	113	ice shock.
	-1.0	C-4	153	Under-ice shock.
Contact	0	C-4	170R	Airblast
bursts	0	A-60	110	Airblast and under- ice shock.
	1.0	C-4	154B	Airblast
Above	1.0	A-60	154C	and air-
surface	1.0	7S	154D	induced
bursts	1.0	5S	154E	under-ice
	1.0	A-60	154F	shock.

travel velocity was measured using all four types of explosive with charges ranging from 2.5 to 40 lb and at various positions above, in contact with, and below the ice surface.

COMPILATION OF THE DATA

The data are compiled and tabulated in the appendix so that either a conventional analysis or an analysis based upon the Livingston crater equations may be made. A conventional analysis may be made using data sheets A and B, in which the various blasts are arranged in numerical order. Figure 10 shows the blasts according to the type of explosive, weight of charge, and depth of charge.

Data sheet C gives the crater data arranged according to charge weight and type in order of increasing charge depth. When these data are so arranged, the strain energy factor, the critical depth, and the materials behavior index are constants for all shots on any given data sheet.

Data sheet D summarizes seismic data, arranged numerically by blast number. The average charge-to-gage velocity and the frequency of each of the three components of vibration are recorded. The frequency recorded is the average of the first five pulses.

SYMBOLS AND NOMENCLATURE

Charge depth (d_c)

Distance from surface to center of gravity of charge.

Charge weight (W)

Net weight of explosive in charge.

Crater shape factor (K_s)

The crater shape factor is the variable K_s in the equation for crater volume

$$V = K_s \pi r^2 h$$

where V = volume
r = crater radius
h = crater depth.

If K_s equals 1/3, V is the volume of a cone. Thus a shape factor of 1/3 indicates a conical-shaped crater. A shape factor of less than 1/3 indicates a convex or trumpet shaped crater. A shape factor of more than 1/3 indicates a concave shape or indicated conversion of the crater shape to parabolic or spherical form.

Critical depth (N)

The minimum depth (measured vertically from the surface to the center of gravity of the explosive charge) at which the energy of the explosion is dissipated into a mass of earth or rock without materially damaging the surface above the charge.

Depth ratio (Δ)

Ratio of the depth of center of gravity of the charge to the critical depth.

Energy utilization number (A)

Explained in text.

Flyrock travel height (T_v)

The maximum vertical height above the ground surface to which particles from a blast are thrown.

Materials behavior index (Ξ)

Explained in text.

Optimum depth (d_{co})

The depth at which a given weight and shape of explosive produce the greatest volume of excavation per unit weight of explosive.

Strain-energy factor (E)

A measure of the energy absorption capacity of the medium in crater blasting.

$$N = E \sqrt[3]{W}$$

where N = critical depth (ft)
W = weight of explosive (lb).

Stress distribution number (C)

Explained in text.

Figure 23 illustrates crater and camouflet nomenclature adopted here. It is similar to that used by Waterways Experiment Station for blasts in soils. However, practical difficulties when blasting in rocks and frozen ground, and field conditions at the test site for explosions in ice make it impractical accurately to determine the limit of complete rupture and the limit of extreme rupture. The practice is to excavate all material loosened by the blast, and to describe the resulting excavation in brittle materials as the "true crater".

EMPIRICAL EVALUATION OF VENTING PHENOMENA

Introduction

The breakage process when blasting in ice appears to be a combination of deformation without loss of cohesion and of deformation in which fracturing occurs. As the depth of the charge is increased at constant weight, a point is reached at which the material is not fractured at the surface or is not deformed beyond a specified limit.

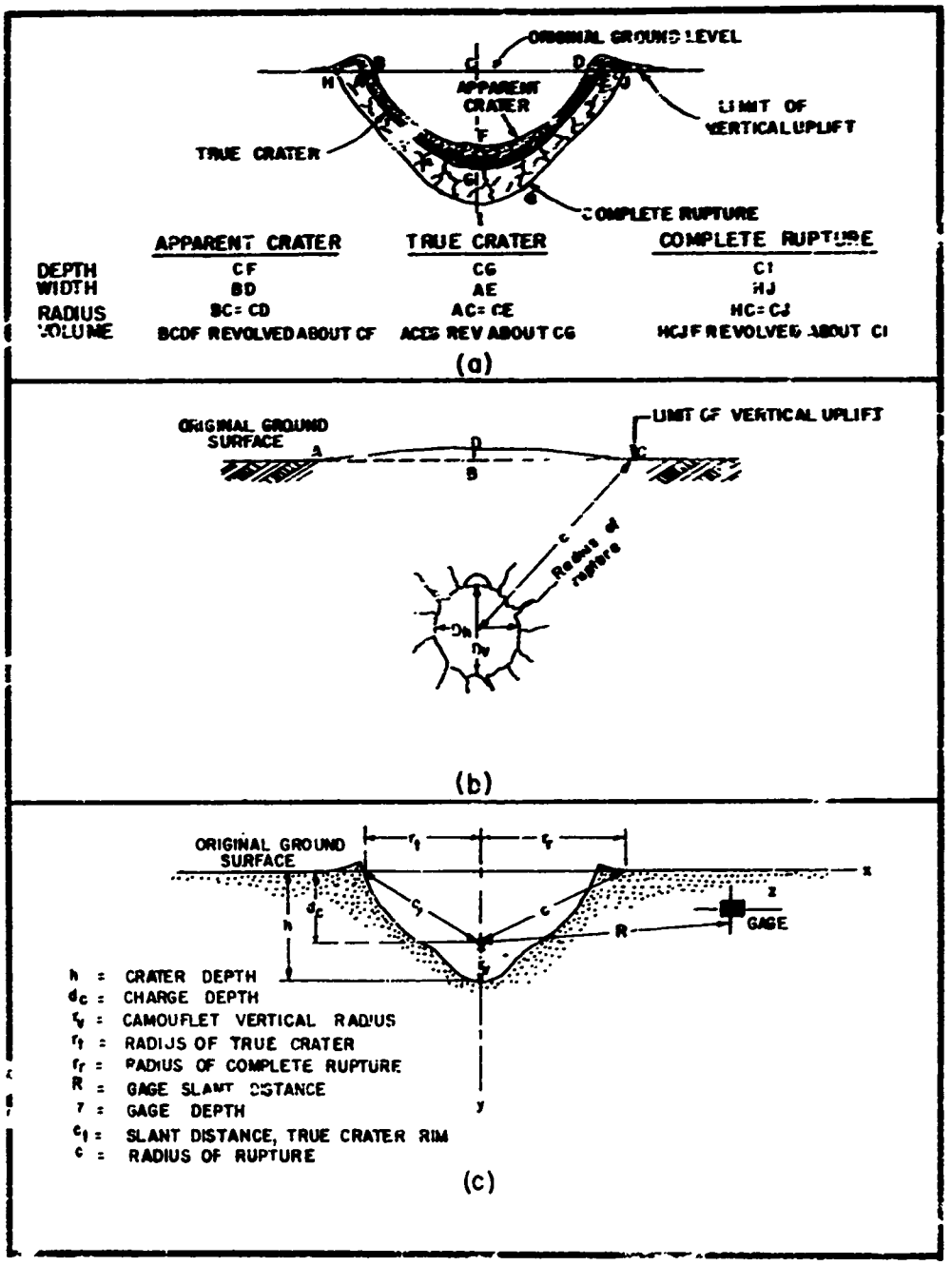

Figure 23. Crater and camouflet nomenclature.

This depth is known as the "critical depth." If the depth of the charge equals or is greater than the critical depth N, deformation without loss of cohesion predominates. The charge depth at which the maximum volume of material is broken per pound of explosive is the "optimum depth." The weight of explosive at that depth is the "optimum weight." If the depth of the charge is less than the critical depth but greater than the optimum depth d_{co}, fracturing occurs and part of the energy of the explosion is partitioned to the fracture process. If the depth of the charge is less than the optimum depth, material isolated by the fracturing process is accelerated, the size of the isolated particle is reduced, and partitioning of energy to the atmosphere begins.

Energy utilized in deforming the material without loss of cohesion is not available to the fracture process. Energy utilized to fracture and isolate the material from its surroundings is not available for accelerating the isolated fragments. It follows that energy utilized to accelerate the material or energy remaining in the gas bubble after breakthrough to the surface is not utilized in prior events. As the sequence of events begins at the instant of detonation with a disturbance propagated outwardly from the explosion cavity, later events depend upon whether energy is available and upon the quantity of energy available.

It is difficult to measure the quantity of energy utilized in each event or to describe it in absolute units. It is possible, however, to observe the development of each of the various events and to relate the beginning or the ending of the event to the depth ratio, which is a measure of the energy density in the material.

Evidence bearing upon the theory of relative behavior of materials, upon cube-root scaling, and upon the partitioning of energy to the breakage process may be obtained by studying the height to which the material is thrown by the explosion. In following paragraphs the evaluation of the crater data begins with events that are later than those comprising the breakage process. By doing so, it is intended to demonstrate that the explosive and the material are not separate and independent variables, and that energy utilized to impart motion is that left over and not required for earlier events.

Flyrock travel height

Motion pictures were taken to record the maximum height to which particles of ice were thrown when blasting with various weights and types of explosive at various depths below the surface. This maximum height divided by the critical depth is referred to here as the "N-scaled flyrock travel height." Figures 24-27 summarize the variation in N-scaled flyrock travel height with the depth ratio Δ.

A comprehensive analysis of flyrock travel phenomena is beyond the scope of the present report. The data are sufficient, however, to demonstrate:

1) that the height to which the material is thrown is a function of the depth ratio, and

2) that the breakaway velocity of the material at any given depth ratio is not independent of the type of explosive or of the weight of the charge.

The maximum height to which material is thrown by a charge of given weight is not always greater for a contact burst ($\Delta = 0$) than for an underground burst ($\Delta > 0$). Nor does the maximum height appear to depend upon the energy density of the explosive or upon the velocity of detonation (Table II).

Although the relation cannot be established positively at this time, the data suggest that the N-scaled flyrock travel height for an underground burst increases to a maximum at the transition between the fragmentation range (Livingston, 1959a) and the airblast range. At low values of Δ, (within the airblast range) upward acceleration of the material appears to be influenced both by pressure within the rising gas bubble and by the velocity of the gas in its scouring action above the broken material.

At depth ratios greater than the transition between the airblast range and the fragmentation range, the strain energy factor E, the energy utilization number A, and the

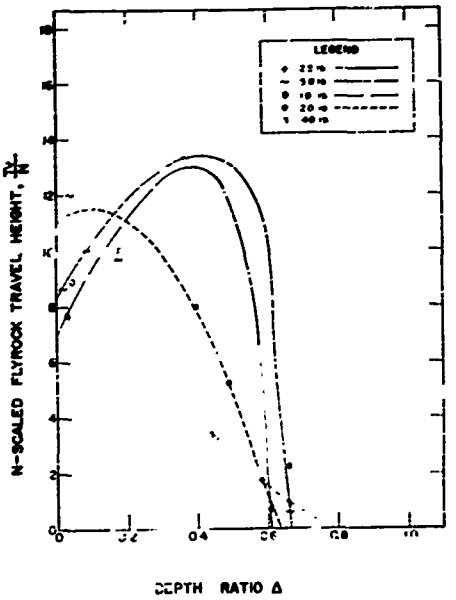

Figure 24. N-scaled flyrock travel height, A-60.

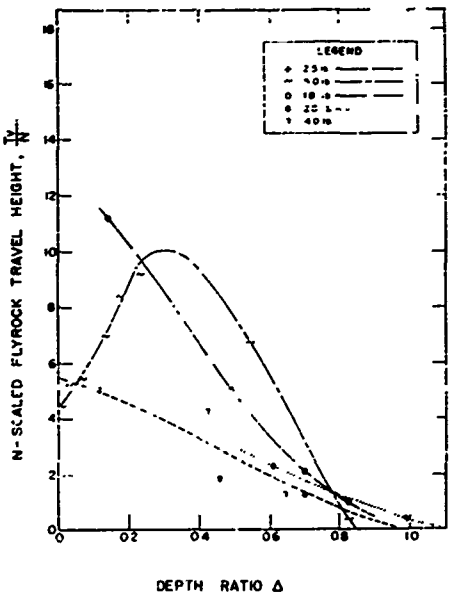

Figure 25. N-scaled flyrock travel height, C-4.

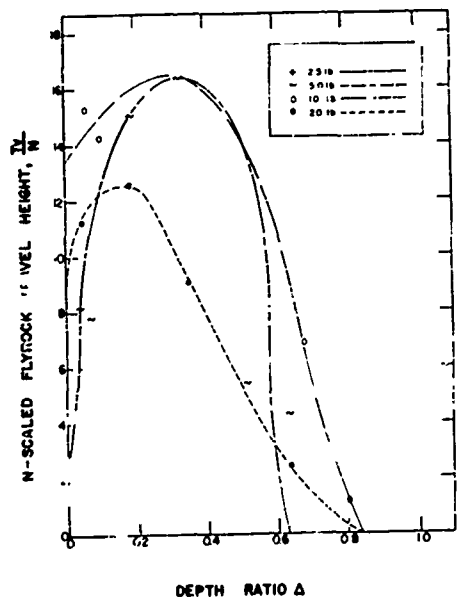

Figure 26. N-scaled flyrock travel height, 7S.

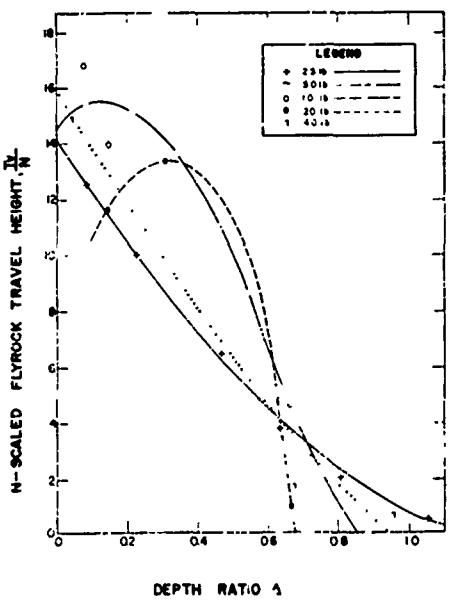

Figure 27. N-scaled flyrock travel height, 5S.

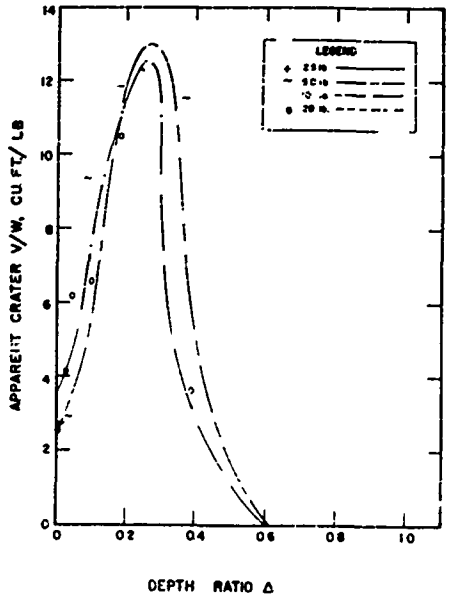

Figure 28. Apparent crater V/W vs Δ. A-30.

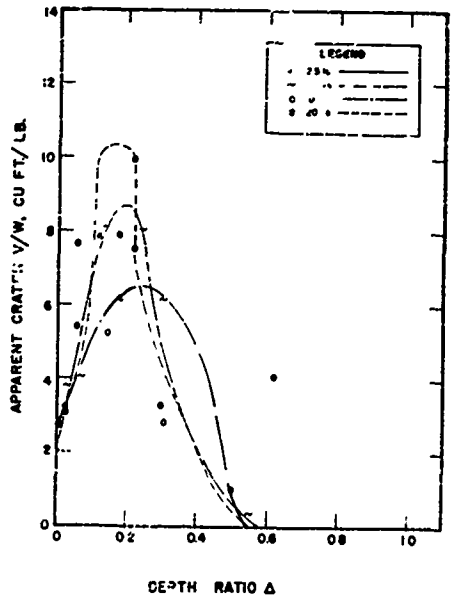

Figure 29. Apparent crater V/W vs Δ, C-4.

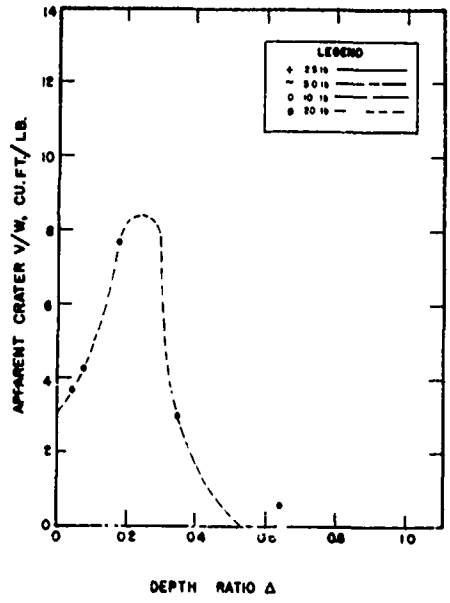

Figure 30. Apparent crater V/W vs Δ, C7S.

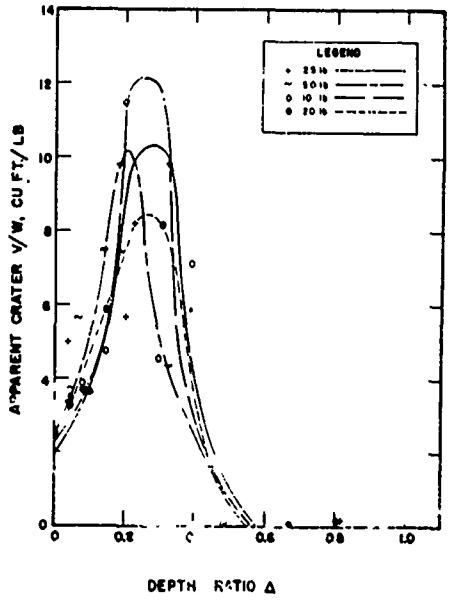

Figure 31. Apparent crater V/W vs Δ, C5S.

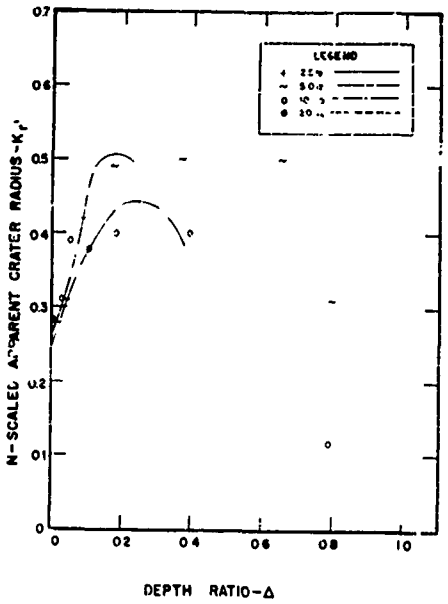

Figure 32. N-scaled apparent crater radius, A-60
$K_{r'}=r'/N$, where r' = radius of apparent crater.

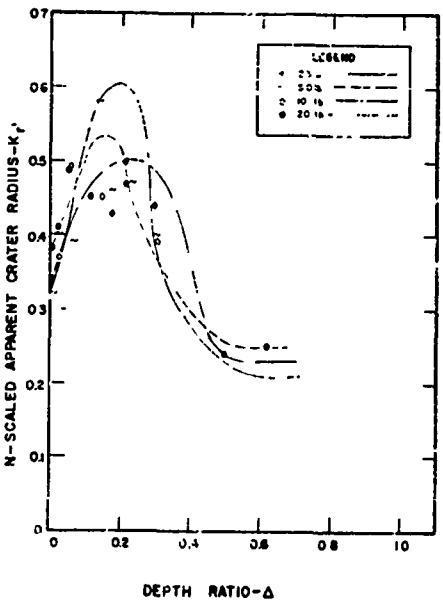

Figure 33. N-scaled apparent crater radius, C-4.

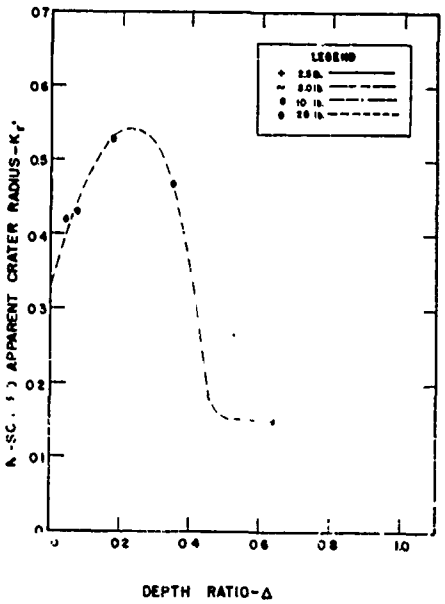

Figure 34. N-scaled apparent crater radius, C7S.

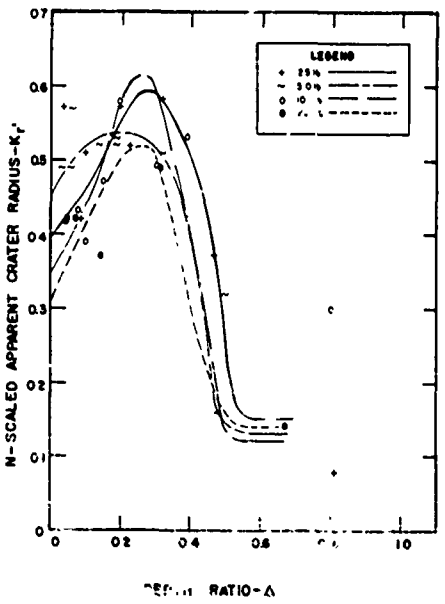

Figure 35. N-scaled apparent crater radius, C5S.

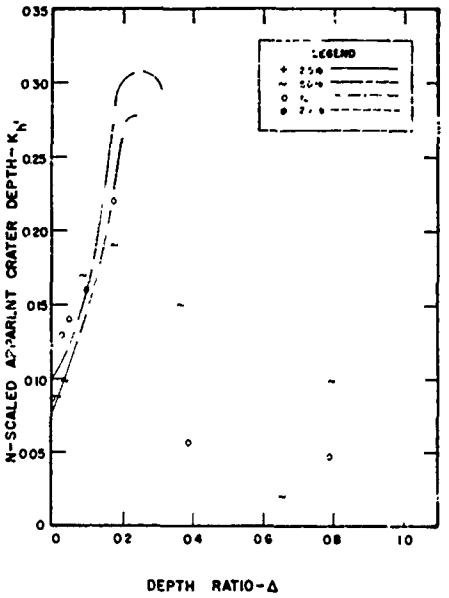

Figure 36. N-scaled apparent crater depth. $K_{h'} = h'/N$, where h' = depth of apparent crater.

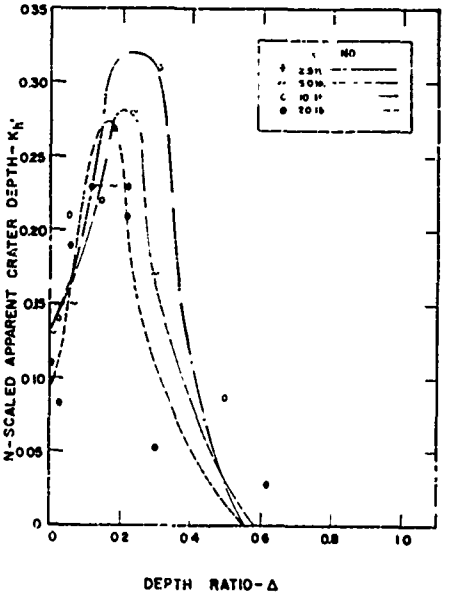

Figure 37. N-scaled apparent crater depth, C-4.

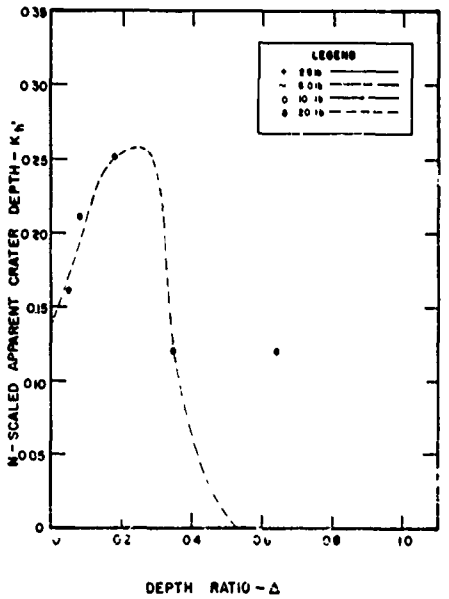

Figure 38. N-scaled apparent crater depth, C7S.

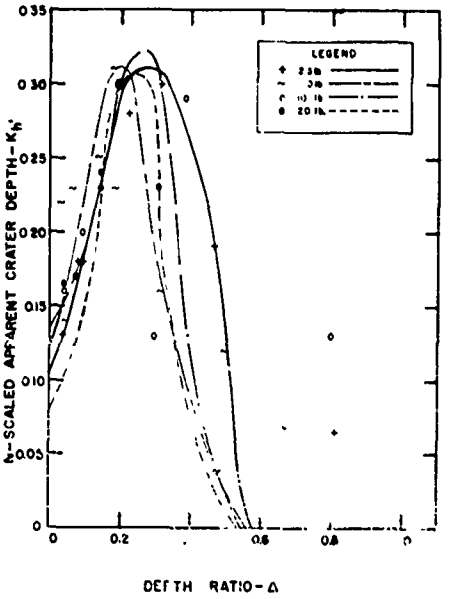

Figure 39. N-scaled apparent crater depth, C5S.

materials behavior index B, appear to be parameters affecting flyrock travel height. Such an interpretation accounts for the variation in flyrock travel with explosives type, materials type, and the charge weight at a given value of Δ.

The apparent crater

The "apparent" crater is the excavation as it appears to an observer immediately after a blast at a depth sufficiently shallow that fall-back does not fill the depression completely. The term as used here does not apply to charges that dome rather than break the surface, nor does it apply to craters that are filled beyond the level of the original ground surface by broken material falling back.

An apparent crater may be formed by an underground burst, a contact burst, or an airburst. A contact burst is one in which the depth ratio is zero. An airburst is one for which, in convention used here, the depth ratio is negative.

When blasts were fired with 10-lb charges of each of the test explosives at a distance (in ft) above the surface of the ice equal to the cube-root of the charge weight (in lb), no crater was formed. The lower limit at which a crater is formed in ice is somewhere in the region $-1 < \lambda_c < 0$, but the exact height at which the ice surface ceases to be damaged by an airburst was not determined. The upper limit in ice (where fall-back fills the crater to the level of the original surface), depends upon both the weight and the type of explosive. It is at a depth ratio slightly less than the optimum Δ_o.

Figures 28-31 summarize the variation in V/W, volume of the apparent crater per pound of explosive, with depth ratio Δ. Maximum V/W is reached in the region $0.18 < \Delta < 0.30$, depending upon the weight of the charge and the type of explosive. The apparent crater is filled by fall-back and ceases to exist in the region $0.52 < \Delta < 0.58$. For a contact burst, V/W varies from 15 to 40% of the maximum for an underground burst, depending upon the weight of the charge and the type of explosive. The fact that a single V/W curve cannot be used to represent the 2.5-, 5.0-, 10-, and 20-lb charges of a given explosive is consistent with variation in the N-scale flyrock travel height with charge weight (Fig. 24-27). An increase in the flyrock travel height is accompanied, for all types of explosive, by an increase in V/W of the apparent crater. V/W of the apparent crater and the N-scaled flyrock travel height both approach a maximum value at low values of Δ.

Figures 32-39 show the variation in the N-scaled radius and depth of the apparent crater with the depth ratio.

The height to which the flyrock is thrown and the dimensions of the apparent crater depend more upon events subsequent to the breakage process than upon events coincident with it. Both are greatest at low values of Δ, where the breakage process is inefficient. Both are dependent upon the explosive, the material, and the scale of the experiment. The observed relations are compatible with the theory of relative behavior of materials and are cited here in its support.

CRATER EVALUATION THEORY

Method of evaluating the data

The method of evaluating crater data employed in following pages differs somewhat from conventional cube-root scaling in that energy partitioning and variation in the behavior of the material with charge weight are taken into consideration. The method embodies the "theory of relative behavior of materials" and makes use of the Livingston crater equations. The equations were derived as a result of the Fort Churchill Blast Tests (Livingston and Murphy, 1959), and the theory of relative behavior of materials was first stated when applying the equations to small blasts in loess and clay (Livingston, 1959a).

Variables that exert the predominant influence on the cratering process are:

1) the explosive
2) the geometry
3) the material.

Experience has shown that the explosive and the material are not separate and independent variables. Experience also has shown that the behavior of the material is not necessarily constant. Moreover, depending upon the depth of the charge, a part of the energy of the explosion is partitioned to the atmosphere and is not available to do work upon the material. The Livingston crater equations take into account the variables that affect the cratering process and may be classified as:

1) those involving a length or damage distance and containing coefficients depending upon the critical depth;

2) those involving volume measurements and containing coefficients dependent upon optimum weight.

The general equation is of the first type, and is:

$$d_c = \Delta^E \sqrt[3]{W} \tag{1}$$

where: d_c is the depth of the charge, ft
Δ is the depth ratio = d_c/N
E is the strain-energy factor
W is the weight of explosive, lb.

Any linear dimension of a crater, a gage distance, or the distance from the shot to a given type of damage may be described using the general equation and suitable coefficients. The coefficients used here, such as K_r to describe the radius of the true crater and K_h to describe the depth of the crater, are N-scaled distances. Instead of using the cube-root of the charge weight as a scaling factor, as is conventional, the critical depth $N = E\sqrt[3]{W}$ is used. In some materials, dependent upon the scale of the experiment and the range of charge weights, E is a variable rather than a constant.

The equation for crater volume is typical of the second type. It may be written in the form

$$V/W = E^3ABC. \tag{2}$$

Because of test geometry, and because charges of spherical shape were used (except for 2.5-lb charges of Atlas 60), the equation as applied to most of the blasts in ice reduces to

$$V/W = E^3AB. \tag{3}$$

For a charge of spherical shape and a given type and weight of explosive is used when blasting in a given material, E and B are constants and the equation reduces to

$$V/W = K'A. \tag{4}$$

The energy utilization number A of eq 4 is the ratio of the volume of the crater at charge depth d_c to the volume at optimum depth, where fracturing reaches its greatest stage of development. Since both the energy utilization number and the volume of material broken per pound of explosive can be measured with certainty, deviation from cube-root scaling may be observed by comparing values of V/W at various charge weights using a given explosive when blasting in a given material.

The interdependence of coefficients that relate to measurements of length and those that relate to measurements of volume is as follows:

$$\pi K_s (K_r)^2 K_h = \tfrac{1}{3}BC = K$$

where K = N-scaled crater volume = V/N^3
K_s is the crater shape factor
K_r is the N-scaled crater radius = r/N
K_h is the N-scaled crater depth = h/N.

Determining critical depth and optimum depth

As failure in blasting may be of the shock type, the shear type, or the viscous damping type, and as certain of the principles set forth here are thought to be applicable to solids, liquids, and gases, the critical depth should be thought of as the depth at which the displacement of the surface above the charge no longer exceeds a specified limit (Livingston, 1959b). Suitable standards of displacement may be chosen for a wide variety of materials such as rocks, soils, ice, snow, water, and air; and the strain-energy equation may be applied not only to brittle-acting or to plastic-acting solids, but also to other materials of the earth's crust. So as to establish a standard to which the factor that relates to deviation of the stressed volume from spherical shape can be referred, critical depth further is specified as being measured in a homogeneous medium using a given type of explosive and a charge of spherical shape.

Because of instrument limitations, it usually is necessary:

1) to measure displacement at some point other than vertically above the charge;
2) to relate displacement to particle velocity or acceleration;
3) to measure displacement using motion pictures;
4) to measure displacement using standard survey techniques which record permanent rather than maximum displacement;
5) to measure displacement using strain gages that measure relative rather than absolute strain;
6) to relate displacement of the surface above the charge to failure criteria such as:
   a) the beginning of the slabbing action due to reflection of the shock wave,
   b) the beginning of shearing-type failure at the explosion cavity,
   c) the beginning of doming of the surface sufficient to cause radial cracks to form in materials such as snow and ice.

As many as possible of the above methods should be used in the field. A sufficient number of shots should be made to pinpoint the critical depth at three or more charge weights, and blasts should be fired with charge depths slightly greater and less than the critical depth. Hence, it becomes unnecessary to extrapolate for critical depth within the interval between a charge that is too deep and another that is too shallow.

Critical depth may be determined by direct observation, supplemented, if desired, by motion-picture records. Some skill and experience is required, because brittle-acting substances and less brittle-acting substances show different effects. The unskilled observer may find it necessary to resort to the "maximum radius of rupture" method of determining critical depth. The skilled observer also may use this method to supplement his observations and to obtain evidence concerning the relative "elastic" or "plastic" behavior of the material.

The maximum radius of rupture method as applied to brittle-acting materials consists of computing the slant distance from the center of the explosive charge to the limit of extreme rupture at the ground surface. More plastic-acting materials are domed at the surface before fracturing begins, and the slant distance is measured to the limit of vertical uplift (see Fig. 23). The charge depth at which the slant distance is maximum is the critical depth for a charge of given weight.

Uplift and doming without loss of cohesion of the surface above a contained explosive charge does not occur in ideal brittle substances. Therefore, the slant distance from

the center of the charge to the limit of extreme rupture becomes a vertical distance. If the material does not behave as an ideal brittle substance, doming occurs, and the slant distance exceeds the charge depth. The extent of the difference indicates the ductility of the material, but is not a satisfactory measure of it because the behavior of the material is dependent on the type and the weight of the explosive.* Low-energy, low-velocity explosives tend to minimize doming. Small charges also minimize doming – both because of the scale of the experiment and because of the small volume of adjacent material that is deformed plastically. The behavior of the material depends upon the energy density† at the point of observation. Ductile behavior increases as the energy increases – or brittle behavior increases as the energy density decreas. At distances approaching the critical distance for a charge of given weight, more of the brittle than of the ductile effects becomes apparent to an observer.

Field experience shows that the maximum volume of material is broken per pound of explosive at that charge depth at which the surface is uplifted in nearly hemispherical shape, and the pressure that remains within the expanded gas bubble inside the uplifted material is insufficient to destroy the hemispherical shape before the uplifted material falls back. This charge depth is taken as the optimum depth. It is the depth at which the energy partitioned to the breakage process is maximum. Positive displacement measurements at the surface beyond the crater substantiate field observations and demonstrate that the scaled displacement of the material approaches a maximum at that charge depth where the volume of material broken per pound of explosive also is maximum. The expulsion of flyrock and of plumes from the vented gas bubble at high velocity is characteristic of charges detonated at depths less than the optimum depth.

The energy utilization number $\underline{A}$ (available) relates to loss or incomplete use of available energy for the breakage process, and is 1.0 at optimum weight where fracturing reaches its greatest stage of development. At charge depths less than optimum, energy is left in the escaping gas bubble, or is used in fragmenting and accelerating material previously isolated. As the total quantity of energy released by a charge of given weight remains constant, the quantity that is used in the breakage process is less at other charge depths in which a crater is formed than at optimum depth. Accordingly, $\underline{A}$ is less than 1.0 at charge depths other than optimum depth.

The optimum depth can be estimated by sight and hearing almost as accurately as it can be determined by excavating, measuring, and plotting the variation of crater volume with depth at constant charge weight. At a depth slightly less than optimum the gas bubble breaks through, the hemispherical shape of the uplifted material is destroyed, the noise of the explosion increases, the rate of acceleration of flyrock increases, the type of fragmentation changes, and ground motion begins in a downward direction or inward towards the vertically rising column of ejected material. A series of motion pictures of blasts at various depths recording the displacement of the surface above the charge or breakthrough of the gas bubble; or a series of measurements recording the noise level or the air-blast pressure at a given position will be useful in determining the depth at which a new phenomenon begins or in pinpointing the critical depth or the optimum depth.

Evaluation procedure

When blasts of various types of explosives and various weights of charge are fired, it may be incorrect to assume that the behavior of the material is independent of the

* For a more complete discussion, see Livingston 1959a.

† The term "energy density" is used with respect to the material as the disturbance propagates through it in the same manner that, in conventional terminology, is used to describe the energy of an explosive per unit of weight.

weight of the charge and of the type of explosive. Accordingly, a change in charge type or weight might be considered as being analogous to a change in material.

Test conditions for explosions were controlled as follows: charges of spherical shape were detonated at the center of the charge and were placed below a near horizontal surface of semi-infinite lateral extent. The diameter of the blast hole did not greatly exceed the diameter of the charge. The hole was backfilled with stemming material and the stemming compacted.

The above "prototype" conditions cause the stress distribution number C to equal 1.0. Under such conditions the parameters W, E, B, and C of the Livingston crater equations are constants for a given material, weight of charge and explosive. (W, E, and B can be measured accurately, and C is fixed by the test conditions.) The strain energy factor E can be determined from blasts at critical depth within limits of accuracy that depend upon the variation in the properties of the material.

The materials behavior index B is computed from

$$B = \frac{V_o}{N^3} .$$

Both V_o and N can be measured accurately.

The stress distribution number C provides a means of describing the effect upon the breakage process of:

a) physical and geologic properties of the material such as alteration, degree of cementation, stratification, bedding, jointing, sheeting, and faulting;

b) the shape of the explosive charge;

c) the geometry of the explosive charge with respect to the charge hole and the material;

d) the type of stemming and its physical properties after compaction;

e) the method and the geometry of the detonation process.

Test conditions may be established so that C = 1.0 — as was done for these tests.

The energy utilization number A is a variable. For a blast at any depth

$$A = \frac{V}{V_o} .$$

The volume of the true crater at any charge depth V and the volume at optimum depth V_o can be measured with the same accuracy as the charge weight or the charge depth.

Limitations placed upon the analyst by the crater equations and by measurements that can be made in the field with accuracy leave little choice when drawing curves to summarize the data. These limitations become apparent if the crater equations are analyzed. For example,

$$ABC = K_s \pi (K_r)^2 K_h = K.$$

Accordingly, if $K = V/N^3$ is determined, the product ABC also is determined; or if K_s, K_h, and K are determined, then K_r is determined. Also, since W, E, B, and C, for single shot blasts under prototype test conditions, are constants for a given weight of charge, explosive, and material:

a) the volume of the true crater is a constant (WE^3BC) times the energy utilization number A;

b) the volume of material broken per pound of explosive is a constant (E^3BC) times A;

c) the N-scaled crater volume K is a constant (BC) times A.

Furthermore, the volume of the crater as measured in the field must satisfy all three of the following equations:

$$V = K_s \pi r^2 h$$

$$V = WE^3ABC$$

$$V = KN^3.$$

The following procedure is suggested in evaluating the data:

1)* Determine whether the strain energy factor is a constant or a variable within the range of the experiments. If more than one type of explosive is used or if blasts are fired in dissimilar materials, determine the variation in $\underline{E}$ for the test conditions.

2) Determine whether or not the materials behavior index is a constant or a variable within the range of the experiments.

3) Plot V/W of the limits of complete rupture vs Δ, to observe transition limits between ranges of similar behavior.

4) Using the shape of the V/W vs Δ curves and the transition limits (which occur at maxima, minima, or points of inflection), construct preliminary curves to summarize the variation of $\underline{A}$ with Δ. (Note: A = 1.0 at optimum weight).

5) Plot $\underline{K_h}$ vs Δ using the field data and the transition limits. Average the data, using smooth curves.

6) Plot $\underline{K_s}$ vs Δ using the field data and the transition limits. Average the data, using smooth curves to obtain preliminary values of $\underline{K_s}$ at various values of Δ.

7) Calculate values of $\underline{K_r}$ for various values of Δ using the equation

$$K_r = \frac{\sqrt{ABC}}{\sqrt{K_s \pi K_h}}.$$

8) Compare values of $\underline{K_r}$ determined directly from field measurements of the crater radius with the calculated values to determine whether inconsistencies in $\underline{A}$ or $\underline{K_s}$ appear. If so, revise the preliminary values of $\underline{A}$ and $\underline{K_s}$.

9) Calculate V/W and $\underline{V}$ at various assumed values of $\underline{\Delta}$, making use of the fact that V/W is a constant (E^3BC) times A and that V is another constant (WE^3BC) times A.

10) Compare values of $\underline{V}$ at any given value of Δ obtained from

$$V = K_s \pi r^2 h$$

$$V = WE^3ABC$$

$$V = KN^3.$$

Critical depth and the strain energy factor

The method of pinpointing was used in the field to determine the critical depth. This method minimizes the number of shots to be fired and increases the accuracy with which the determination is made. The critical depth first was determined by "cut and try," using 2.5-lb charges of Atlas 60 Percent Straight Gelatin at various depths below the surface to observe the minimum depth at which the charge was completely contained. It was determined, for example (see Fig. 1.7), that critical depth was somewhere between 7.6 ft (shot H) and 8.6 ft (shot 75). An approximate value of $\underline{E}$ was calculated, assuming N to be 8.0 ft, from

$$N = E\sqrt[3]{W}$$

and tested using a 5-lb charge (shot 70). The process of computation and extrapolation was repeated for other charge weights and types of explosive. Field observation later

* Note: Steps 1 and 2 should be investigated during the field work rather than after the analysis begins.

Table VI. Explosions in glacier ice. Constants for charge of spherical shape

Charge wt, W (lb)	Materials behavior index, B	Strain energy factor, E	E^3	BC	E^3BC	WE^3BC	Δ_o
Atlas 60							
2.5	0.56*	5.96	211.71	0.40†	84.68†	211.7†	0.67
5	0.55	5.96	211.71	0.55	116.44	582.2	0.68
10	0.54	5.86	201.23	0.54	108.66	1086.6	0.67
20	0.50	5.65	180.36	0.50	90.18	1803.6	0.65
40	0.38	5.41	158.34	0.38	60.17	2405.8	0.63
C-4							
2.5	1.29	4.19	73.56	1.29	94.89	237.2	0.74
5	0.89	4.56	94.82	0.89	84.39	422.0	0.71
10	0.67	4.79	109.90	0.67	73.63	736.3	0.70
20	0.51	4.91	118.37	0.51	60.37	1207.4	0.68
40	0.32	5.00	125.00	0.32	40.00	1600.0	0.64
Coalite 7S							
2.5	0.83	4.41	85.77	0.83	71.19	178.0	0.70
5	0.82	4.50	91.12	0.82	74.72	373.6	0.69
10	0.80	4.51	91.73	0.80	73.78	733.8	0.66
20	0.78	4.50	91.12	0.78	71.07	1421.4	0.63
40							
Coalite 5S							
2.5	1.14	3.98	63.05	1.14	71.88	179.7	0.70
5	0.91	4.21	74.62	0.91	67.90	339.5	0.68
10	0.81	4.28	78.40	0.81	63.50	635.0	0.67
20	0.71	4.28	78.40	0.71	55.66	1113.2	0.66
40							

* Estimated
† Valid only at Δ_o

was supplemented by studying motion pictures of the blasts. The curved lines marked "critical" on the correlation diagrams (Fig. 10) are the result of this study. Because the lines are not straight on log-log paper and do not follow a one-third slope, it follows that the behavior of the material is not constant and therefore that geometric similarity cannot be achieved when employing conventional methods of cube-root scaling. The curves for all four types of explosives are concave downward. Depending upon the type of explosive and the range of the experiment, the slope may be either greater or less than one-third.

Values of the strain-energy factor E are summarized in Table VI. The range of values is from 3.98 to 5.96 and is greater for the smaller than for the larger charges. The maximum value of E for each type of explosive within the range of the experiments is as follows:

5.96 Atlas 60
5.00 C-4
4.51 Coalite 7S
4.28 Coalite 5S.

The maximum value of E occurs where the slope of the tangent to the log-log curves is one-third (Fig. 10).

Optimum depth and the materials behavior index

Essentially the same procedure was used in the field to determine optimum depth as to determine critical depth. The criterion for optimum depth determined by sight and sound is that the blast must cause the material to be uplifted in igloo-shape without noise and without plumes being shot out. Motion pictures of blasts at near optimum depth were reviewed, and graphs were constructed summarizing the variation of V/W with Δ. The curved lines of Figure 10 marked "optimum" are the result. The curves for all four types of explosive are concave downward. Their slope at any given position within the range of the experiments may be either greater than or less than one-third. The flatter slopes occur at the larger charge weights. In general, the slope is less than one-third for blasts in glacier ice if the weight of the charge is greater than 10 lb.

The depth ratios at optimum depth Δ_o are summarized in Table VI.

From the correlation diagrams and Table VI, one may conclude that the performance of an explosive depends upon the charge weight. For example, the strain energy factor for C-4 steadily increases with charge weight whereas the strain energy factor for Atlas 60 steadily decreases for charges heavier than 5 lb. At some weight in excess of 40 lb, the performance of the two explosives may be similar. The performance of Atlas 60 at 2.5 lb is vastly superior to that of C-4 relative to that particular energy level at which the material begins to lose its cohesion. The data show that as the charge weight changes, the behavior of the material also changes. We thus are provided with experimental verification of the concept stated in the theory of relative behavior of materials (Livingston, 1959a, Ch. II), that a change in energy density within a given material is analogous to a change in the type of material at constant energy density.

The materials behavior index $\underline{B}$ is a ratio of lengths to the third power. Both the length that is determined by $\underline{V}_o$ and the length that is determined by $\underline{N}$ are dependent upon the breakage process. These lengths describe the geometry of the breakage process at two different stages — the stage where fracturing begins and the stage where the fractures* extend so as completely to isolate the material within the limits of complete rupture from its surroundings. The energy level within the material at the beginning of the breakage process is that at which the depth ratio is 1.0. At the end of the process, the energy level is that at which the depth ratio is Δ_o. Until additional basic research has been accomplished, it is necessary to describe the materials behavior index in relative rather than absolute units.

The variation in $\underline{B}$ with charge weight and explosive type is shown in Table VI. Although $\underline{B}$ is a constant for a given material, weight of charge, and type of explosive, it varies both with the weight of the charge and with the type of explosive. The view held here, in accordance with the theory of relative behavior of materials, is that a decrease in $\underline{B}$ with increase in charge weight represents a decrease in the elastic behavior, or an increase in the ductile behavior of the material.

It may be unwise to assume that the constants of Table VI apply without modifications to lake ice and to sea ice. It also appears unwise to assume that the constants apply to all types of glacier ice, or for that matter to ice of the Thule ramp at all temperatures.

TRUE CRATER EVALUATION

Variation of V/W of the true crater with Δ

It was impractical, because of conditions at the test site, to differentiate between the limit of the true crater and the limit of complete rupture. When determining the crater limit, all material loosened by the blast was excavated. The crater walls as

* The fracture process in ice is determined by a shear rather than a shock failure (Livingston, 1959b).

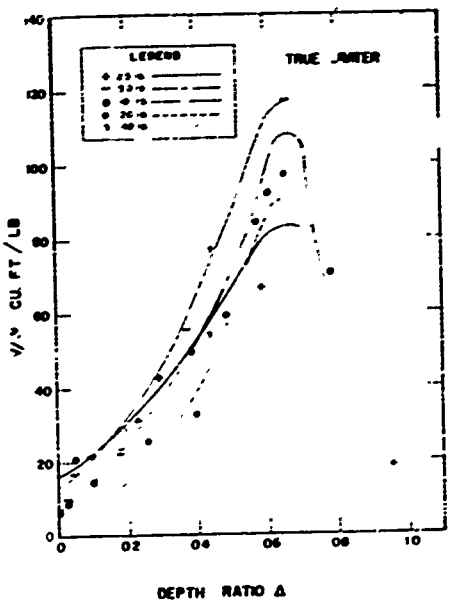

Figure 40. V/W vs Δ, A-60.

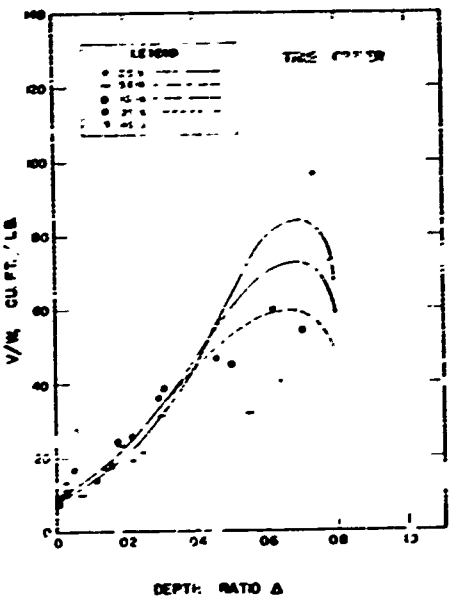

Figure 41. V/W vs Δ, C-4.

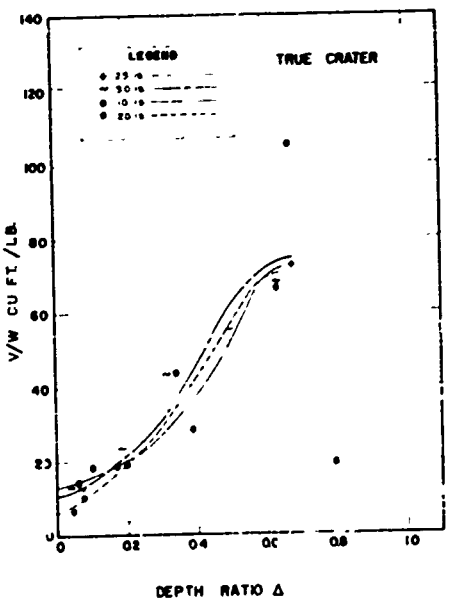

Figure 42. V/W vs Δ, C7S.

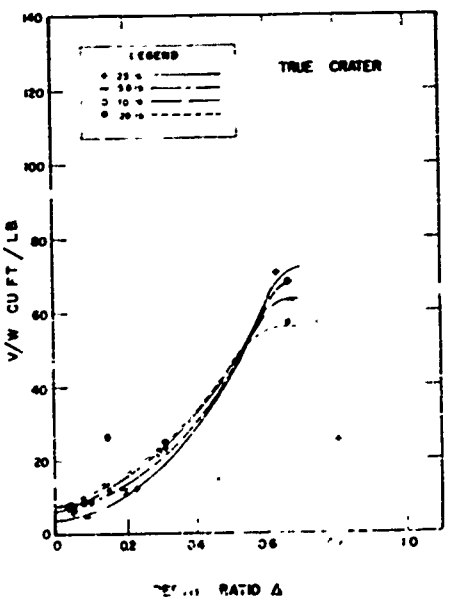

Figure 43. V/W vs Δ, C5S.

excavated probably represent the limit of complete rupture as defined for blasts in soils (USA WES, 1958) and in snow (Livingston, 1960). When blasting in rocks and in frozen ground, it is impractical also to determine the limit as defined for soils. It should be recognized, therefore, that the "true crater" as determined for brittle substances and as also determined here for ice may not be identical with the limit as defined for soils, for snow,* and for other materials where the colored column technique is practical.

Figures 40-43 summarize the variation in V/W with the depth ratio Δ. It is evident that

1) the behavior of the material is not independent of the type of explosive, and

2) that the behavior of the material is not independent of the weight of the charge or of the scale of the experiment.

Physical properties of the upper 2 ft of ice differ from those of the colder ice below, and the effect of the warmer surface layer is greater for small than for large charges. The 2.5-lb charges of Atlas 60 were of cylindrical shape of height equal to diameter, but all other charges were of spherical shape. Because of the test conditions, the 2.5-lb charges of each of the test explosives should be evaluated separately as if in a different material. The effect of charge shape must be considered for the 2.5-lb charges of Atlas 60.

Eq 3 expresses the volume of material broken per pound of explosive, for charges of spherical shape, as a function of the strain energy factor E, the energy utilization number A, and the materials behavior index B.

$$V/W = E^3AB. \qquad (3)$$

As E and B are constants for a given explosive and weight of charge, the variation in V/W with Δ depends upon the energy utilization number A, which is a relative measure of the energy partitioned to the fracture process. From eq 3 and Figures 40-43 it follows that the partitioning of energy to the fracture process varies with the depth ratio. At some value of Δ (Δ_o by definition), the quantity of energy partitioned to the breakage process is maximum.

Applying a similar argument to the phenomenon of flyrock travel, it follows that the maximum flyrock travel height must occur at that value of Δ where the proportion of the energy of the explosion available to impart motion to the material is maximum. From the law of conservation of energy, the energy partitioned to plastic deformation and to fracturing the material is less at the depth ratio where T_v/N is maximum than that at higher values of Δ. This is in accordance with the relations of Figures 24-27 and 40-43.

Regardless of the detailed manner in which energy is partitioned to the material or to the atmosphere and regardless of the sequence of events, it appears from comparison of the flyrock travel and the V/W relations for the true crater that:

1) energy utilized in deforming the material without loss of cohesion is not available to the fracture process,

2) energy utilized in deforming without loss of cohesion and in fracturing the material is not available to accelerate the isolated fragments,

3) the variation both of V/W with Δ and of T_v/N with Δ are dependent upon the weight and type of explosive, upon the material, and upon the shape of the charge.

* See Explosions in snow for further discussion.

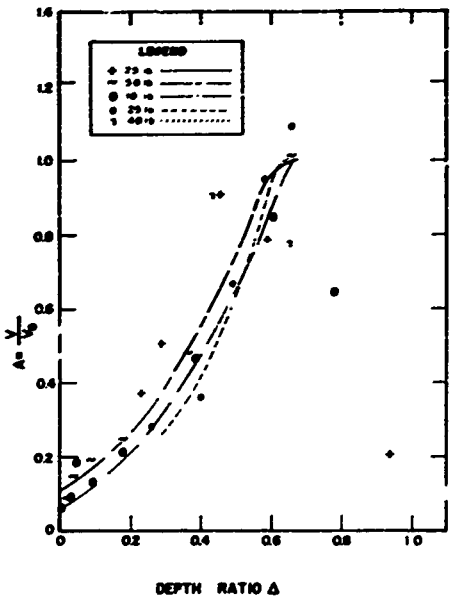

Figure 44. A-60 energy utilization number.

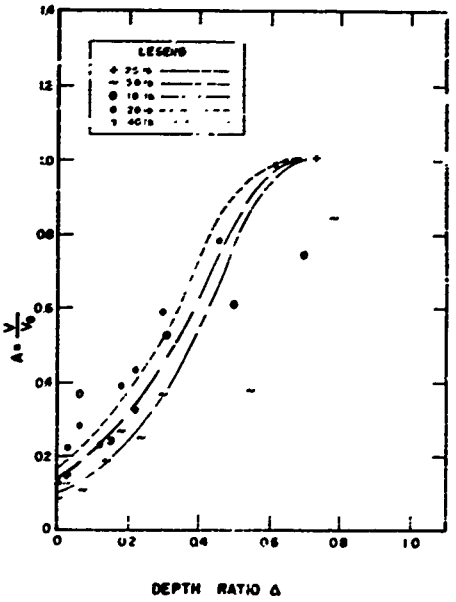

Figure 45. C-4 energy utilization number.

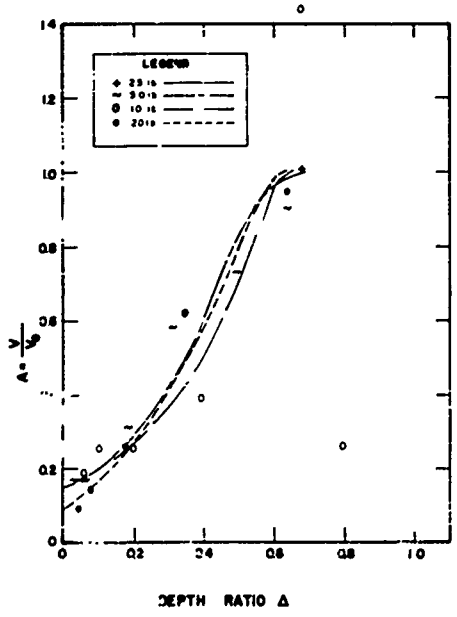

Figure 46. 7S energy utilization number.

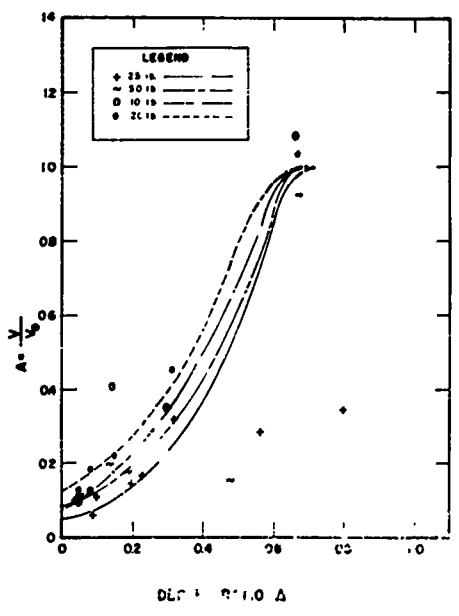

Figure 47. 5S energy utilization number.

Energy utilization number, A

Variation of the energy utilization number A with depth ratio is summarized in Figures 44-47. The curves were obtained by dividing the V/W vs Δ curves by the constant $E^{3}BC$ (Table VI) for type and weight of explosive. The curves have not been extended beyond Δ_o because the region was not explored fully. Points were calculated for each blast from

$$A = \frac{V}{V_o}$$

where V is the volume of the true crater and V_o is the volume at optimum depth. The position of the points with respect to the corresponding curve indicates the dispersion of the data.

The curves are concave upwards at low values of Δ and concave downwards at higher values. The depth ratio at the point of inflection depends both upon the type of explosive and the weight of charge. The relations imply that the behavior of the material is independent neither of the type of explosive nor of the weight of the charge. They also imply that partitioning of energy to the breakage process changes from an increasing function to a decreasing function at some particular charge depth. As a first approximation, it appears that the transition occurs at the limit between the airblast range (Livingston, 1959a) and the fragmentation range where V/W of the apparent crater is maximum (Figs. 28-31) and the height of flyrock travel (Figs. 24-27) also is maximum.

Depth of the true crater, K_h

The depth of the true crater is the sum of the depth to the center of gravity of the charge, d_c, and the vertical radius, r_v, of the explosion cavity (Fig. 23).

Figures 48-51 show the variation of the N-scaled depth of the true crater K_h and the N-scaled gas bubble radius K_v with the depth ratio. For example, except for charges of cylindrical shape (2.5 lb Atlas 60), K_{cv} is larger for a contact burst than for a charge at optimum depth. It appears that K_h and K_{cv} depend not only upon the critical depth, but also upon the explosion pressure.

For charges of spherical shape K_{cv} varies with the weight of the charge. The variation is less for a charge at optimum depth than for a contact burst. Part of the observed variation may be due to physical properties of the 2-ft surface layer of 32F ice. As the curves (Fig. 48) for spherical charges of 5, 10, 20, and 40 lb of Atlas 60 appear identical, the observed difference between the curve for the 2.5-lb charge (cylindrical shape) and the curve for the other charges appears to be due to the effect of charge shape.

Crater shape factor, K_s

The shape of the true crater may be inferred from the crater shape factor K_s where

$$K_s = \frac{V}{\pi r^2 h} .$$

If K_s is less than 1/3, the crater is trumpet-shaped. If K_s = 1/3, the crater is cone-shaped. If K_s = 2/3, the crater is hemispherical. If K_s is greater than 2/3, the crater is bowl- or dish-shaped. The shape varies with the depth ratio and appears to be indicative of the mechanics of failure and of the scouring action of the gas bubble.

Figures 52-55 summarize the variation of K_s with Δ. Because of the dispersion, the curves were computed using a "cut and try" method and the equation

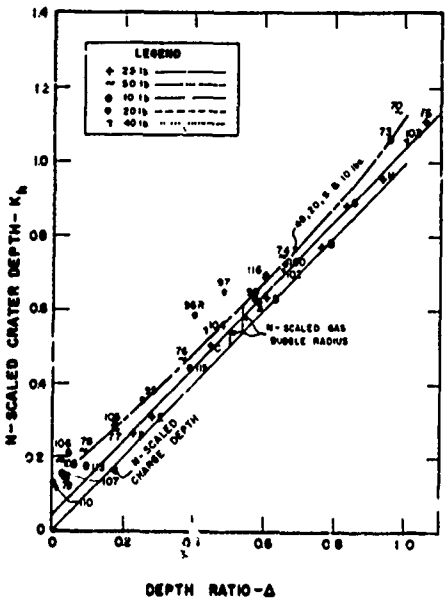

Figure 48. N-scaled true crater depth, A-60.

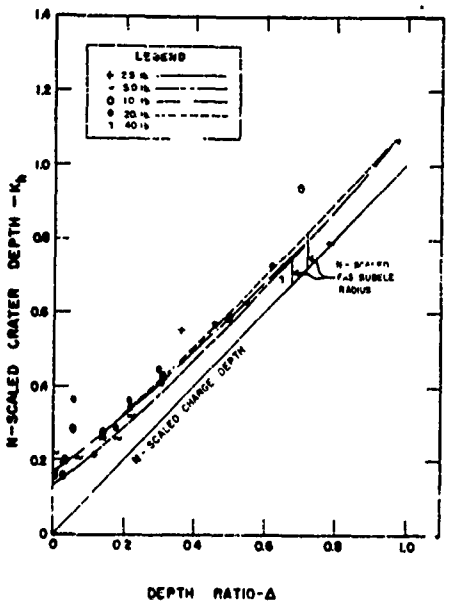

Figure 49. N-scaled true crater depth, C-4.

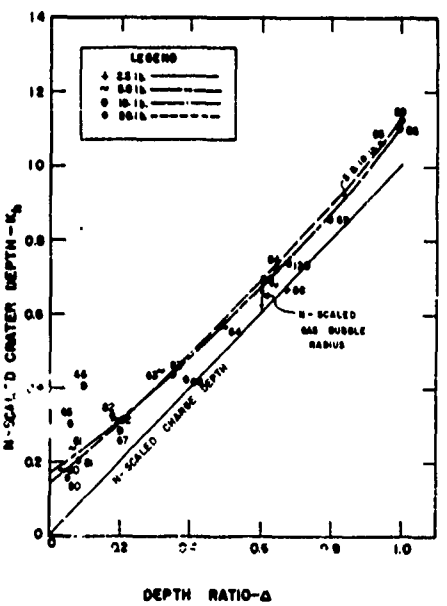

Figure 50. N-scaled true crater depth, C7S.

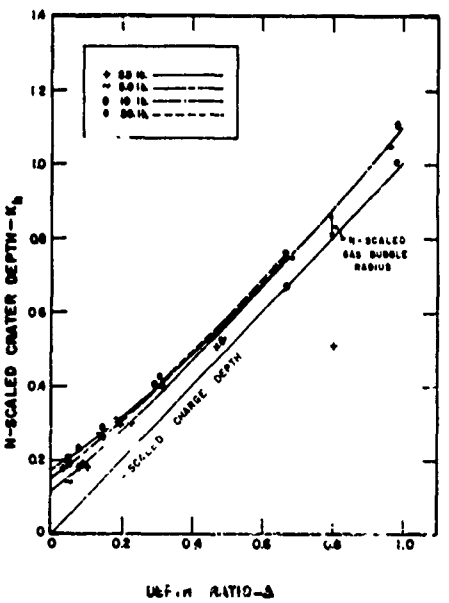

Figure 51. N-scaled true crater depth, C5S.

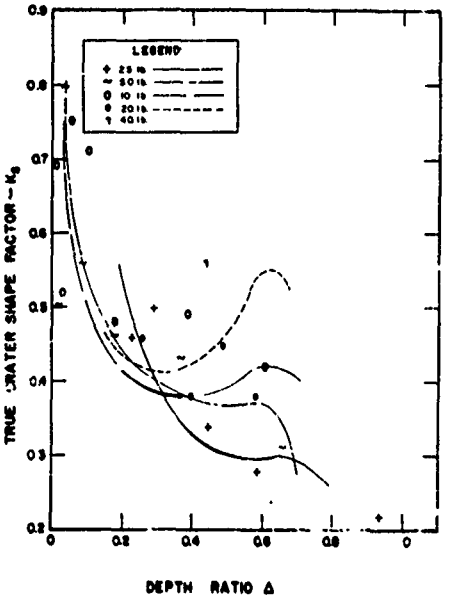

Figure 52. A-60 crater shape factor.

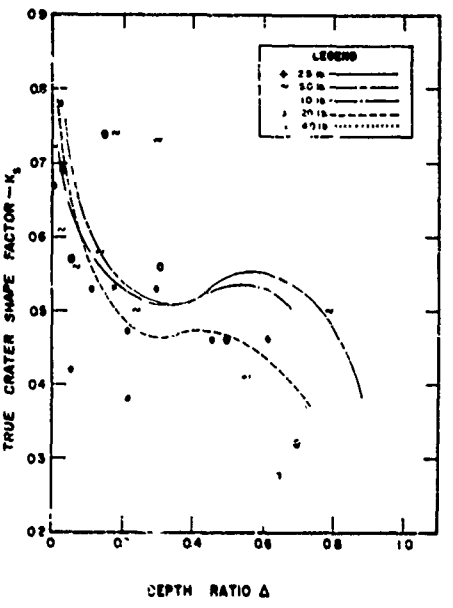

Figure 53. C-4 crater shape factor.

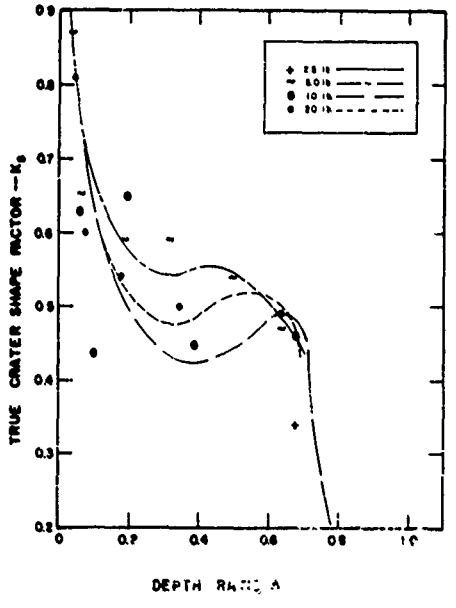

Figure 54. 7S crater shape factor.

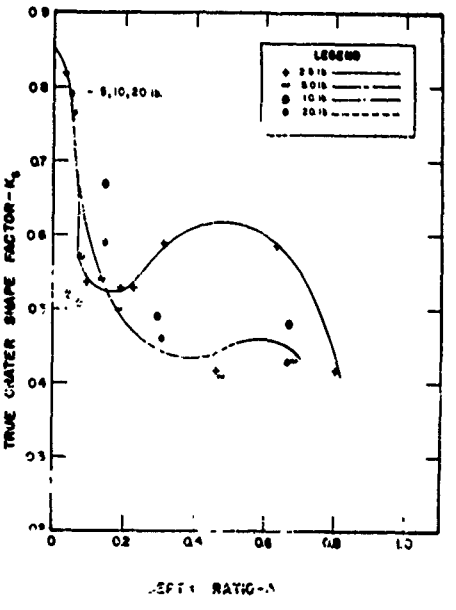

Figure 55. 5S crater shape factor.

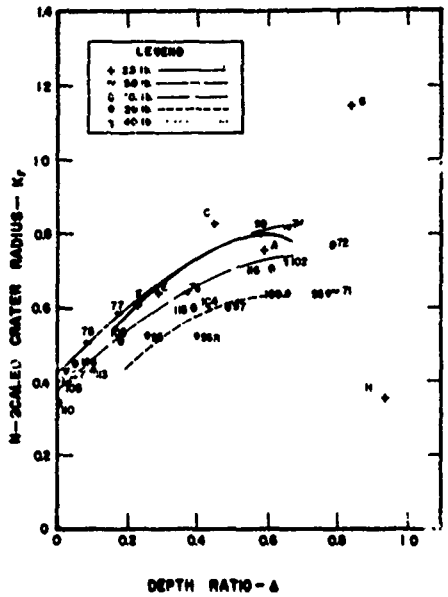

Figure 56. N-scaled true crater radius, A-60.

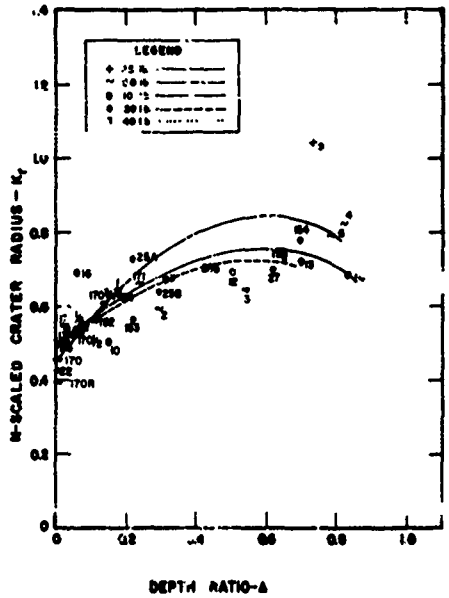

Figure 57. N-scaled true crater radius, C-4.

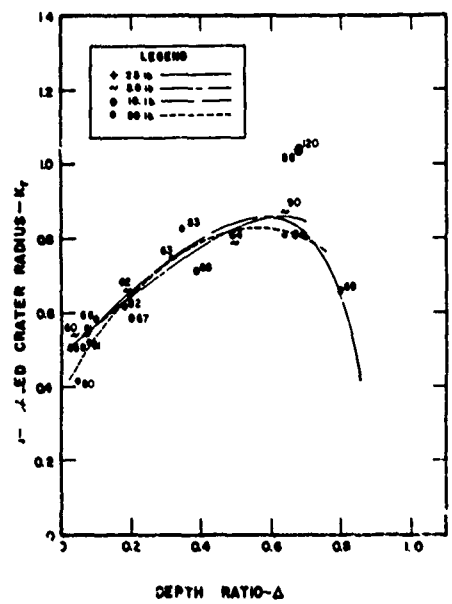

Figure 58. N-scaled true crater radius, C7S.

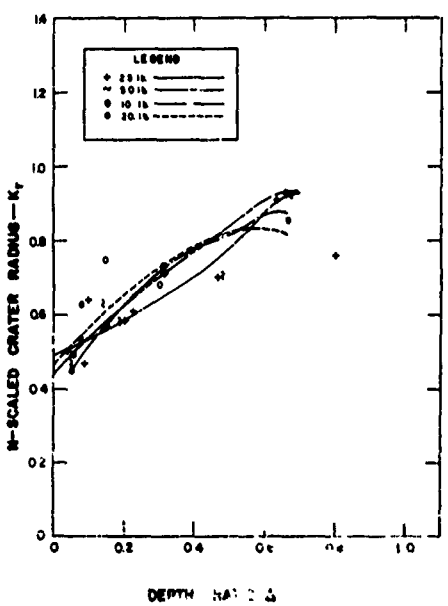

Figure 59. N-scaled true crater radius, C5S.

$$K_s = \frac{ABC}{\pi (K_r)^2 K_h} .$$

Values of K_r and of K_s were adjusted to obtain the best agreement between the computed curves and the experimental data. This resulted in a family of K_s curves for each type of explosive, except for Coalite 5S, where a single curve fits the test data.

The curves show that a contact burst produces a bowl- or dish-shaped true crater which changes gradually to hemispherical shape as the depth of the charge is increased within the airblast range. A local maximum and a local minimum occur within the fragmentation range. The local minimum occurs near the transition from the airblast range to the fragmentation range, and the local maximum occurs near the transition from the fragmentation range to the shear range. The variation in the shape of the true crater within the fragmentation range is considerably less than in the other ranges. Such is consistent with the premises that a scouring action predominates in the airblast range, particle size is reduced in the fragmentation range, and the material is isolated from its surroundings in the shear range.

True crater radius, K_r

Figures 56-59 summarize the variation in the N-scaled true crater radius K_r with Δ. The curves were computed from

$$K_r = \sqrt{\frac{ABC}{\pi K_s K_h}}$$

using values of B from Table VI and the curves for A, K_s, and K_h.

AIR AND UNDER-ICE SHOCK

Twenty-four instrumented shots were fired during the test program. A comprehensive analysis at this time is beyond the scope of this report, and additional data are needed. The following preliminary comments are intended only to aid future work. Figures 10 and 11 show the charge weight-charge depth relations. Test conditions and results are summarized in Figures A1-23.

Under-ice pressure records

The shape of the pressure pulse, although different than in water or in air, is thought to be representative of materials that deviate from ideal elastic behavior. On certain shots, higher pressures were recorded at gages beyond the crater than within it. It is doubtful that this effect could be observed in an ideal brittle substance or in fluids. Rather than being anomalous, it may represent both the shape of the disturbance that proceeds outwardly from the explosion cavity in materials that fail in shear, and a fundamental difference between shock and shear failure in blasting. Shearing failure predominates over shock failure in ice, and the rise to maximum pressure at scaled distances K greater than 1.5λ is gradual rather than abrupt. Failure, rather than being caused by the reflection of the shock wave, is due to outward displacement from the explosion cavity. Depending upon the depth ratio of the shot and upon the gage position with respect to limits of the potential crater, the gage possibly may be set in motion before the maximum pressure at that distance is reached.

Figure 60 illustrates the variation in the shape of the pressure pulse with distance and the effect of depth ratio and of the place of observation upon the shape. The lower maximum pressure of record (e) compared to record (b) (518 vs 783 psi) at the same scaled distance (3.3λ) may indicate that the direction of displacement is different for the deeper charge, and that the time at which movement begins also is different.

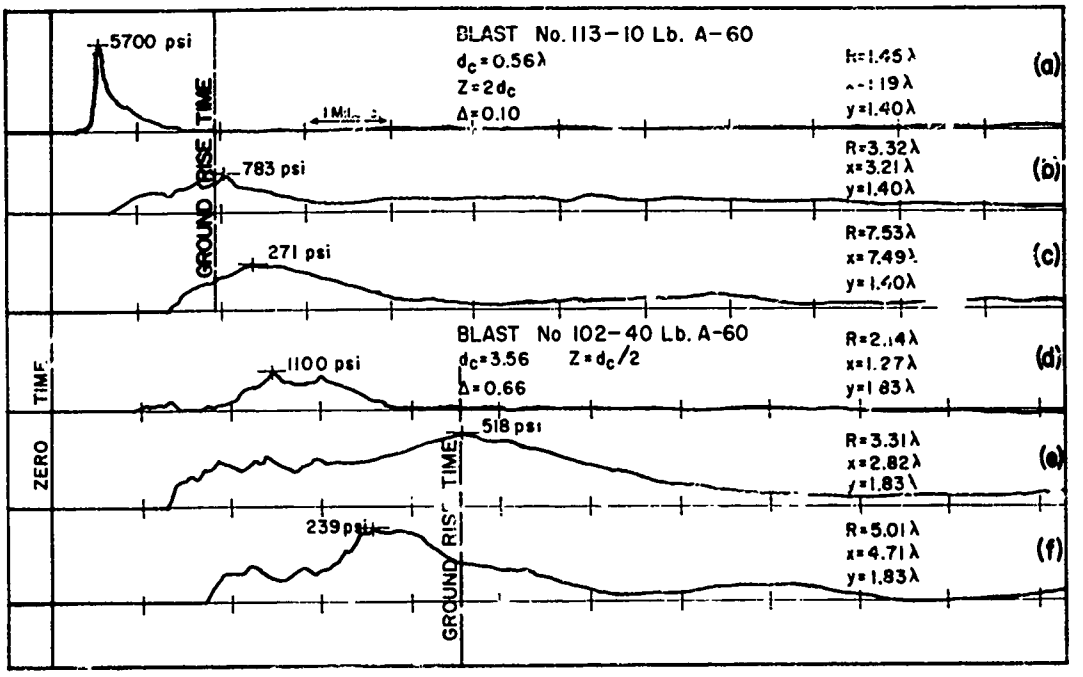

Figure 60. Under-ice pressure records - typical variation with distance. For gage layout see Fig. A121, 125.

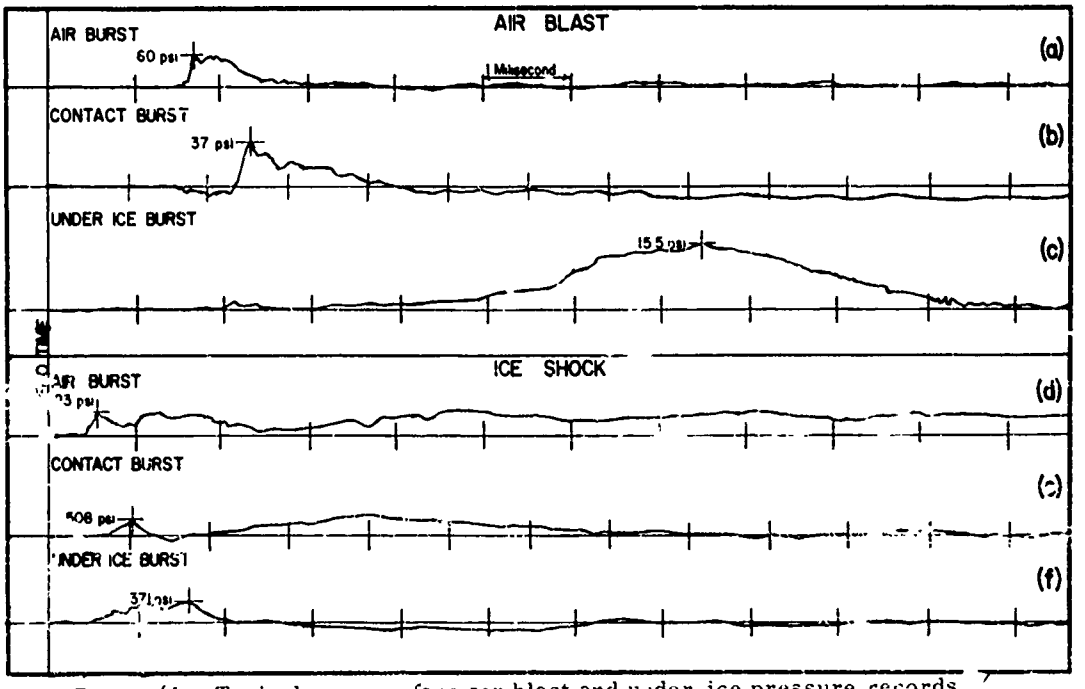

Figure 61. Typical near surface, air blast and under-ice pressure records. Gage geometry is shown in Fig. A119, A133, A137.

When studying crater limits using a trenching machine, it was observed that incipient planes of shear continue beyond the crater walls if the depth of the charge favors shearing rather than the type of deformation illustrated in Figure 14.

At scaled distances of 1.5λ or less (record 79a), the shape of the pressure pulse is similar to that in air or in water, but as the distance increases, the shape changes so that the pressure at the shock front is small compared to that some distance behind it.

Near-surface airblast and under-ice pressure

The presence of a nearby ice surface affects the magnitude and shape of both airblast and under-ice shock records. Consistent with the 2W correction, the airblast pressure for an ice-surface contact burst is higher at a given scaled distance than for an airburst. A comparatively shallow depth of cover substantially reduces the airblast pressure. Similarly, if the shot is fired at a comparatively small distance above the surface of the ice, the under-ice shock is substantially reduced. A change in the magnitude of the pressure peak due to the presence of the nearby interface is accompanied by certain characteristic changes in the form of the pressure record. As was observed also for deeper under-ice shots, the pressure record is affected both by the depth ratio of the shot and by the place of observation.

Figure 61 illustrates the effect of the charge position and place of observation upon the shape and magnitude of the pressure pulse in air and under ice. The records were chosen so that the effect of distance upon the form and magnitude of the pressure pulse is minimized.

Records (a), (b), and (c) illustrate the variation in the shape of the pressure pulse in air in the range $3.59\lambda < R < 4.25\lambda$ as the charge position successively changes from airburst to contact burst to shallow underground burst. At the reference gage position for a contact burst (position 9, Fig. A3), record (b) shows that a negative phase precedes the positive phase. The form of the pressure pulse in air from a shallow under-ice burst (record c) as recorded at the reference gage position (position 2, Fig. A12) differs from that for a contact or airburst (record a). The low intensity shock first arriving at the airblast gage is followed by a gradual pressure rise as the vented bubble rises and engulfs the gage.

Records (d), (e), and (f) illustrate the variation in the form of the under-ice pressure pulse at the range of composite air plus ice slant distance $2.17\lambda < R < 2.43\lambda$. The scaled distance through which the disturbance travels in air decreases and the distance in ice increases as the charge position is lowered. The depth of the gage below the ice surface remains constant at 1.40λ. The contact burst (record e) shows an initial pulse due to the direct shock followed by a gradual rise of pressure within the ice. The gradual rise may be a result of air-induced under-ice shock as the expanding gas bubble sweeps across the ice surface. The under-ice pressure pulse due to the shallow burst (Fig. 61) illustrates the gradual rise to maximum pressure that is characteristic of deeper shots in bubbly ice. The maximum pressure is lower for the under-ice burst than for the contact burst. The lower pressure (371 psi vs 508 psi) at nearly the same scaled slant distance again suggests that, depending upon the depth ratio and the gage position, a gage may be set into motion before the maximum pressure at that distance is reached.

Direct under-ice shock

Figure 62 summarizes the relation between maximum under-ice pressure and scaled slant distance to the gage using spherical charges of Atlas 60 Percent Straight Gelatin. The observed relations are summarized empirically and are offered as preliminary data subject to modification when an analysis is undertaken.

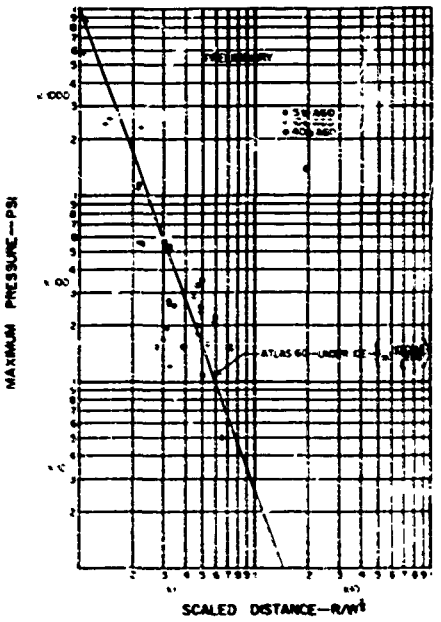

Figure 62. Under-ice shock pressure, A-60.

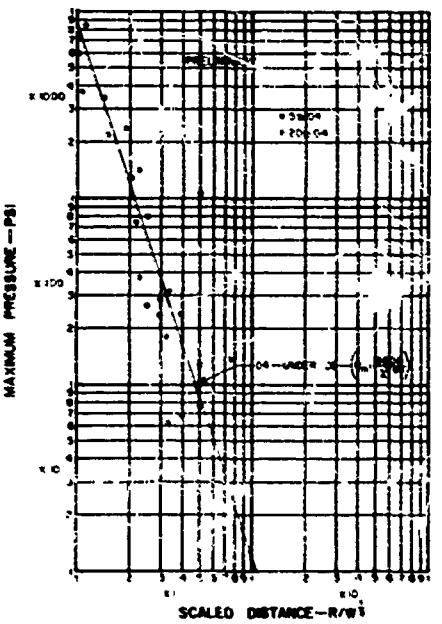

Figure 63. Under-ice shock pressure, C-4.

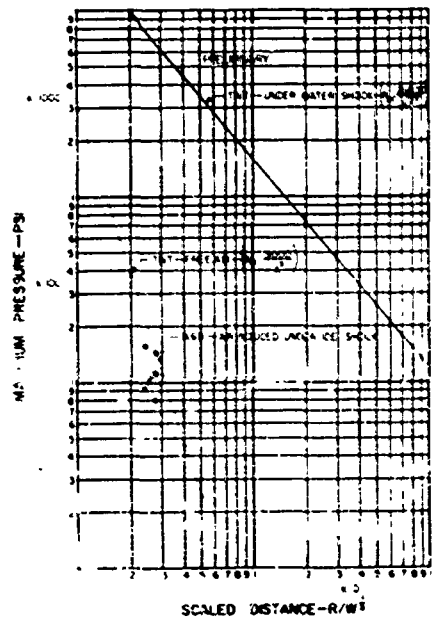

Figure 64. Air-induced under-ice shock, A-60.

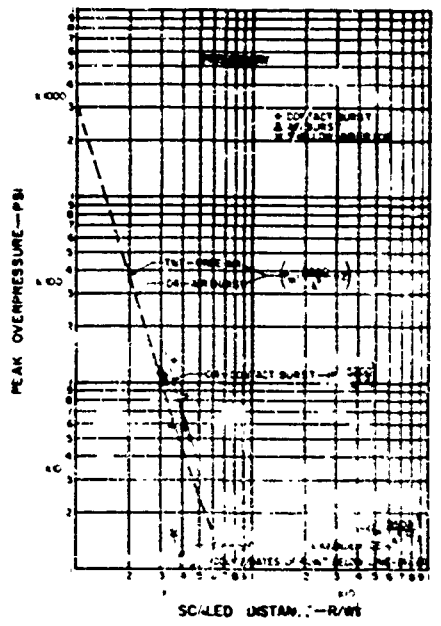

Figure 65. Air blast pressure, C-4.

A first approximation of the relation between maximum under-ice pressure and scaled slant distance, independent of charge depth and gage geometry, is given for under-ice blasts of Atlas 60 by the equation

$$P_m = \frac{10,000}{\lambda_s^{2.56}} \qquad \text{(Atlas 60 prelim.)}$$

where P_m is the maximum pressure and λ is the scaled slant distance to the gage $\lambda_s = R/\lambda$.

Figure 63 summarizes the relation between maximum under-ice pressure and scaled slant distance for blasts of C-4. The equation

$$P_m = \frac{8,600}{\lambda_s^{2.84}} \qquad \text{(C-4 prelim.)}$$

is a first approximation and does not take the depth ratio or the gage position into account.

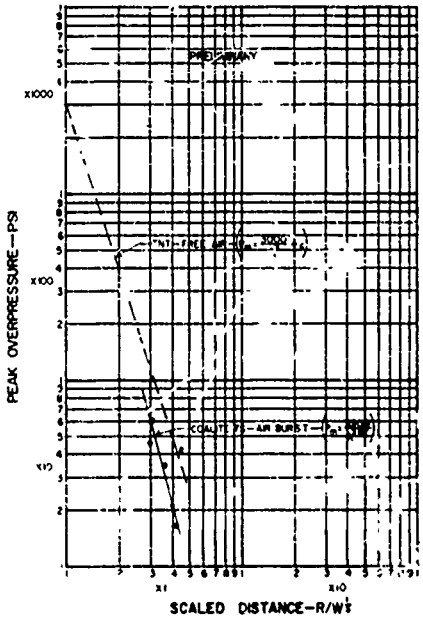

Figure 66. Air blast pressure, C7S.

Air-induced under-ice shock

Figure 64 compares the observed air-induced under-ice shock from two 10 lb charges of Atlas 60 (blasts 154c, 154f) with the shock pressure produced by explosions of TNT in water (Cole, 1948) and free air. The gage geometry and the scaled slant distance to which the under-ice shock pressure is referred are illustrated in appendix drawings A1 and A2. The charges were of spherical shape and were suspended in air at a distance of 1λ above the ice surface.

Near-surface air blast pressure

Within limitations of the available data, Figure 65 compares the observed peak overpressure from 10-lb blasts of C-4 detonated at 1λ above the ice surface, in contact with the ice surface, and at 0.56λ below the ice surface with the peak overpressure from blasts of TNT in free air. The overpressure using C-4 appears to be comparable to that using TNT. The overpressure from a contact burst is greater than that in free air, and the overpressure in air from a shallow under-ice burst is considerably less than that from a free air blast.

Figure 66 indicates as a first approximation that Coalite 7S produces a lower overpressure than TNT in free air.

SEISMIC MEASUREMENTS

A detailed analysis of the seismic measurements is beyond the scope of this report. The following comments are of a preliminary nature and are intended only to aid future work. Figure 10 shows the charge weight-explosive type-charge depth relations for blasts where seismic measurements were taken; and data sheets 5 record the distance to the geophones, the charge-to-gage travel velocity, and the frequency of each of the three components of vibration.

Effect of charge depth at constant weight

Figures 67-69 are typical seismic records illustrating the effect of varying the depth of the charge at constant weight.

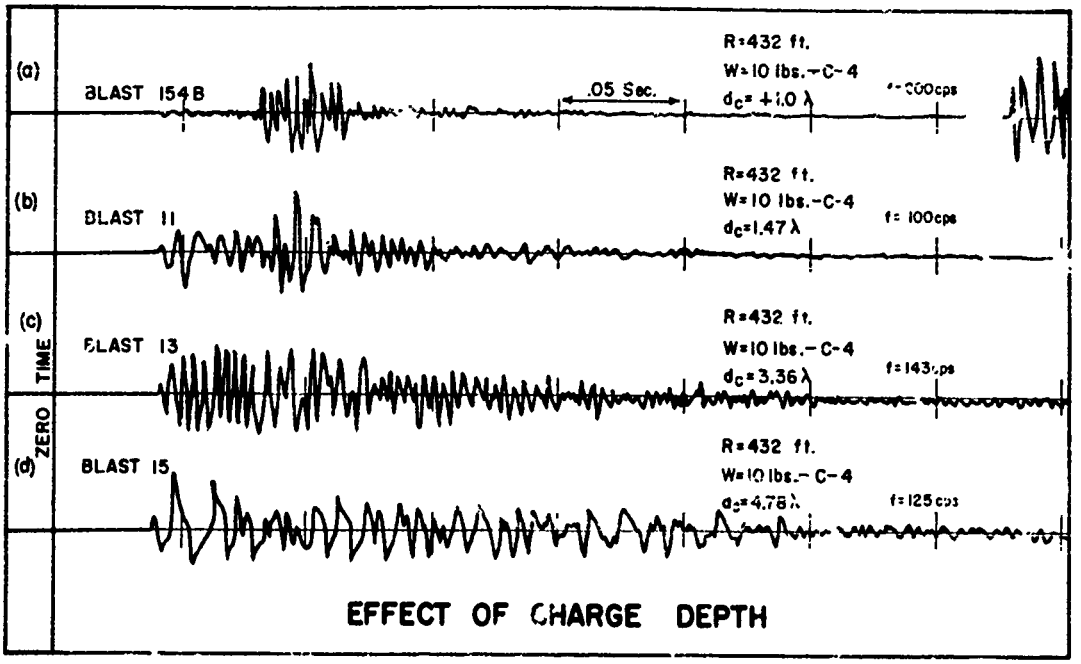

Figure 67. Typical seismic records, longitudinal component.

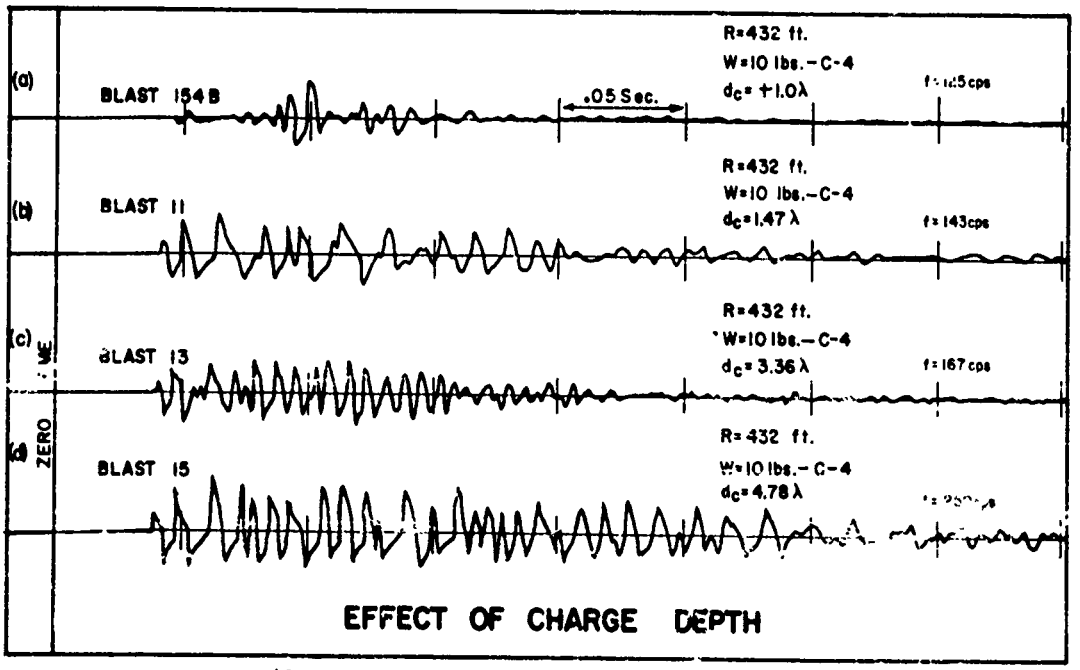

Figure 68. Typical seismic records, vertical component.

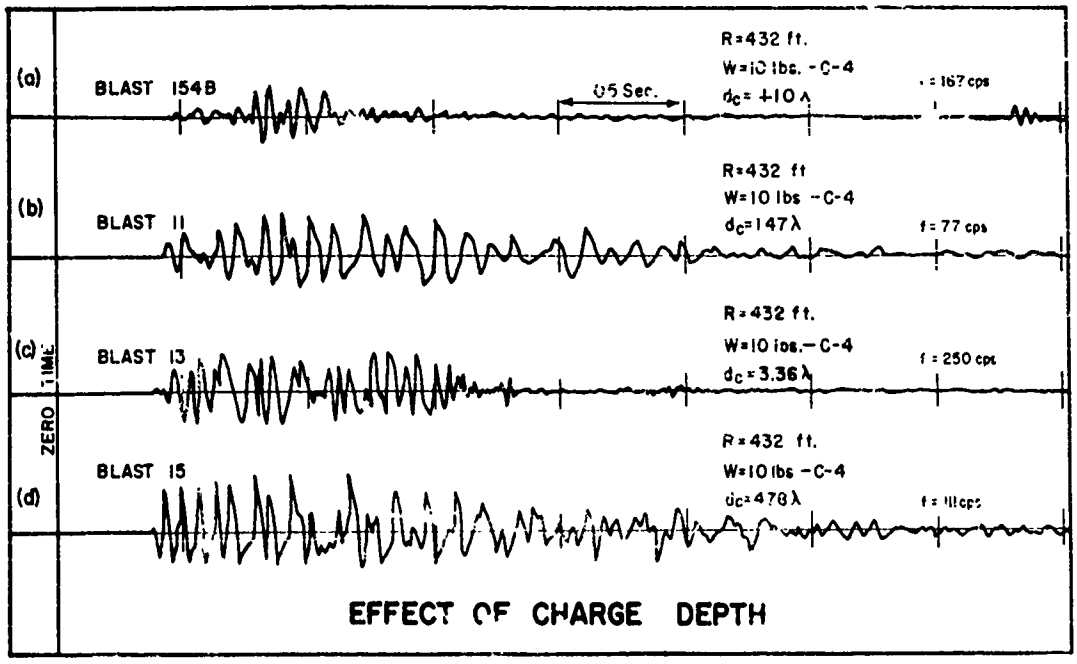

Figure 69. Typical seismic records, transverse component.

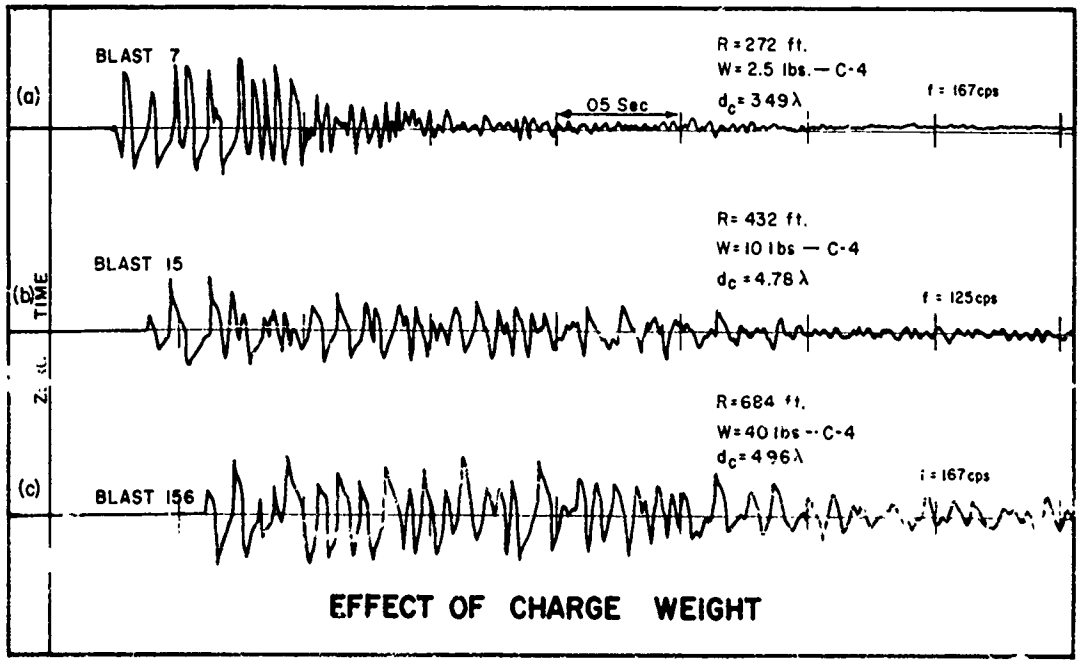

Figure 70. Typical seismic records, longitudinal component.

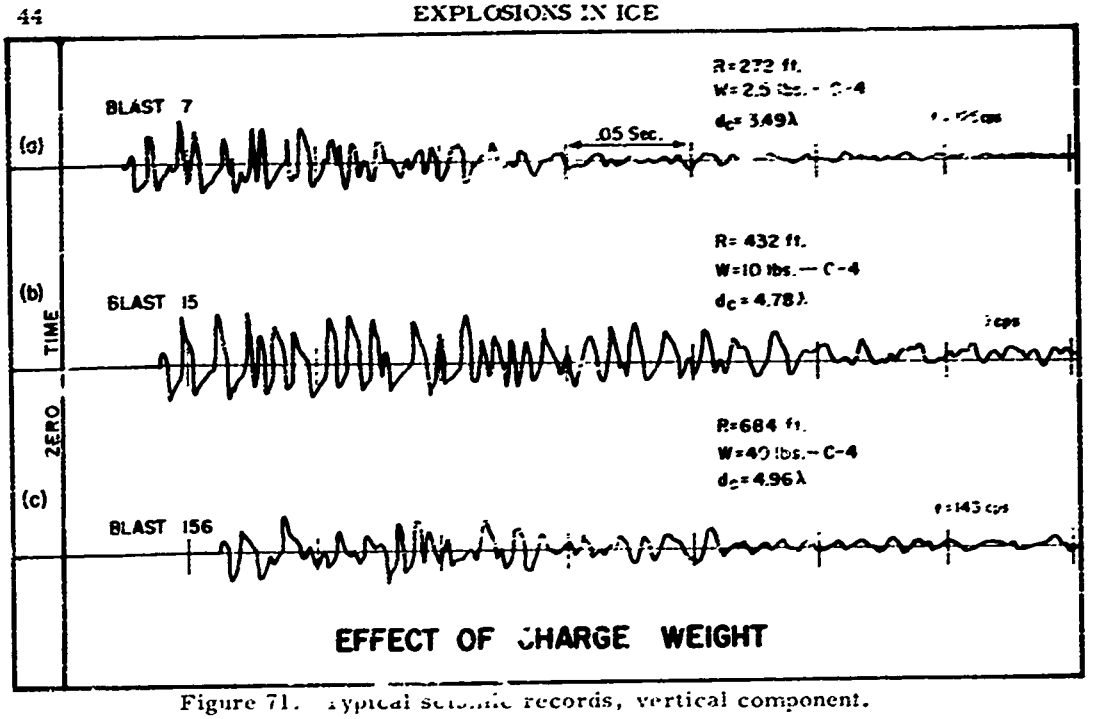

Figure 71. Typical seismic records, vertical component.

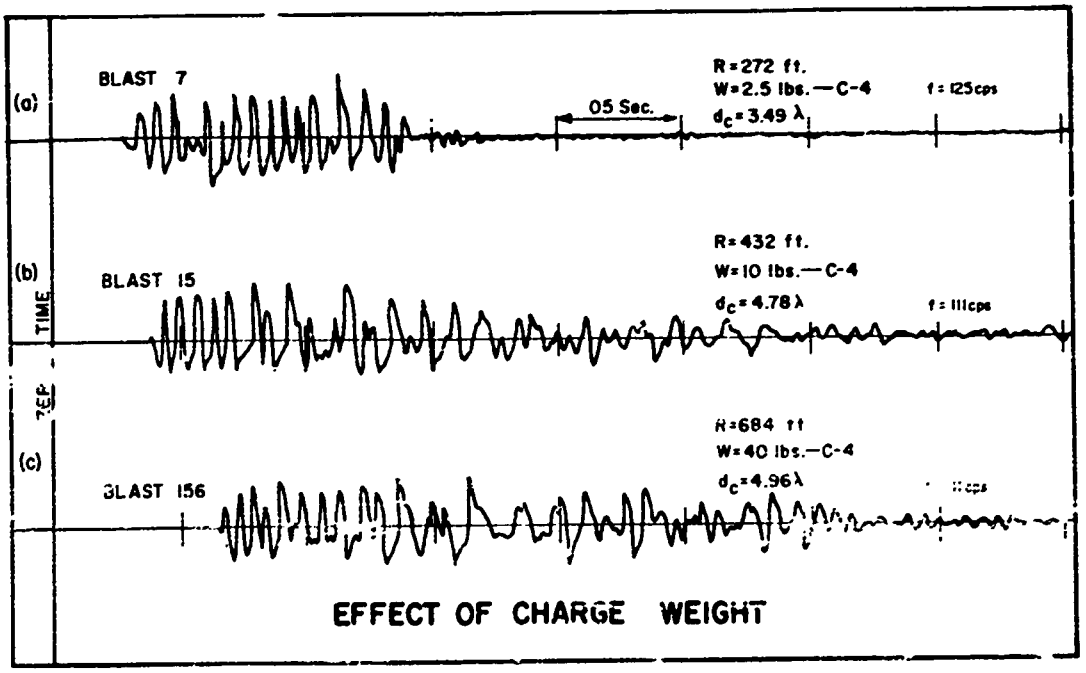

Figure 72. Typical seismic records, transverse component.

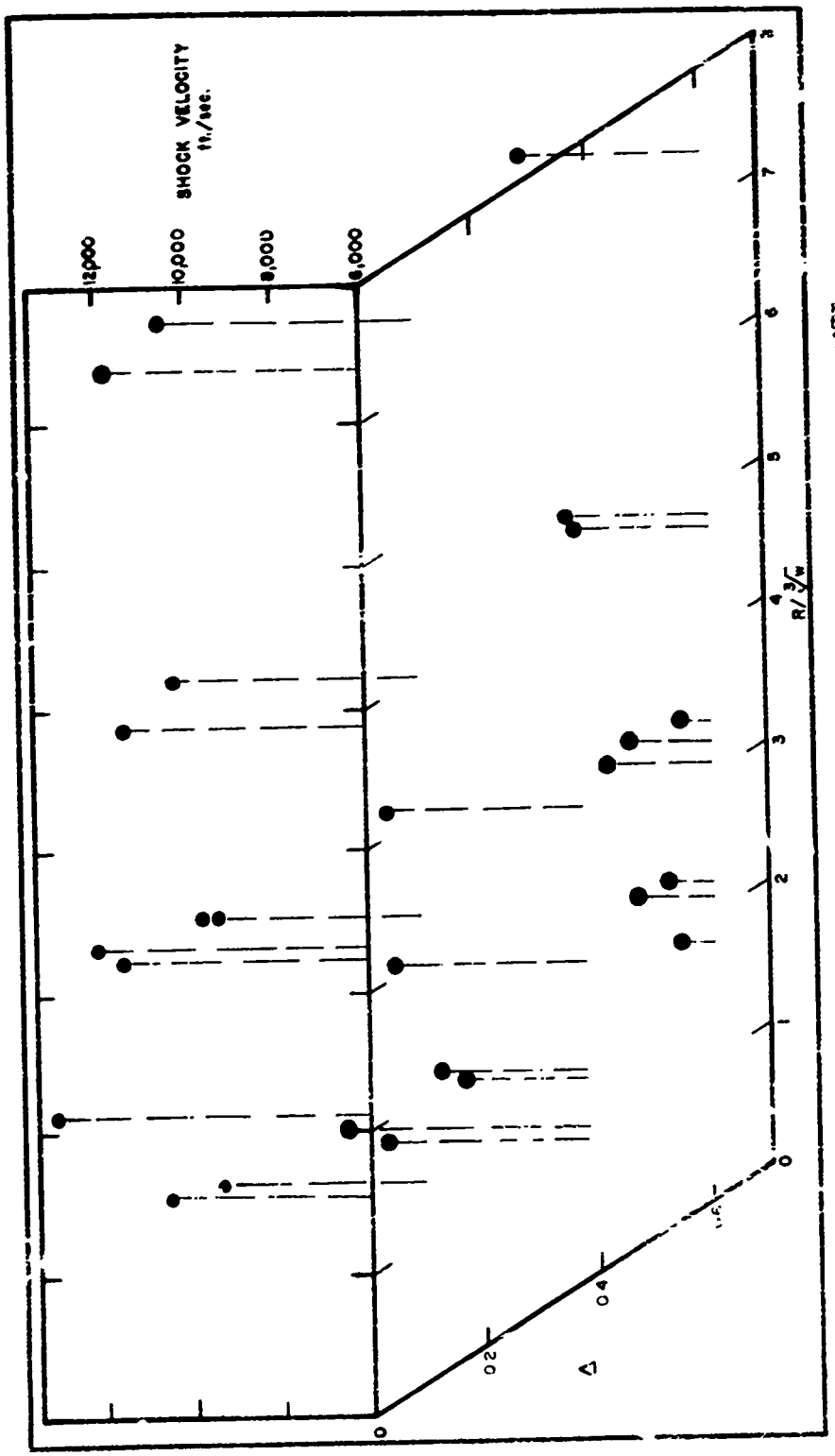

Figure 73. 10 lb A-60, isometric - under ice V vs Δ and $R/\sqrt[3]{W}$.

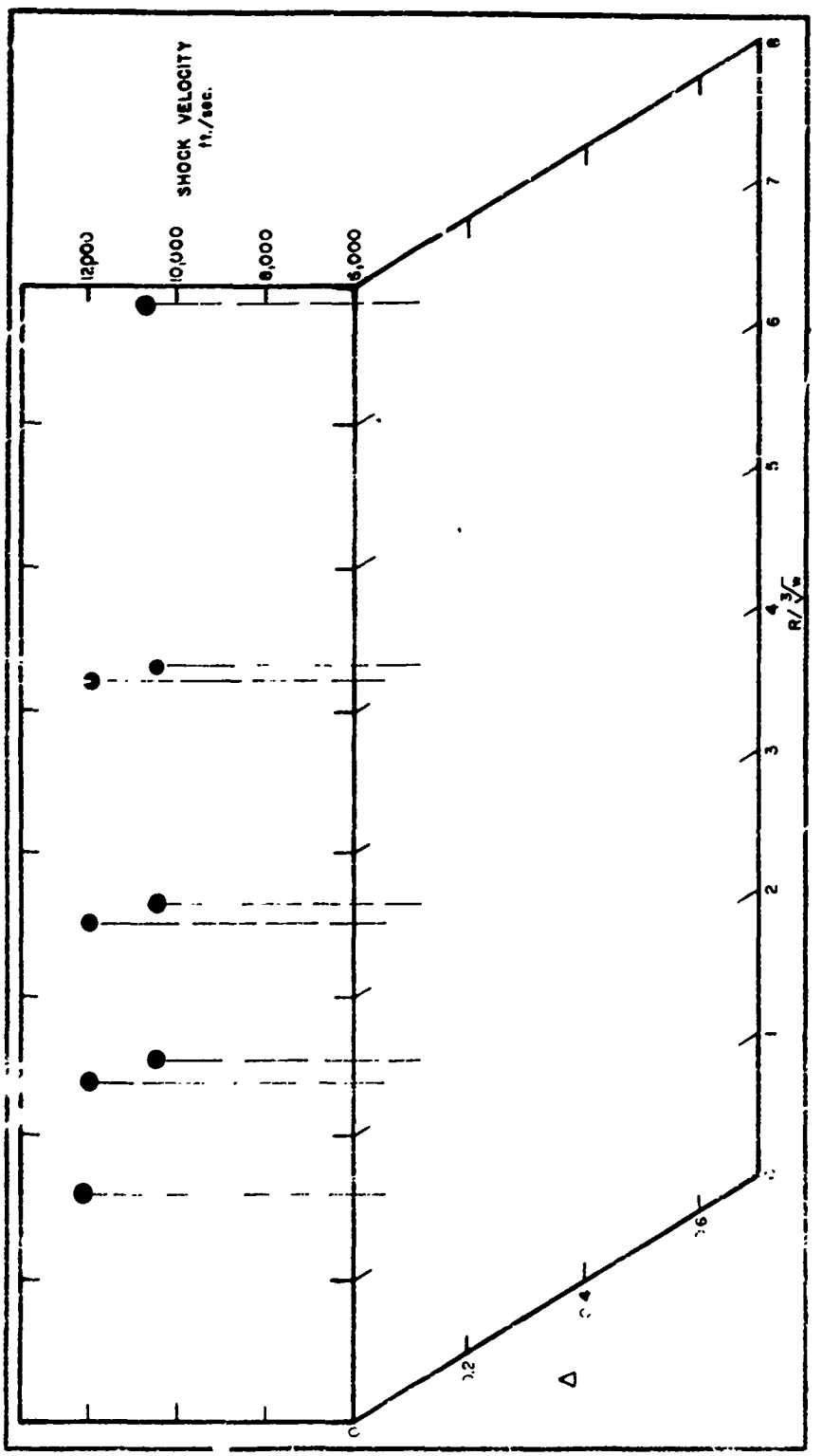

Figure 74. 20 lb C-4, isometric - under ice V vs Δ and $R/\sqrt[3]{W}$.

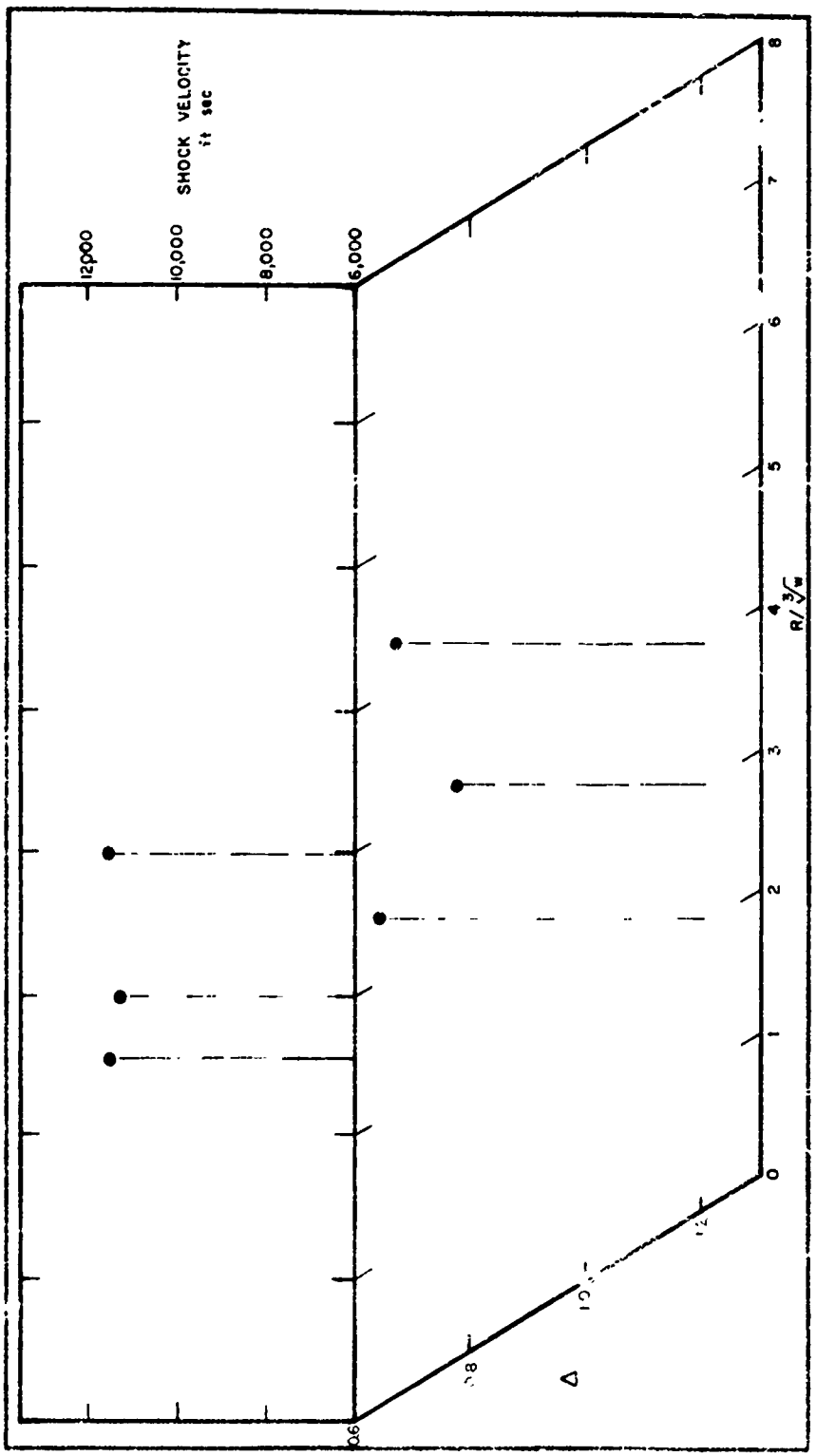

Figure 75. 5 lb C-4, isometric - under ice V vs Δ and $R/\sqrt[3]{W}$.

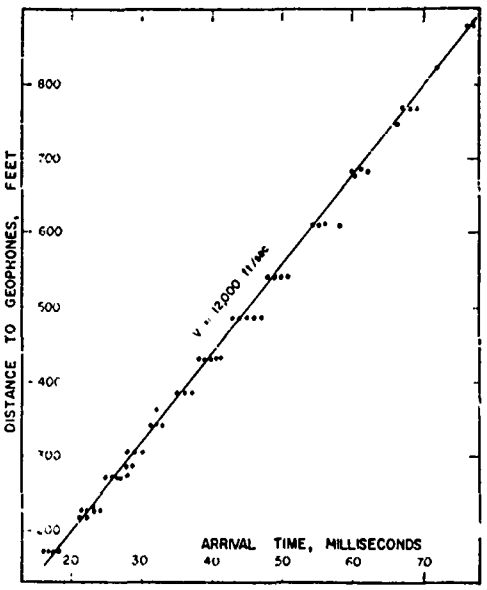

Figure 76. Longitudinal wave velocity.

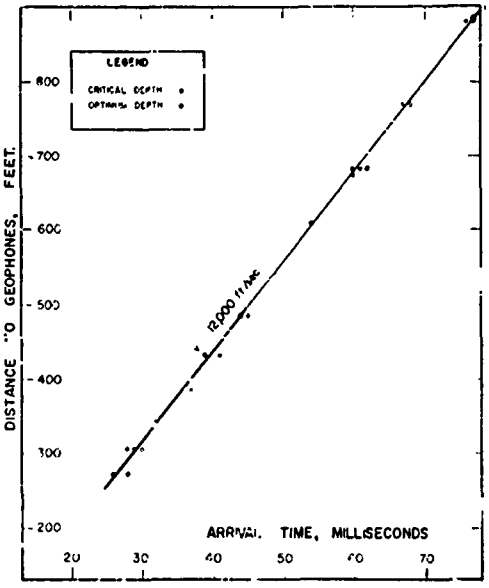

Figure 77. Longitudinal wave velocity for optimum and critical depths.

Record (a) for air burst shot 154b shows the arrival both of the direct under-ice shock and of the air-induced under-ice shock. The record of the direct under ice shock is characterized by vibrations of low amplitude, followed by vibrations of much higher amplitude. The record of the air-induced under-ice shock is characterized by the high amplitude of the longitudinal component, the moderately low amplitude of the transverse component, and the very low amplitude (or the apparent absence) of the vertical component.

The amplitude of the vibrations first arriving at the geophones increases as the charge depth increases. The fact that the record for a blast at optimum depth (c) differs from that at near critical depth (d) suggests that seismic effects are not independent of breakage effects.

Effect of charge weight at critical depth

If critical depth is used as point of reference, the form of the record is not affected by the charge depth; and seismic measurements may be correlated with the breakage process, because all of the energy of the explosion is partitioned to the material and fracturing is about to begin. At critical depth, all of the energy of the explosion is partitioned to processes that precede fracturing. In glacier ice, these are: 1) deformation without loss of cohesion, 2) seismic effects, and 3) heating and melting of the cavity walls.

Figures 70-72 are typical vibration measurements in glacier ice at a scaled distance of 200λ from blasts of 2.5, 10, and 40 lb of C-4 at critical depth. The duration of high amplitude vibration increases with charge weight — otherwise, the records for a given component are similar. If geometric, kinematic, and dynamic similarity were achieved and the behavior of the ice were independent of the scale of the experiment, the duration of vibration would be expected to scale with the length-scale ratio. For example, the duration of record (c) (40 lb) in relation to record (a) (2.5 lb) would be expected to be in the ratio of the cube-roots of the charge weights, or 2.51 times greater.

Seismic velocity vs charge-to-pressure gage shock velocity

Region near the charge. Figures 73-75 are isometric drawings in which the charge-to-pressure gage shock velocity is referred both to the scaled distance and to the depth ratio when blasting. The variation of the under-ice shock velocity with charge-depth, explosive type, and scaled slant distance appears to be as follows:

1) If shock gages are placed at given scaled slant distances, the under-ice shock velocity of blasts at a given depth of charge depends both upon the type and the weight of explosive.

2) If shock gages are placed in the range where plastic deformation and fracturing occur, the under-ice charge-gage shock velocity approaches a minimum if the charge is placed at the optimum depth for a given type of explosive and weight of charge.

3) When blasting at optimum depth with a given explosive and weight of charge, the under-ice charge-to-gage shock velocity increases with the scaled distance, in the range where fracturing predominates over plastic deformation.

Region remote from the charge. The region in which the under-ice shock velocity was observed to vary with depth ratio and scaled slant distance is small compared to that in which seismic measurements usually are made. The scaled distance to the most remote shock gage is less than 5% of that to the nearest geophone. The path of the disturbance from the blast to the geophone probably is longer than the measured horizontal distance. A variation in charge-to-gage velocity such as observed close to the shot becomes increasingly difficult to detect at greater distances.

Figure 76 summarizes the relation between distance and time of arrival of the longitudinal component of vibration for all blasts, independent of explosive type, charge weight, or charge depth. Figure 77 summarizes similar relations for blasts at optimum depth and critical depth only. It appears that dispersion increases if parameters such as the weight and type of explosive and the depth ratio of the charge are disregarded.

The relations suggest that when seismic measurements are to be used to supplement studies of the breakage process, both 1) energy partitioning to the material, and 2) the change in behavior of the material with the depth ratio must be taken into account when planning the experiments and when evaluating the measurements.

REFERENCES

Bishop, B. C. (1957) Shear moraines in the Thule area, Northwest Greenland, U. S. Army Snow Ice and Permafrost Research Establishment, Corps of Engineers, Research Report 17.

Butkovich, T. R. (1959) Some physical properties of ice from the TUTO tunnel and ramp, Thule, Greenland, U. S. Army Snow Ice and Permafrost Research Establishment, Corps of Engineers, Research Report 47.

Cole, Robert H. (1948) Underwater explosions. Princeton University Press.

Livingston, C. W. (1956) Excavations in frozen ground, Part I. Explosion tests in Keweenaw silt, USA SIPRE, Research Report 30, pt I.

_____ (1957) Behavior of materials of the earth's crust, Second annual symposium on rock mechanics, Quarterly of the Colorado School of Mines, vol. 52, no. 3.

_____ (1959a) Application of the Livingston crater theory to blasts in loess and clay. (Confidential) Prepared for Waterways Experiment Station, Corps of Engineers. U. S. Army.

_____ (1959b) Fundamentals of blasting, Proceedings, Foundations and Materials Branch, American Society of Civil Engineers.

_____ (1960) Bomb penetration tests, Fort Churchill, Canada, USA SIPRE Technical Report 71.

_____ (1960) Explosions in snow, USA SIPRE Technical Report 86, (in preparation).

_____ and Murphy, Glenn (1959) Excavations in frozen ground, Part 2, Explosion tests in Churchill till, USA SIPRE Report 30, pt. 2.

Schmitt, V. L. (1955) Glaciological investigations in the Thule Ramp area, USA SIPRE Report 28.

U. S. Army Waterways Experiment Station, Corps of Engineers (1958) Cratering effects of surface and burial HE charges in loess and clay, Technical Report no. 2-482, Vicksburg, Miss.

APPENDIX

Data Sheets

A. Blast hole and apparent crater data.

r_c = Charge radius (ft)

W = Charge weight (lb)

θ_1 = Tonnage utilization factor

d_c = Charge depth (ft)

h_c = Compression distance (ft)

T_v = Flyrock travel height (ft)

N = Critical depth (ft)

v = Initial flyrock velocity (ft/sec)

h' = Apparent crater depth (ft)

r' = Apparent crater radius (ft)

c' = Max radius of rupture (ft)

$K_{h'}$ = h'/N

$K_{r'}$ = r'/N

$K_{c'}$ = c'/N

V' = Apparent crater volume (ft^3)

B. True crater measurements and energy utilization factors.

V_t = Avg total volume (ft^3)

V_{TP} = Model total volume (ft^3)

h = Crater depth (ft)

K_s = Crater shape factor

r = Crater radius (ft) (Plan)

K_r = r/N

K_h = h/N

K = V/N^3

E = Strain energy factor

Δ = Depth ratio

A = Energy utilization number

B = Materials behavior index

C = Stress distribution number
= 1 for these tests

ABC - Compare to N-scaled crater volume K to which it is numerically equal.

C. Crater coefficients (same symbols as Data sheets A-B).

D. Seismic data.

Figures A1-23. Shock data.

Data sheet A: Blast hole and apparent crater data.*

Hole no.	r_c (ft)	W (lb)	θ_1	Hole depth (ft)	d_c (ft)	h_c (ft)	T_Y (ft)	T_Y/N	v (ft/sec)	h' (ft)	r' (ft)	c' (ft)	$K_{h'}$	$K_{r'}$	$K_{c'}$	V'	V'/W	Lip ht (ft)
	Explosive: -4			Density of material: 0.886 - 0.896g/cm³														
1	0.23	5.0	0.63	1.42	1.20	0.80	65.20	3.36	479.0	1.8	3.6	3.9	0.23	0.46	0.50	30.73	6.12	0.90
2	0.23	5.0	0.87	2.37	2.06	1.25			484.0	1.3	3.1	3.6	0.17	0.40	0.46	30.97	6.17	0.92
3	0.23	5.0	0.82	3.96	3.73	1.20	52.50	6.74	50.7							1.87	0.37	0.50
4	0.23	5.0		6.00	5.66		2.40	0.31	115.4									
5	0.23	5.0		8.32	8.22													
6	0.23	5.0	2.04	5.60	5.34	0.80												
7	0.18	2.5		6.10	5.97		7.66	1.34	35.4									
8	0.18	2.5	2.69	4.41	4.20	0.70												
10	0.29	10.0	0.49	1.75	1.51	1.40	115.60	11.21	341.0	2.3	4.6	5.1	0.22	0.45	0.50	52.25	5.23	0.61
11	0.29	10.0	1.07	3.67	3.17	1.30			152.1	3.2	4.0	5.2	0.31	0.39	0.50	28.25	2.83	0.71
12	0.29	10.0	1.25	5.38	5.20	0.90	51.90	5.04	78.0	0.9	2.5	6.6	0.087	0.24	0.64	10.10	1.01	0.51
13	0.29	10.0	1.50	7.37	7.23	0.70	21.00	2.04	429.0									
14	0.29	10.0		9.08	8.59		9.80	0.95	22.7									
15	0.29	10.0		10.54	10.30	1.30			71.0									
16	0.29	10.0	0.76	0.97	0.65	1.45				2.2	5.0	5.04	0.21	0.49	0.49	54.25	5.43	0.30
17	0.29	10.0	0.30	0.62	0.32	1.08				1.4	3.8	3.87	0.14	0.37	0.38	32.43	3.24	0.31
22	0.37	20.0	0.22	0.41	0.03	1.86				1.5	5.0	5.0	0.11	0.38	0.38	55.08	2.75	0.28
23	0.37	20.0	0.36	0.73	0.38	1.35				1.8	5.4	5.41	0.083	0.41	0.41	61.90	3.10	0.38
24	0.37	20.0	0.56	2.75	2.37	1.55			370.0	3.6	5.7	6.2	0.27	0.43	0.47	157.63	7.88	0.84
25a	0.37	20.0	0.72	3.83	2.92	1.70				2.8	6.2	6.8	0.21	0.47	0.51	150.23	7.51	1.50
25b	0.37	20.0	1.01	4.73	4.05	1.80				0.7	5.8	7.0	0.053	0.44	0.53	65.80	3.29	1.02
26	0.37	20.0	1.32	6.62	6.07	1.50	18.40	1.82	101.5									0.31
27	0.37	20.0	1.67	8.50	8.18	1.48	29.80	2.24	65.1	0.4	3.3	8.6	0.030	0.25	0.65	8.35	0.41	1.50
29	0.37	20.0		13.10	12.98	1.25			23.2									
	Explosive: Coalite 5S			Density of material: 0.877 - 0.896 g/cm³														
30	0.23	2.5	0.22	0.45	0.23	0.70				0.7	3.1	3.1	0.13	0.57	0.57	12.42	4.99	0.01
31	0.23	2.5	0.33	0.70	0.48	0.50	68.20	12.59	427.0	1.0	2.25	2.27	0.18	0.42	0.42	8.95	3.58	0.30
32	0.23	2.5	0.34	1.58	1.27	0.40	54.20	10.00	273.0	1.5	2.8	3.0	0.28	0.52	0.55	20.53	8.21	0.39
33	0.23	2.5	0.59	2.88	2.52	0.25	35.00	6.47	72.0	1.1	2.0	3.6	0.19	0.37	0.35	4.13	1.65	0.68
34	0.23	2.5	0.70	4.55	4.38		10.82	2.00	36.9	0.35	0.42	4.5	0.065	0.078	0.83	0.43	0.17	0.64
35	0.23	2.5		5.90	5.74		2.40	0.44	7.98									
36	0.23	2.5	0.65	1.95	1.74	0.40				1.6	3.15	3.5	0.30	0.58	0.67	24.52	9.81	0.57
37	0.23	2.5	0.29	1.26	1.09	0.45			271.0	1.6	3.1	3.35	0.30	0.57	0.62	14.15	5.66	0.52
38	0.23	2.5	0.22	0.77	0.54	0.45			447.0	1.0	2.75	4.9	0.18	0.51	0.54	9.26	3.70	0.56
39	0.23	2.5	1.96	3.69	3.44	0.45	20.00	3.70	45.75									
40	0.27	5.0	0.73	0.91	0.38	0.60	108.00	15.00	607.0	1.1	3.75	3.8	0.14	0.49	0.49	18.88	3.78	0.69
41	0.27	5.0	0.38	1.28	1.04	0.90			370.0	1.9	4.0	4.1	0.25	0.52	0.53	37.51	7.50	0.46
42	0.27	5.0	0.54	1.57	1.39	0.80				1.8	4.0	4.3	0.23	0.52	0.56	37.37	7.47	0.59
43	0.27	5.0	0.69	3.73	3.48	0.30	48.00	6.76	71.0	0.3	1.2	4.4	0.039	0.16	0.57	0.62	0.12	0.52
44	0.27	5.0	1.77	5.10	4.88	0.40	12.74	1.77	32.2									
45	0.27	5.0	0.00	7.21	6.90	0.60	4.91	0.68	25.72									
46	0.34	10.0	0.18	0.87	0.44	1.10				1.5	3.85	3.88	0.16	0.42	0.42	32.65	3.27	0.18
47	0.34	10.0	0.22	1.05	0.72	0.87	154.80	16.82	448.0	1.6	4.0	4.62	0.17	0.43	0.44	38.78	3.88	0.30

*Additional blast hole and crater data are available on request.

Data sheet A: Blast hole and apparent crater data (cont'd).

Hole no	r_c (ft)	W (lb)	θ_1	I. h depth (ft)	d_c (ft)	h_c (ft)	T_V (ft)	T_V/N	v (ft/sec)	h' (ft)	r' (ft)	c' (ft)	$K_{h'}$	$K_{r'}$	$K_{c'}$	V'	V'/W	Lip ht (ft)
	Explosive: Coalite 5S (cont'd)																	
48	0.34	10.0	0.73	1.79	0.69	0.80	128.2	13.96	379.0	2.1	4.35	4.5	0.23	0.47	0.49	47.88	4.79	0.43
49	0.34	10.0	0.62	3.02	0.62	0.84	172.6	18.76	168.2	1.2	4.5	5.2	0.13	0.49	0.57	45.93	4.59	0.68
50	0.34	10.0	1.90	6.39	0.86	0.10	41.5	4.51	101.2									
51		10.0																
52	0.43	20.0	0.21	1.05	0.27	1.30			468.0	1.9	4.90	4.95	0.164	0.42	0.43	70.23	3.51	0.92
53	0.43	20.0	0.28	1.35	0.36	1.15				0.8	4.90	4.95	0.069	0.42	0.43	74.03	3.70	0.90
54	0.43	20.0	0.34	2.23	0.33	1.05	134.1	11.56	561.0	2.8	5.5	5.7	0.24	0.37	0.49	117.40	5.87	1.96
55	0.43	20.0	0.71	4.15	0.42	1.25	154.0	13.29	173.8	2.7	5.7	6.8	0.23	0.49	0.59	163.50	8.18	1.45
56	0.43	20.0	1.59	8.01	0.49	1.10	10.7	0.92	31.6	0.8	1.6	8.0	0.069	0.14	0.69	1.10	0.06	1.29
57	0.43	20.0		11.76														
60	0.27	5.	0.36	0.60	0.83	1.03	62.4	8.10	332.0	1.7	3.75	3.8	0.22	0.49	0.49	17.01	3.40	0.42
61	0.27	5.0	0.35	1.09	0.83	1.30	60.0	7.79	222.0	1.8	4.35	4.4	0.23	0.57	0.57	28.32	5.66	0.31
62	0.27	5.0	0.65	1.74	1.01	1.00	117.0	15.21	362.0	2.4	4.05	4.3	0.31	0.53	0.56	49.21	9.84	0.37
63	0.27	5.0	1.22	3.10	1.16	1.00	127.0	16.49	126.9	1.2	3.9	4.1	0.16	0.51	0.61	21.92	4.38	0.65
64	0.27	5.0	1.54	5.35	3.84	0.55	41.4	5.37	70.2	0.95	2.5	4.2	0.12	0.32	0.68	8.89	1.78	0.54
65	0.33	10.0	0.40	0.75	0.49		148.5	15.31	307.0									
66	0.33	10.0	0.71	1.20	0.92	1.00	138.0	14.23	452.0	1.9	3.8	4.0	0.20	0.39	0.41	36.64	3.66	0.39
67	0.33	10.0	0.62	2.00	1.72	1.10	200.0	20.62	846.0	2.9	5.6	5.9	0.30	0.58	0.61	115.23	11.52	0.24
68	0.33	10.0	0.80	3.75	3.39	0.75	Off		211.0	2.8	5.1	6.1	0.29	0.53	0.63	71.50	7.15	0.52
69	0.33	10.0	0.54	7.75	7.01	1.35	10.8	1.11	45.5	1.3	2.9	7.7	0.13	0.30	0.79	19.69	1.97	1.10
	Explosive: Atlas 60			Density of material 0.886 - 0.896 g/cm³														
70	0.23	5.0		10.12	10.09		136.0	13.32	77.4									
71	0.23	5.0		8.3	8.14		No			1.0	5.15	8.3	0.098	0.31	0.86	18.89	3.78	0.50
72	0.29	10.0		10.15	9.92					0.6	1.5	10.1	0.048	0.12	0.80	1.75	0.18	1.55
73	0.29	10.0		12.38	12.10													
74	0.23	5.0	3.26	6.95	6.69	0.85	5.7	0.57	10.1	0.2	5.05	6.2	0.02	0.50	0.67	0.07	2.04	1.38
75	0.18	2.5		8.70	8.61		Off											
76	0.23	5.0	1.55	4.17	3.80	0.90	136.0	13.32	72.8	1.5	5.05	6.4	0.15	0.50	0.63	57.68	11.54	0.40
77	0.23	5.0	0.79	2.20	1.82	0.90	98.7	9.68	287.0	1.9	4.95	5.4	0.19	0.49	0.51	59.24	11.85	0.34
78	0.23	2.0	0.60	1.15	0.88	1.35	102.6	10.10	374.0	1.7	4.25	4.3	0.17	0.42	0.42	46.83	9.37	0.10
79	0.23	5	0.55	0.68	0.40	0.85	112.3	12.00	333.0	1.6	3.2	3.27	0.098	0.31	0.32	14.65	2.92	0.50
	Explosive: Coalite 7S			Density of material 0.886 - 0.896 g/cm³														
80	0.43	20.0	0.17	0.98	0.55	1.35	136.5	11.20	437.0	1.9	5.15	5.2	0.16	0.42	0.43	72.67	3.63	0.60
81	0.43	20.0	0.37	1.54	1.01	1.55	Off		472.0	2.5	5.2	5.5	0.21	0.42	0.45	85.08	4.25	0.30
82	0.43	20.0	0.57	2.70	2.21	0.90	154.0	12.62	369.0	3.1	6.45	6.75	0.25	0.53	0.55	153.00	7.65	0.40
83	0.43	20.0	1.25	4.68	4.33	1.05	110.0	9.02	126.0	1.5	5.7	7.3	0.12	0.47	0.60	59.49	2.97	1.30
84	0.43	20.0	1.86	8.14	7.80	1.10	29.8	2.44	80.5	1.5	1.8	8.4	0.12	0.15	0.69	11.86	0.59	1.82
85	0.27	5.0		7.55	7.28													
86	0.33	10.0		10.30	9.74													
87	0.21	2.5		6.05	5.97													
88	0.21	2.5	2.02	4.35	4.09				92.2	0.3	0.75	4.8	0.05	0.13	0.80	0.23	0.09	1.04
89	0.43	20.0		12.51	12.19													
90	0.27	5.0	1.89	5.54	4.89	0.30	33.1	4.30	38.6									

Data sheet A: Blast hole and apparent crater data (cont'd)

Hole no.	r_c (ft)	W (lb)	θ_i	H dept (ft)	d_c (ft)	h_c (ft)	T_v (ft)	T_v/N	v (ft/sec)	h' (ft)	r' (ft)	c' (ft)	$K_{h'}$	$K_{r'}$	$K_{c'}$	V'	V'/W	Lip ht (ft)
	Explosive: Atlas 60			Density of material 0.886 - 0.896 g/cm³														
95	0.35	20	0.71	4.25	4.05	1.50				3.3	6.8	8.0	0.22	0.44	0.52	250.60	12.53	0.35
96	0.35	20.0		6.80	6.40													
96R	0.35	20.0	0.89	6.40	6.15	2.30	121.0	7.92	141.0	0.5	6.5	8.6	0.033	0.42	0.56	80.12	4.01	0.65
97	0.35	20.0	1.65	8.00	7.46	2.60	80.0	5.23	78.9	1.0	7.2	10.0	0.065	0.47	0.65	129.35	6.47	0.70
98	0.35	20.0		12.65	12.01													
99	0.35	20.0	2.34	9.30	8.95	0.70	26.1	1.71	46.3	1.1	8.3	10.1	0.072	0.54	0.66	43.78	2.19	1.71
100	0.35	20.0	2.52	10.48	10.10	1.00	34.0	2.22	28.4	1.05	8.6	10.8	0.069	0.56	0.71	77.13	3.86	1.80
101	0.35	20.0		14.85	14.47		No											
102	0.46	40.0		12.81	12.16	0.95	16.8	0.91	29.8	1.55	4.2	11.3	0.084	0.23	0.61	32.34	0.81	2.10
103	0.46	40.0		19.10	18.67													
104	0.46	40.0	1.52	8.50	8.10	2.00	63.0	3.41	74.5	1.75	6.2	8.4	0.095	0.34	0.45	180.58	4.51	2.86
105	0.29	10.0	0.63	2.64	2.31	1.25	125.0	9.93	321.0	2.8	5.1	6.0	0.22	0.40	0.48	104.80	10.48	0.48
106	0.29	10.0	0.57	0.90	0.62	1.20	111.2	8.84	440.0	1.7	4.9	5.0	0.14	0.39	0.40	62.24	6.22	0.36
107	0.29	10.0	0.25	0.65	0.35	1.20	96.5	7.66	324.0	1.6	3.9	3.95	0.13	0.31	0.31	41.86	4.19	0.42
108	0.23	5.0	0.27	0.47	0.21	1.65	90.0	8.83	319.0	0.9	2.88	2.9	0.88	0.28	0.28	13.97	2.[illegible]	0.34
110	0.29	10.0	0.18	0.30	0.00	1.60	Off		323.0	1.1	3.5	3.5	0.087	0.28	0.28	25.54	2.55	0.3[illegible]
113	0.29	10.0	0.40	1.53	1.20	0.95	Off		177.5	2.0	4.8	4.[illegible]9	0.16	0.38	0.40	65.95	6.60	0.68
115	0.29	10.0	1.58	5.20	4.93	0.65				0.7	5.1	6.[illegible]5	0.056	0.40	0.55	35.89	3.[illegible]9	0.65
116	0.29	10.0	2.56	9.00	7.65	1.05	8.0	0.64	16.7									
	Explosive: Coalite 7S			Density of material 0.893 g/cm³														
120	0.33	10.0	2.94	6.34	6.00	1.20	66.5	6.86	119.2	0.3	2.1	6.[illegible]	0.031	0.22	0.69	1.58	0.16	0.77
	Explosive: C-4			Density of material 0.877 - 0.896 g/cm³														
151	0.37	20.0	0.47	1.10	0.83	3.10				2.5	6.5	6.8	0.19	0.49	0.51	153.78	7.69	0.49
152	0.37	20.0	0.39	1.90	1.53	1.35	66.5	5.00	252.5	3.0	6.0	6.2	0.23	0.45	0.47	156.10	7.81	0.72
153	0.37	20.0	0.55	4.35	2.94	1.80	Off		361.0	3.0	6.6	7.2	0.23	0.50	0.54	198.73	9.94	1.05
154	0.37	20.0		9.53	9.33		17.0	1.28	31.4									
155	0.46	40.0	1.13	11.54	11.07		22.6	1.32	31.0	0.7	1.6	11.6	0.041	0.094	0.68	1.14	0.03	1.75
156	0.46	40.0		17.35	16.95		7.7	0.45	29.5									
157	0.46	40.0		7.90	7.39		73.6	4.31	98.0									
170	0.23	5.0	0.21	0.23	0.00		34.0	4.36	71.0	0.9	2.5	2.5	0.12	0.32	0.32	9.95	.99	0.20
170R	0.23	5.0	0.20	0.23	0.00													
170¼	0.23	5.0	0.30	0.46	0.23		40.4	5.19	146.6	1.2	3.1	3.15	0.15	0.40	0.40	18.22	3.80	0.35
170½	0.23	5.0	0.26	0.68	0.46	0.70	41.8	5.36	284.5	1.2	3.05	3.1	0.15	0.39	0.40	19.99	4.00	0.22
170¾	0.23	5.0	0.45	1.15	0.92	1.00	46.2	6.93	239.0	1.8	4.5	4.6	0.23	0.58	0.59	40.45	8.09	0.80
171	0.23	5.0	0.58	1.92	1.65	0.85	71.4	9.15	253.5	2.2	3.7	4.1	0.28	0.47	0.53	40.20	8.04	1.41
	Explosive: Atlas 60			Density of material 0.892 - 0.896 g/cm³														
A*	0.18	2.5	1.86	5.05	4.74													
B*	0.18	2.5		6.85	6.20		8.1	1.00	11.2									
C*	0.18	2.5	2.14	4.02	3.61	0.90												
D*	0.18	2.5		5.13	4.94		9.6	1.19	32.3									
E*	0.18	2.5	1.18	2.55	2.36	1.40												
F*	0.18	2.5	0.96	2.13	1.89	0.70												
G*	0.18	2.5		7.10	6.80													
H*	0.18	2.5	0.50	7.66	7.58		3.75	0.46	11.0									

*Cylindrical charges. All other charges were spheres.

DATA SHEET B: True crater measurements and energy utilization factors.

Hole no.	Plan area (ft^2)	V_t (ft^3)	V_{TP} (ft^3)	h (ft	K_s	r (ft)	$\frac{V}{W}$	K_r	K_h	K	E	$\sqrt[3]{W}$	N	Δ	A	B	ABC
	Explosive: C-4																
1	77.56	114.15	14.27	2.0	0.74	4.97	22.83	0.64	0.26	0.24	4.56	1.71	7.80	0.18	0.27	0.89	0.24
2	66.32	1[illegible].74	4.30	3.2	0.73	4.59	31.15	0.59	0.41	0.33	4.56	1.71	7.80	0.30	0.37	0.89	0.33
3	78.60	157.86	1.32	4.93	0.41	5.00	31.57	0.64	0.63	0.33	4.56	1.71	7.80	0.55	0.38	0.89	0.34
4	127.72					6.38		0.82			4.56	1.71	7.80	0.83		0.89	
5											4.56	1.71	7.80	1.21		0.89	
6	118.76	365.66	1.58	6.14	0.50	6.15	73.13	0.79	0.79	0.77	4.56	1.71	7.80	0.79	0.85	0.89	0.76
7											4.19	1.36	5.70	1.05		1.29	
8	109.32	240.95	2.10	4.35	0.45	5.90	96.38	1.04	0.85	1.30	4.19	1.36	5.70	0.74	1.01	1.29	1.30
10	82.04	175.66	7.13	2.[illegible]	0.74	5.11	17.57	0.50	0.28	0.16	4.79	2.15	10.30	0.15	0.24	0.67	0.16
11	151.88	381.29	4.27	4.47	0.56	6.95	38.13	0.67	0.43	0.35	4.79	2.15	10.30	0.31	0.52	0.67	0.35
12	158.24	448.74	1.98	6.10	0.46	7.10	44.87	0.69	0.59	0.41	4.79	2.15	10.30	0.50	0.61	0.67	0.41
13	174.52	538.76	1.08	9.65	0.32	7.45	53.88	0.72	0.94	0.49	4.79	2.15	10.30	0.70	0.74	0.67	0.50
14	152.20					6.96		0.68			4.79	2.15	10.30	0.83		0.67	
15				11.60					1.13		4.79	2.15	10.30	1.00		0.67	
16	1[illegible]0.64	271.68	2.85	2.95	0.57	7.15	27.17	0.69	0.29	0.25	4.79	2.15	10.30	0.06	0.37	0.67	0.25
17	97.16	109.52	39.97	1.63	0.69	5.56	10.95	0.54	0.16	0.10	4.79	2.15	10.30	0.03	0.15	0.67	0.10
22	101.12	155.29	23.[illegible]1	2.28	0.67	5.67	7.77	0.43	0.17	0.066	4.91	2.71	13.30	0.002	0.13	0.51	0.066
23	146.96	261.86	50.[illegible]5	2.63	0.78	6.84	13.10	0.51	0.20	0.11	4.91	2.71	13.30	0.03	0.22	0.51	0.11
24	227.28	470.66	7.81	3.92	0.53	8.51	23.53	0.64	0.29	0.20	4.91	2.71	13.30	0.18	0.39	0.51	0.20
25a	293.72	517.05	5.24	4.62	0.38	9.67	25.85	0.73	0.35	0.22	4.91	2.71	13.30	0.22	0.43	0.51	0.22
25b	230.76	719.51	3.59	5.85	0.53	8.57	35.97	0.64	0.45	0.31	4.91	2.71	13.30	0.30	0.59	0.51	0.30
26	274.08	944.60	2.18	7.57	0.46	9.34	47.23	0.70	0.57	0.40	4.91	2.71	13.30	0.46	0.78	0.51	0.40
27	269.40	1201.81	1.33	9.66	0.46	9.26	60.09	0.70	0.73	0.51	4.91	2.71	13.30	0.62	0.99	0.51	0.50
29				14.25					1.07		4.91	2.71	13.30	0.98		0.51	
	Explosive: Coalite 5S																
30	23.36	18.44	23.[illegible]	0.95	0.82	2.73	7.38	0.50	0.18	0.12	3.98	1.36	5.41	0.04	0.10	1.19	0.11
31	20.64	11.74	12.49	1.00	0.57	2.56	4.70	0.47	0.18	0.074	3.98	1.36	5.41	0.09	0.065	1.14	0.074
32	34.36	30.1[illegible]	6.46	1.65	0.53	3.31	12.04	0.61	0.30	0.19	3.98	1.36	5.41	0.23	0.17	1.14	0.19
33	44.52	52.94	2.49	2.77	0.42	3.80	21.18	0.70	0.51	0.33	3.98	1.36	5.41	0.47	0.29	[illegible]	0.33
34	54.72	62.8[illegible]		2.75	0.42	4.17	25.14	0.77	0.51	0.40	3.98	1.36	5.41	0.81	0.35	1.14	0.40
35											3.98	1.36	5.41	1.06		1.14	
36	45.76	58.[illegible]	5.94	2.15	0.59	3.82	23.28	0.71	0.40	0.37	3.98	1.36	5.41	0.32	0.32	1.14	0.36
37	31.24	36.3[illegible]	7.23	1.60	0.53	3.15	10.35	0.58	0.30	0.17	3.98	1.36	5.41	0.20	0.15	1.14	0.17
38	37.44	30.04	20.6	1.00	0.54	3.45	8.02	0.64	0.18	0.13	3.98	1.36	5.41	0.10	0.11	1.14	0.13
39	76.32	[illegible]5.52	2.78	3.90	0.59	4.93	70.20	0.91	0.72	1.11	3.98	1.36	5.41	0.64	0.98	1.14	1.12
40	35.72	42.81	44.18	1.00	1.17	3.37	8.36	0.47	0.14	0.11	4.21	1.71	7.20	0.05	0.12	0.91	0.11
41	65.24	69.01	9.45	1.[illegible]5	0.54	4.56	13.80	0.63	0.27	0.18	4.21	1.71	7.20	0.1[illegible]	0.20	0.91	0.18
42	55.56	61.60	[illegible].37	2.20	0.50	4.21	12.32	0.58	0.31	0.17	4.21	1.71	7.20	19	0.18	0.9[illegible]	0.16
43	80.72	123.16	2.28	3.76	0.41	5.07	24.63	0.70	0.52	0.33	4.21	1.71	7.20	46	0.36	[illegible]1	0.33
44	137.84	315.99	2.15	5.30	0.43	6.62	63.20	0.92	0.74	0.85	4.21	1.71	7.20	0.68	0.93	0.91	0.85
45				7.50					1.04		4.21	1.71	7.20	0.96		0.91	
46	62.76	66.04	18.09	1.85	0.52	4.47	6.60	0.49	0.20	0.085	4.28	[illegible]15	9.20	0.05	0.10	0.81	0.081
47	76.1[illegible]	80.26	19.97	2.05	0.51	4.92	8.03	0.53	0.22	0.10	4.28	2.15	9.20	0.0[illegible]	0.13	0.81	0.11

*Additional blast hole and crater data are available on request.

DATA SHEET B: (cont'd)

Hole no.	Plan area (ft^2)	V_t (ft^3)	V_{TP} (ft^3)	h (ft)	K_s	r (ft)	$\frac{V}{W}$	K_r	K_h	K	E	$\sqrt[3]{W}$	N	Δ	A	B	ABC
	Explosive: Coalite 8S (cont'd)																
48	148.16	260.33	25.83	2.60	0.67	6.87	26.03	0.75	0.28	0.33	4.28	2.15	9.20	0.15	0.41	0.81	0.33
49	121.84	222.50	4.85	3.71	0.49	6.23	22.26	0.68	0.40	0.29	4.28	2.15	9.20	0.30	0.35	0.81	0.28
50	230.00	680.96	2.81	6.18	0.48	8.555	68.06	0.93	0.67	0.37	4.28	2.15	9.20	0.67	1.08	0.81	0.87
51				10.10					1.10		4.28	2.15	9.20	0.99		0.81	
52	86.76	149.76	24.04	2.20	0.79	5.25	7.49	0.45	0.19	0.096	4.28	2.71	11.60	0.05	0.13	0.71	0.092
53	163.04	203.42	22.60	2.20	0.57	7.21	10.17	0.62	0.19	0.13	4.28	2.71	11.60	0.08	0.18	0.71	0.13
54	137.80	245.67	10.72	3.00	0.59	6.62	12.19	0.56	0.26	0.16	4.28	2.71	11.60	0.15	0.22	0.71	0.16
55	222.56	503.82	3.31	4.55	0.46	8.42	25.19	0.73	0.43	0.32	4.28	2.71	11.60	0.31	0.45	0.71	0.32
56	304.88	1144.02	1.66	8.80	0.43	9.85	57.20	0.85	0.76	0.73	4.28	2.71	11.60	0.67	1.03	0.71	0.73
57				11.70					1.01		4.28	2.71	11.60	0.99		0.71	
60	54.56	64.35	26.16	1.35	0.87	4.17	12.87	0.54	0.18	0.14	4.50	.71	7.70	0.04	0.17	0.82	0.14
61	54.16	63.65	10.73	1.81	0.65	4.15	12.73	0.54	0.24	0.14	4.50	.	7.70	0.07	0.17	0.82	0.14
62	80.92	115.93	7.98	2.44	0.59	5.07	23.19	0.66	0.32	..25	4.50		7.70	0.19	0.31	0.8	0.25
63	105.92	218.93	5.10	3.48	0.59	5.81	43.79	0.75	0.45	0.48	4.50	.1	7.70	0.32	0.58	0.82	0.48
64	116.24	275.73	3.46	4.39	0.54	6.98	55.16	0.79	0.57	0.60	4.50	1.71	7.70	0.50	0.73	0.82	0.60
65	75.32	141.78		3.00	0.63	4.90	14.18	0.51	0.31	0.16	4.51	2.15	9.70	0.06	0.16	0.99	0.16
66	103.48	181.58	49.20	4.02	0.44	5.74	18.17	0.59	0.41	0.20	4.51	2.15	9.70	0.10	0.20	0.99	0.20
67	103.16	187.07	8.31	2.82	0.65	5.73	18.77	0.59	0.29	0.21	4.51	2.15	9.70	0.20	0.21	0.99	0.21
68	153.00	285.55	4.02	4.14	0.45	6.98	28.56	0.72	0.43	0.31	4.51	2.15	9.70	0.39	0.32	0.99	0.32
69	127.32	192.90	0.53	8.36	0.18	6.37	19.29	0.66	0.86	0.21	4.51	2.15	9.70	0.80	0.21	0.99	0.21
	Explosive: Atlas 60																
70				11.50					1.13		5.96	1.71	10.20	0.99		0.55	
71	138.04					6.63		0.65			5.96	1.71	10.20	0.80		0.55	
72	298.08	700.22	0.37			9.74	70.02	0.77		0.35	5.86	2.15	12.60	0.79	0.65	0.54	0.35
73				13.40					1.06		5.86	2.15	12.60	0.96		0.54	
74	219.40	584.64	1.39	7.50	0.31	8.36	116.93	0.82	0.74	0.55	5.96	1.71	10.20	0.66	1.01	0.55	0.56
75				9.00						1.11	5.96	1.36	8.10	1.06		0.40	
76	135.44	276.96	2.67	4.70	0.43	6.57	55.39	0.64	0.46	0.26	5.96	1.71	10.20	0.37	0.48	0.55	0.26
77	113.88	141.9	7.05	2.72	0.46	6.02	28.39	0.59	0.27	0.13	5.96	..71	10.20	0.18	0.24	0.55	0.13
78	86.32	108.3	9.77	2.25		5.24	21.68	0.51	0.22	0.10	5.96	1.71	10.20	0.09	0.19	0.55	0.10
79		82.32	42.06	1.45			16.40		0.14	0.077	5.96	1.71	10.20	0.04	0.14	0.55	0.077
	Explosive: Coalite 7S																
80	81.20	124.95	18.2	1.90	0.81	5.08	6.25	0.42	0.16	0.069	4.50	2.71	12.20	0.05	0.089	0.78	0.069
81	124.88	193.31	11.2	2.56	0.60	6.31	9.57	0.52	0.21	0.11	4.50	2.71	12.20	0.08	0.14	0.78	0.11
82	177.36	370.60	12.32	3.90	0.54	7.51	18.53	0.62	0.32	0.20	4.50	2.71	12.20	0.18	0.26	0.78	0.20
83	322.56	877.04	5.63	5.40	0.50	10.13	43.85	0.83	0.44	0.48	4.50	2.71	12.20	0.35	0.62	0.78	0.48
84	302.64	1033.16	1.59	8.90	0.49	9.89	66.66	0.81	0.73	0.73	4.50	2.71	12.20	0.94	0.95	0.78	0.74
85				8.2*					1.06		4.50	1.71	7.70	5		0.1	
86				10.80					1.11		4.51	2.15	9.70	.11		0.99	
87											4.4.	1.36	6.00	0.99		0.83	
88	122.32	181.18		4.40	0.34	6.24	72.47	1.04	0.67	0.84	4.41	.36	6.00	0.68	1.01	0.83	0.84
89				13.8*					1.13		4.50	2.71	12.20	1.00		0.78	
90	139.64	338.37	2.42	5.20	0.47	6.67	67.67	0.87	0.68	0.74	4.50	1.71	7.70	0.64	0.90	0.82	0.74

*Estimated data.

DATA SHEET B: (Cont'd)

Hole no.	Plan area (ft^2)	V (ft^3)	V_{TP} (ft^3)	(ft)	K_s	(ft)	$\frac{V}{W}$	K_r		K	E	$\sqrt{W}$	N	Δ	A	B	ABC
	Explosive:	Atlas 60															
95	201.64	5[illegible]5.33	2.96	5.45	0.46	8.01	25.27	0.52	0.[illegible]6	0.14	5.65	2.71	15.30	0.26	0.28	0.50	0.14
96											5.65	2.71	15.30	0.42			
96R	189.52	642.17	1.06	8.80	0.38	7.77	32.16	0.52	0.58	0.18	5.65	2.71	15.30	0.40	0.36	0.50	0.18
97	264.48	1180.15	1.16	10.00	0.45	9.17	59.01	0.60	0.65	0.33	5.65	2.71	15.30	0.49	0.66	0.50	0.33
98	302.56			4.85		9.81		0.69	0.32		5.65	2.71	15.30	0.78		0.50	
99	468.24	1682.38	1.87	9.50	0.38	12.21	84.17	0.80	0.62	0.47	5.65	2.71	15.30	0.58	0.95	0.50	0.48
100	299.16	1944.29	1.42	11.20		9.76	97.21	0.69	0.73	0.54	5.65	2.71	15.30	0.66	1.09	0.50	0.54
101											5.65	2.71	15.30	0.95		0.50	
102	573.72	1874.85		13.10		13.51		0.73	0.71	0.30	5.41	3.42	18.50	0.66	0.78	0.38	0.30
103				19.60					1.06		5.41	3.42	18.50	1.01			
104	383.08	2181.70	2.12	10.10	0.56	11.04	54.54	0.60	0.55	0.34	5.41	3.42	18.50	0.44	0.91	.38	0.35
105	130.32	224.32	4.97	3.56	0.48	6.44	22.43	0.51	0.20	0.11	5.86	2.15	12.60	0.18	0.21	0.54	0.11
106	102.20	202.93	3[illegible].65	2.65	0.75	5.70	20.29	0.45	0.21	0.10	5.86	2.15	12.60	0.05	0.19	0.54	0.10
107	93.00	91.96	24.72	1.90	0.52	5.44	9.20	0.43	0.15	0.046	5.86	2.15	12.60	0.03	0.085	0.54	0.046
108	52.08	49.59	7.71	1.90	0.50	4.08	9.92	0.40	0.19	0.047	5.96	1.71	10.20	0.02	0.086	0.55	0.047
110	57.92	63.61	15.51	1.60	0.69	4.29	6.36	0.34	0.13	0.032	5.86	2.15	12.60	0	0.05[illegible]	0.54	0.032
113	93.40	143.34	2.59	2.15	0.71	5.45	14.33	0.43	0.17	0.072	5.8	2.15	12.60	0.10	0.13	0.54	0.07
115	180.96	495.15	2.85	5.60	0.49	7.59	49.52	0.60	0.44	0.[illegible]5	5.85	2.15	12.60	0.39	0.46	0.54	0.25
116	251.64	917.63	1.39	8.70	0.42	8.95	91.76	0.71	0.69	0.46	5.65	2.15	12.60	0.61	0.85	0.54	0.46
	Explosive:	Coalite 7S															
120	318.84	1055.88	2.83	7.18	0.46	10.07	105.59	1.04	0.74	1.16	4.51	2.15	9.70	0.68	1.17	0.99	0.16
	Explosive:	C-4															
151	164.84	339.09	5.30	4.93	0.42	7.24	16.95	0.54	0.37	0.14	4.91	2.71	13.30	0.06	0.28	0.51	0.14
152	182.08	280.93	4.72	2.88	0.53	7.61	14.00	0.57	0.22	0.12	4.91	2.71	13.30	0.12	0.23	0.51	0.12
153	177.68	396.19	3.72	4.74	0.47	7.52	19.80	0.57	0.36	0.17	4.91	2.71	13.30	0.22	0.33	0.51	0.17
154	337.44					10.36		0.78			4.91	2.71	13.30	0.70		0.51	
155	495.00	1620.99		11.90	0.28	12.55	40.52	0.73	0.70	0.32	5.00	3.42	17.10	0.65	1.00	0.32	0.32
156											5.00	3.42	17.10	0.99		0.32	
157											5.00	3.42	17.10	0.43		0.32	
160	38.76	37.50		1.35	4.21	3.51	7.51	0.45	0.029	0.079	4.56	1.71	7.80	0	0.089	0.89	0.079
170R	29.36	36.0[illegible]		1.70	5.32	3.06	7.21	0.39	0.029	0.076	4.56	1.71	7.80	0	0.086	0.89	0.077
170¼	55.84	54.5[illegible]		1.58	2.12	4.22	10.91	0.59	0.059	0.11	4.56	1.71	7.80	0.03	0.13	0.89	0.12
170½	51.88	47.07	36.17	1.60	1.34	4.06	9.31	0.52	0.087	0.099	4.56	1.71	7.80	0.07	0.11	0.89	0.098
170¾	69.48	81.81	11.56	2.01	1.02	4.70	16.36	0.60	0.15	0.17	4.56	1.71	7.80	0.14	0.19	0.89	0.17
171	84.36	106.0[illegible]	6.78	2.50	0.65	5.18	21.21	0.66	0.25	0.22	4.56	1.71	7.80	0.24	0.25	0.89	0.22
A	119.04	165.9[illegible]		5.05	0.28	6.15	66.38	0.76	0.62	0.31	5.96	1.36	8.10	[illegible].59	0.79	.40	0.32
B				6.39					0.79		5.96	1.36	8.10	0.77		[illegible].40	
C	141.36	192.02	2.09	4.02	0.34	6.71	76.81	0.83	0.50	0.36	5.96	1.36	8.10	0.45	0.91	0.40	0.36
D				5.13					0.63		5.96	1.36	8.10	0.61		0.40	
E	84.36	106.17	2.00	2.51	0.50	5.18	42.58	0.64	0.31	0.20	5.96	1.36	8.10	0.	0.51	0.40	0.20
F	77.76	76.96	4.43	2.13	0.46	4.98	30.78	0.61	0.26	0.14	5.96	1.36	8.10	0.23	0.37	0.40	0.15
G	67.62			7.10		9.28		1.15	0.86		5.96	1.36	8.10	0.84		0.40	
H	36.76	44.76		7.66	0.22	2.92	17.91	0.36	0.95	0.084	5.96	1.36	8.10	0.94	0.21	0.40	0.084

C1

Data sheet C: Crater coefficients.

Hole no.	d_c (ft)	Δ	V/W	$K=V/N^3$	$K_s=V/wx^2a$	$A=V/V_o$	$K_r=r/N$	$K_h=h/N$	$K_c=c/N$	$K_{cw}=r_w/N$
Atlas 60 (2.5 lb): E = 5.96 N = 8.[illegible] B = 0.40 H/D = 1.0										
F	-1.89	0.23	30.78	[illegible]:4	0.46	0.37	0.61	0.26	0.63	0.039
E	-2.36	0.29	42.58	[illegible]	0.50	0.51	0.64	0.31	0.65	0.019
C	-3.61	0.45	76.81	[illegible]	[illegible]	0.91	0.83	0.50	[illegible]	[illegible]
A	-4.74	0.59	66.38	0.51	0	0.79	0.76	[illegible]	[illegible]	0.038
D	-4.94	0.61						[illegible]		[illegible]
B	-6.20	0.77						[illegible]		0.023
G	-6.80	0.84					1.15	0.88	1.67	0.037
H	-7.58	0.94	17.91	0.084	0.22	0.21	0.36	0.95	1.21	0.010
75	-8.61	1.06						1.11		[illegible]
Atlas 60 (5.0 lb): E = 5.96 N= 10.20 B = 0.55 C = 1.0										
108	-0.21	0.02	9.92	0.047	0.50	0.086	0.40	0.19	0.41	[illegible]
79	-0.40	0.04	16.40	0 077		0.14		0.14	0.48	0.10
78	-0.88	0.09	21.68	0.10		0.19	0.51	0.22	[illegible]	[illegible]
[illegible]	[illegible] 22	0.18	28.39	0.13	0.46	0.24	0.59	[illegible]	0.60	0.088
76	-3.80	0.37	55.39	0.26	0.42	0.48	0 69	0.46	0.79	0.088
74	-6.69	0.66	116.93	0.55	0.31	1.01	0.82	0 74	[illegible]	0.079
71	-8.14	0.80					0.65		[illegible]	
70	-10.09	0.99						[illegible]		0.14
Atlas 60 (10.0 lb). E = 5.86 N = 12.60 B = 0.54 C = 1.0										
154C	+2.15	-0.17	0.00							
154F	+2.15	-0.17	0.00							
110	0.00	0.00	6.36	0.032	0.69	0.059	0.23	0 13	0.40	0.. 3
107	-0.35	0.03	9.20	0.046	0.52	0.085	0.33	[illegible]	0.44	0.12
106	-0.62	0.05	20.29	0.10	0.75	0.19	0.45	[illegible]	0.48	0.16
113	-1.20	0.10	14.33	0.072	0.71	0 13	0.43	[illegible]	0.52	0.075
105	-2.31	0.18	22.43	0.11	0.48	0.21	0.51	[illegible]	0.58	0.099
115	-4.93	0.39	49.52	0.25	0.49	0.46	0.60	0.41	0.73	0.053
116	[illegible] 65	0 61	91.76	[illegible]	[illegible] 42	0.85	0.71	[illegible]	0.94	0.083*
72	-9.92	0 79	70.62	[illegible]		0.65	0.77		1.14	0.20
73	-12.10	0 96						1.06		0 10
Atlas [illegible] (20.0 lb): E = 5.65 N = 15.30 B = 0.50 C = 1.0										
95	-4.05	0.26	25.27	0.14	0.46	0.28	0.52	0.36	0.74	0.092
96R	-6.15	0.40	32.16	0 18	0.38	0 36	0 52	[illegible]	0 62	0.17
97	-7.46	0 49	59.01	0.33	0.45	0.66	0.60	0.65	0.76	0.17
99	-8.95	0.58	84.17	0.47	0.38	0.95	0.80	0.62	1.11	0.036
100	-10.10	0.66	97.21	0.54		1.09	0.64	0.73	1.05	0.072*
98	-12.01	0.78					0.64	[illegible] 32	1.0	0.34
Atlas 60 (40.0 lb): E = 5.41 N = 18.50 B = 0.38 C = 1.0										
104	-8.10	0.44	54.54	0.34	0.56	0.91	0.60	0 55	0 95	0.11
102	-12.16	0.66		0.30		0.78	0.73	0.71	[illegible] 09	0.051
103	-18.67	1.01						1 06		0.050
C-4 (2.5 lb). E = 4.19 N = 5.70 B = 1.29 C = 1.0										
8	-4.20	0.74	96.38	1.30	0.45	1 01	1 04	0 85	1.30	0.11
7	-5 97	1.05								
C-4 (5.0 lb). E = 4.56 N = 7.80 B = 0.89 C = 1.0										
170	0.00	0.00	7.51	0.079	0.72	0.089	0.45	0 17	0.45	0.029
170R	0.00	0.00	7.21	0.076	0.72	0.086	0.39	0 22	0.41	0.029
171	-0.23	0.03	10.91	0 11	[illegible].61	0 13	0.54	0.20	0 5	0 020
[illegible]	-0.46	0.07	9 31	0.099	0.56	0 11	0.52	0.21	0.5[illegible]	0.028
[illegible]	-0 96	0.14	16.56	0.17	0.58	0.19	0 [illegible]	0 26	0 65	0 021
1	-1.20	0.18	22.83	0.24	0.74	0.27	[illegible] 1	0 [illegible]	0.[illegible]	0 10
171	-1.65	0.24	21.21	0.22	0 56	0 25	[illegible] 01	0 32	0.73	0.035
2	-2.06	0.30	31.15	0.33	0.73	0.37	[illegible] 59	0.41	0.75	0.15
3	-3.73	0 55	31.57	0 33	[illegible] 41	0.39	[illegible] 64	0.63	[illegible].69	0.15
6	-5.34	0.79	73.13	0 77	0.59	0.85	0.79	0.79	1.15	[illegible] 10
4	-5 66	0.83					0 82		[illegible]	
5	-8.22	1.21								
C-4 (10.0 lb) E = 4.79 N = 10.30 B = 0.67 C 1 0										
154B	+2.15	[illegible] 21	0.00							
17	-0.32	0.03	10.95	0.10	0.69	0.15	0.54	0 16	[illegible].58	0 13
16	-0.6[illegible]	0.06	27.17	0 25	0.57	[illegible] 37	0.69	0 29	0 70	0.22
10	-1.51	0.15	17.57	0.16	0 74	0.24	0 50	0 28	0.60	0 14
11	-3.17	0.31	38.13	0.35	0.56	0.52	0.67	0 43	[illegible] 75	0 13
12	-5.20	0.50	44.87	0.41	0.46	0.61	0.69	0.56	0 88	0.087
13	-7 23	0 70	53 88	0 49	0.32	0 74	0 72	0.94	1.13	0.23
14	-8.59	0 83					0.68		1.12	
15	-10.30	1.00						1 13		0 13

*Estimated data

Data sheet C (cont'd).

Hole no.	d_c (ft)	Δ	V/W	$K=V/N^2$	$K_e=V/\pi r^2 h$	$A=V/V_e$	$K_r=r/N$	$K_h=h/N$	$K_c=c/N$	$K_{cv}=r_v/N$
C-4 (20.0 lb): E = 4.91 N = 13.30 B = 0.51 C = 1.0										
22	-0.83	0.002	7.77	0.06[illegible]	0.67	[illegible]	0.43	0.17	[illegible]	0.17
23	-0.38	0.03	12.10	0.1[illegible]	0.78	0.22	0.51	0.20	0.52	0.17
151	-0.83	0.06	16.95	0.[illegible]	0.42	0.28	0.54	0.[illegible]7	0.61	[illegible]51
152	-1.53	0.12	14.00	0.1[illegible]	0.5[illegible]	0.23	0.57	0.22	0.58	0.10
24	-2.37	0.18	23.53	0.20	0.[illegible]	0.39	0.64	0.29	0.75	0.12
25A	-2.92	0.22	25.85	0.22	[illegible].38	0.43	0.73	0.35	0.68	0.13
153	-2.94	0.22	19.80	0.17	[illegible].47	0.33	0.57	0.36	[illegible].68	0.14
25B	-4.05	0.30	35.97	0.31	0.53	0.59	0.64	0.45	0.74	0.14
26	-6.07	0.46	47.23	0.40	0.46	0.78	0.70	0.57	0.89	0.11
27	-8.17	0.62	60.[illegible]9	0.51	0.46	0.99	0.70	0.73	0.92	[illegible].[illegible]9
154	-9.33	0.70					0.78		1.22	
29	-12.98	0.98						1.07		[illegible].035
C-4 (40.0 lb): E = 5.00 N = 17.10 B = 0.32 C = 1.0										
157	-7.39	0.43								
15[illegible]	-[illegible].07	0.65	40.52	0.32	0.28	[illegible].00	0.73	0.70	0.93	0.049
156	-16.95	0.99								
Coalite 7S (2.5 lb): E = 4.41 N = 6.0 B = 0.83 C = 1.0										
88	-4.09	0.68	72.47	0.84	0.34	1.01	1.04	0.67	1.42	0.052
87	-5.97	0.99								
Coalite 7S (5.0 lb): E = 4.50 N = 7.70 B = 0.82 C = 1.0										
60	-0.32	0.04	12.87	0.14	0.[illegible]7	[illegible].17	0.54	0.[illegible]8	0.74	0.1[illegible]
61	-0.51	0.07	12.73	0.14	0.65	0.17	0.5[illegible]	0.24	0.81	0.17
62	-1.44	0.19	23.19	0.25	0.59	[illegible].31	0.[illegible]6	0.32	0.83	0.13
63	-2.48	0.32	[illegible]3.79	0.48	0.59	[illegible].58	0.[illegible]5	0.45	1.00	0.13
64	-3.84	0.50	55.16	0.60	0.54	0.73	0.79	0 57	1.08	0.071
90	-4.89	0.64	67.67	0.74	0.47	0.90	0.87	0.68*	1.08	0.040*
85	-7.28	0.95						1.06	1.23	0.12
Coalite 7S (10.0 lb): E = 4.51 N = [illegible].2 B = 0.80 C = 1.0										
153D	+2.15	-0.22	0.00							
65	-0.49	0.06	14.18	0.16	0.63	0.19	0.51	0.31	0.53	0.26
66	-0.92	0.10	18.17	0.20	0.44	0.25	0.59	0.41	0.60	0.32
67	-1.72	0.20	18.77	0.21	0.65	0.26	0.59	0.29	0.82	0.11
68	-3.39	0.39	28.56	0.31	0.45	0.39	0.72	0.43	0.81	0.077
120	-6.00	0.68	105.59	1.16	0.46	1.44	1.04	0.74	1.21	0.12
69	-7.01	0.80	19.29	0.21	0.18	0.26	0.66	0.86	0.97	0.14
86	-9.74	1.00						1.11		0.11
Coalite 7S (20.0 lb): E = 4.50 N = 12.20 B = 0.78 C = 1.0										
80	-0.55	0.05	6.25	0.069	0.81	0.089	0.42	0.16	0.56	0.11
81	-1.01	0.08	9.67	0.11	0.60	0.14	0.52	0.21	0.52	0.13
82	-2.21	0.18	18.53	0.20	0.54	0.26	0.62	0.32	0.74	0.14
83	-4.33	0.35	43.85	0.48	0.50	0.62	0.83	0.44	1.04	0.088
84	-7.80	0.64	66.66	0.73	0.49	0.95	0.81	0.73	1.06	0.074
89	-12.19	1.00						1.13*		0.13 *
Coalite 5S (2.5 lb): E = 3.98 N = 5.41 B = 1.14 C = 1.0										
30	-0.23	0.04	7.38	0.12	0.82	0.10	0.50	0.18	0.92	0.13
31	-0.48	0.09	4.70	0.074	0.57	0.065	0.47	0.18	0.55	0.096
38	-0.54	0.10	8.02	0.13	0.54	0.11	0.64	0.18	0.67	0.085
37	-1.09	0.20	10.55	0.17	0.53	0.15	0.58	0.30	0.83	0.094
32	-1.27	0.23	12.04	0.19	0.53	0.17	0.61	0.30	0.72	0.070
[illegible]	-1.74	0.32	23.28	0.37	0.59	0.32	0.71	0.40	1.1[illegible]	0.076
33	-2.52	0.47	21.18	0.33	0.42	0.29	0.76	0.51	0.[illegible]8	0.046
39	-3.44	0.64	70.20	1.11	0.59	0.98	[illegible]	0 7[illegible]	1.5[illegible]	0.094
34	-4.38	0.81	25.14	0.40	0.42	0.35	0.77	0 51	1.16	
35	-5.74	1.06								
Coalite 5S (5.0 lb): E = 4.21 N = 7.20 B = 0.91 C = 1.0										
40	[illegible].38	0.05	8.36	0.11	1.17	0.12	0.47	0.14	0.[illegible]4	0.086
41	-1.0[illegible]	0.1[illegible]	13.80	0.1[illegible]	0.54	0.20	0.63	0.2[illegible]	[illegible].[illegible]5	0.13
42	1.39	0.19	12.32	0.17	0.50	0.18	0.58	0.[illegible]1	0.79	0.11
43	[illegible].48	0.48	24.63	0.33	0.41	0.36	0.70	0.[illegible]2	0.88	0.039
44	-4.88	[illegible].63	63.20	0.85	0.43	0.93	0.92	0.74	[illegible].19	0.058
45	-6.90	0.96						1.04	1.29	0.033
Coalite 5S (10.0 lb): E = 4.28 N = 9.20 B = 0.81 C = 1.0										
154E	+2.15	-0.23	0.00							
46	-0.44	0.05	6.60	0.085	0.52	0.10	0.49	0.20	0.48	0.15
47	-0.72	0.08	8.03	0.10	0.51	0.13	0.53	0.22	0.54	0.14
48	-1.36	0.15	26.03	0.33	0.67	0.41	0.75	0.28	0.84	0 13
49	-2.74	0.30	22.26	0.29	0.49	0.35	0.68	0.40	0.83	0.11
50	-6.13	0.67	68.0[illegible]	0.87	0.48	1.08	0.93	0.67	1.15	0.05
51	-9.07	0.99						1.10		[illegible].11

*Estimated data

C3

Data sheet C (cont'd).

Hole no.	d_c(ft)	Δ	V/W	$K=V/N^3$	$K_s=V/\pi x^2 h$	$A=V/V_o$	$K_r=r/N$	$K_h=h/N$	$K_c=c/N$	$K_{cv}=r_v/N$
Coalite 5S (20.0 lb):		E = 4.28		N = 11.60		B = 0.71	C = 1.0			
52	-0.54	0.05	7.49	0.006	0.79	0.13	0.45	0.19	0.66	0.14
53	-0.93	0.08	10.17	0.13	0.57	0.18	0.62	0.19	0.61	.1
54	-1.79	0.15	12.19	0.16	0.59	0.22	0.57	0.26	0.63	0.10
55	-3.69	0.31	25.19	0.32	0.47	0.45	0.73	0.43	0.82	0.11
56	-7.73	0.67	57.20	0.73	0.43	1.03	0.85	0.76	1.11	0.022
57	-11.46	0.99						1.01	1.59	0.021

Data sheet D: Seismic data.

Blast and jug no.	W (lb)	λ_c Scaled charge depth	$\lambda = \sqrt[3]{W}$	R Jug distance (ft)	$\frac{R}{\lambda}$	Velocity to jug (ft/sec)	Frequency* (cps) L	V	T	$\frac{R}{N}$
Military explosive C-4										
1 - 1	5.0	0.70	1.71	228	133	9,[illegible]		100		29.2
1 - 2	"	"	"	228	133	8,140			100	29.2
1 - 3	"	"	"	228	133	9,910	100			29.2
1 - 4	"	"	"	171	100	9,500		125		21.9
1 - 5	"	"	"	171	100	9,500			143	21.9
1 - 6	"	"	"	171	100	9,500	200			21.9
2 - 1	"	1.20	"	228	133	10,360		167		29.2
2 - 2	"	"	"	228	133	10,360			[illegible]	29.2
2 - 3	"	"	"	228	133	10,360	167			29.2
2 - 4	"	"	"	171	100	10,060		167		21.9
2 - 5	"	"	"	171	100	10,060			125	21.9
2 - 6	"	"	"	171	100	10,690	143			21.9
3 - 1	"	2.18	"	228	133	10,360		100		29.2
3 - 2	"	"	"	228	133	9,500			91	29.2
3 - 3	"	"	"	228	133	9,910	111			29.2
3 - 4	"	"	"	171	100	9,500		143		21.9
3 - 5	"	"	"	171	100	9,500			83	21.9
3 - 6	"	"	"	171	100	10,060	100			21.9
4 - 1	"	3.30	"	385	225					49.4
4 - 2	"	"	"	385	225					49.4
4 - 3	"	"	"	385	225					49.4
4 - 4	"	"	"	342	200					43.8
4 - 5	"	"	"	342	200					43.8
4 - 6	"	"	"	342	200					43.8
5 - 1	"	4.82	"	385	225			100		49.4
5 - 2	"	"	"	385	225				111	49.4
5 - 3	"	"	"	385	225		167			49.4
5 - 4	"	"	"	342	200			200		43.8
5 - 5	"	"	"	342	200				125	43.8
5 - 6	"	"	"	342	200		333			43.8
7 - 1	2.5	3.49	1.36	272	200	10,880		125		47.7
7 - 2	"	"	"	272	200	9,710			125	47.7
7 - 3	"	"	"	272	200	10,460	167			47.7
7 - 4	"	"	"	306	225	10,550		200		53.7
7 - 5	"	"	"	306	225	10,200			143	53.7
7 - 6	"	"	"	306	225	10,550	143			53.7
8 - 1	"	3.09	"	272	200	10,460		143		57.7
8 - 2	"	"	"	272	200	10,070			125	57.7
8 - 3	"	"	"	272	200	10,460	125			57.7
8 - 4	"	"	"	306	225	10,930		167		53.7
8 - 5	"	"	"	306	225	10,200			111	53.7
8 - 6	"	"	"	306	225	10,930	143			53.7
10 - 1	5.0	0.88	1.71	288	168	9,930		91		28.0
10 - 2	"	"	"	288	168	9,930			111	28.0
10 - 3	"	"	"	288	168	9,930	167			28.0
10 - 4	"	"	"	216	126	9,818		200		21.0
10 - 5	"	"	"	216	126	9,818			250	21.0
10 - 6	"	"	"	216	126	10,290	25			21.0
11 - 1	10.0	1.47	2.15	486	226	10,800		91		47.2
11 - 2	"	"	"	486	226	10,125			125	47.2
11 - 3	"	"	"	486	226	10,565	125			47.2
11 - 4	"	"	"	432	200	10,540		[illegible]		41.9
11 - 5	"	"	"	432	200	10,290			77	41.9
11 - 6	"	"	"	432	200	10,540	[illegible]			41.9
12 - 1	"	2.42	"	288	134	9,[illegible]30		143		28.0
12 - 2	"	"	"	288	134	9,600			111	28.0
12 - 3	"	"	"	288	134	10,290	125			28.0
12 - 4	"	"	"	216	100	10,290		143		21.0
12 - 5	"	"	"	216	100	9,820			77	21.0
12 - 6	"	"	"	216	100	10,290	100			21.0
13 - 1	"	3.36	"	486	226	10,800		167		47.2
13 - 2	"	"	"	486	226	10,570			200	47.2
13 - 3	"	"	"	486	226	11,050	200			47.2
13 - 4	"	"	"	432	200	11,080		167		41.9
13 - 5	"	"	"	432	200	10,800			250	41.9
13 - 6	"	"	"	432	200	11,080	143			41.9

*Avg of first five pulses

Data Sheet D: (cont'd)

Blast and jug no.	W (lb)	λ_c Scaled charge depth	$\lambda = \sqrt[3]{W}$	R Jug distance (ft)	$\frac{R}{\lambda}$	Velocity to jug (ft/sec)	Frequency* (cps) L	Frequency* (cps) V	$\frac{R}{N}$
Military explosive C-4 (cont'd)									
14 - 1	10.0	4.0	2.15	486	226	11,3[illegible]		143	47.2
14 - 2	"	"	"	486	226	11,050		125	47.2
14 - 3	"	"	"	486	226	11,300	167		47.2
14 - 4	"	"	"	432	200	11,080		200	41.9
14 - 5	"	"	"	432	200	10,800		250	41.9
14 - 6	"	"	"	432	200	11,370	125		41.9
15 - 1	"	4.78	"	486	226	11,050		100	47.2
15 - 2	"	"	"	486	226	11,050		[illegible]	47.2
15 - 3	"	"	"	486	226	11,050	143		47.2
15 - 4	"	"	"	432	200	11,370		250	41.9
15 - 5	"	"	"	432	200	11,080		111	41.9
15 - 6	"	"	"	432	200	11,080	125		41.9
24 - 1	20.0	0.87	2.71	610	225	10,890		77	45.9
24 - 2	"	"	"	610	225	10,520		83	45.9
24 - 3	"	"	"	610	225	10,890	83		45.9
24 - 4	"	"	"	542	200	10,630		200	40.8
24 - 5	"	"	"	542	200	10,840		167	40.8
24 - 6	"	"	"	542	200	10,630	67		40.8
25A - 1	"	1.08	"	610	225	10,890		91	45.9
25A - 2	"	"	"	610	225	10,520		83	45.9
25A - 3	"	"	"	610	225	10,890	200		45.9
25A - 4	"	"	"	542	200	10,840		91	40.8
25A - 5	"	"	"	542	200	10,630		100	40.8
25A - 6	"	"	"	542	200	10,840	167		40.8
25B - 1	"	1.48	"	610	225	10,890			45.9
25B - 2	"	"	"	610	225	10,890			45.9
25B - 3	"	"	"	610	225	11,090			45.9
25B - 4	"	"	"	542	200	10,840			40.8
25B - 5	"	"	"	542	200	10,630			40.8
25B - 6	"	"	"	542	200	11,060			40.8
26 - 1	"	2.24	"	610	225	10,890		77	45.9
26 - 2	"	"	"	610	225	10,340		71	45.9
26 - 3	"	"	"	610	225	10,890	167		45.9
26 - 4	"	"	"	542	200	10,840		125	40.8
26 - 5	"	"	"	542	200	10,040		100	40.8
26 - 6	"	"	"	542	200	10,840	200		40.8
26B - 1	"	1.50	"	610	225	10,520		91	45.9
26B - 2	"	"	"	610	225	10,340		91	45.9
26B - 3	"	"	"	610	225	10,520	100		45.9
26B - 4	"	"	"	542	200	10,630		83	40.8
26B - 5	"	"	"	542	200	10,630		91	40.8
26B - 6	"	"	"	542	200	10,840	200		40.8
29 - 1	"	4.78	"	542	200	11,060		100	40.8
29 - 2	"	"	"	542	200	10,840		143	40.8
29 - 3	"	"	"	542	200	11,060	83		40.8
29 - 4	"	"	"	610	225	11,300		71	45.9
29 - 5	"	"	"	610	225	11,090		111	45.9
29 - 6	"	"	"	610	225	11,300	125		45.9
Coalite 5S									
30 - 1	2.5	0.19	1.36	272	200				50.3
30 - 2	"	"	"	272	200				50.3
30 - 3	"	"	"	272	200				50.3
30 - 4	"	"	"	306	225				56.6
30 - 5	"	"	"	306	225				56.6
30 - 6	"	"	"	306	225				56.6
31 - 1	"	0.32	"	272	200	10,460		200	50.3
31 - 2	"	"	"	272	200	10,460		167	50.3
31 - 3	"	"	"	272	200	10,460	250		50.3
31 - 4	"	"	"	306	225	10,200		200	56.6
31 - 5	"	"	"	306	225	10,200		200	56.6
31 - 6	"	"	"	306	225	10,930	200		56.6
32 - 1	"	0.93	"	272	200	10,070		143	50.3
32 - 2	"	"	"	272	200	9,710		125	50.3
32 - 3	"	"	"	272	200	10,070	200		50.3

*Avg of first five pulses

Data Sheet D: (cont'd)

Blast and jug no.	W (lb)	λ_c Scaled charge depth	$\lambda = \sqrt[3]{W}$	R Jug distance (ft)	$\frac{R}{\lambda}$	Velocity to jug (ft/sec)	Frequency* (cps) L	V	T	$\frac{R}{\sqrt{W}}$
Coalite 5S (cont'd)										
32 - 4	2.5	0.93	1.36	306	225	10,200		167		56.6
32 - 5	"	"	"	306	225	10,200			143	56.6
32 - 6	"	"	"	306	225	10,200	167			56.6
34 - 1	"	3.22	"	272	200			125		50.3
34 - 2	"	"	"	272	200				125	50.3
34 - 3	"	"	"	272	200		125			50.3
34 - 4	"	"	"	306	225			200		56.6
34 - 5	"	"	"	306	225				100	56.6
34 - 6	"	"	"	306	225		100			56.6
36 - 1	"	1.28	"	272	200	10,880		200		50.3
36 - 2	"	"	"	272	200	10,070			125	50.3
36 - 3	"	"	"	272	200	10,880	200			50.3
36 - 4	"	"	"	306	225	10,930		200		56.6
36 - 5	"	"	"	306	225	10,200			125	56.6
36 - 6	"	"	"	306	225	10,930	143			56.6
37 - 1	"	0.80	"	272	200	10,460		143		50.3
37 - 2	"	"	"	272	200	10,460			167	50.3
37 - 3	"	"	"	272	200	10,880	143			50.3
37 - 4	"	"	"	306	225	10,930		167		56.6
37 - 5	"	"	"	306	225	10,200			167	56.6
37 - 6	"	"	"	306	225	10,550	125			56.6
40 - 1	5.0	0.22	1.71	342	200	10,360		200		47.5
40 - 2	"	"	"	342	200	10,360			167	47.5
40 - 3	"	"	"	342	200	10,690	200			47.5
40 - 4	"	"	"	385	225	10,690		250		53.5
40 - 5	"	"	"	385	225	10,130			143	53.5
40 - 6	"	"	"	385	225	10,690	200			53.5
50 - 1	20.0	0.20	2.71	542	200	10,840		125		46.7
52 - 2	"	"	"	542	200	10,840			100	46.7
52 - 3	"	"	"	542	200	11,060	143			46.7
52 - 4	"	"	"	610	225	11,090		200		52.6
52 - 5	"	"	"	610	225	10,700			111	52.6
52 - 6	"	"	"	610	225	11,090	111			52.6
53 - 1	"	0.34	"	542	200	10,840		1.5		46.7
53 - 2	"	"	"	542	200	10,630			125	46.7
53 - 3	"	"	"	542	200	11,060	143			46.7
53 - 4	"	"	"	610	225	10,890		200		52.6
53 - 5	"	"	"	610	225	10,700			111	52.6
53 - 6	"	"	"	610	225	10,890	111			52.6
54 - 1	"	0.66	"	542	200	11,060		125		46.7
54 - 2	"	"	"	542	200	10,230			91	46.7
54 - 3	"	"	"	542	200	10,840	125			46.7
54 - 4	"	"	"	610	225	10,890		125		52.6
54 - 5	"	"	"	610	225	10,700			100	52.6
54 - 6	"	"	"	610	225	10,890	91			52.6
55 - 1	"	1.36	"	542	200	10,840		111		46.7
55 - 2	"	"	"	542	200	10,630			111	46.7
55 - 3	"	"	"	542	200	10,840	125			46.7
55 - 4	"	"	"	610	225	11,090		100		52.6
55 - 5	"	"	"	610	225	10,890			100	52.6
55 - 6	"	"	"	610	225	11,090	111			52.6
57 - 1	"	4.23	"	880	325	10,350				75.9
57 - 2	"	"	"	813	300	10,560				70.1
57 - 3	"	"	"	745	275	10,490				64.4
57 - 4	"	"	"	677	250	10,920				58.4
57 - 5	"	"	"	610	225	11,090				52.6
57 - 6	"	"	"	542	200	10,840				46.7
Coalite 7S										
60 - 1	5.0	0.19	1.71	385	225	11,000		143		50.1
60 - 2	"	"	"	385	225	10,694			125	50.0
60 - 3	"	"	"	385	225	11,000	143			50.0
60 - 4	"	"	"	342	200	10,690		167		44.4
60 - 5	"	"	"	342	200	10,360			143	44.4
60 - 6	"	"	"	342	200	10,690	200			44.4

*Avg of first five pulses

Data Sheet D: (Cont'd)

Blast and jug no.	W (lb)	ℓ_c Scaled charge depth	$\lambda = \sqrt[3]{W}$	R Jug distance (ft)	$\frac{R}{\sqrt{}}$	Velocity to jug (ft/sec)	Frequency* (cps) L	V	T	$\frac{R}{N}$
Coalite 7S (cont'd)										
61 - 1	5.0	0.30	1.71	385	225	10,405		143		50.0
61 - 2	"	"	"	385	225	10,405			125	50.0
61 - 3	"	"	"	385	225	10,405	167			50.0
61 - 4	"	"	"	342	200	10,360		125		44.4
61 - 5	"	"	"	342	200	10,060			125	44.4
61 - 6	"	"	"	342	200	10,360	167			44.4
62 - 1	"	0.84	"	385	225	10,405		111		50.0
62 - 2	"	"	"	385	225	9,870				50.0
62 - 3	"	"	"	385	225	10,405	143			50.0
62 - 4	"	"	"	342	200	10,360		167		44.4
62 - 5	"	"	"	342	200	9,770			125	44.4
62 - 6	"	"	"	342	200	10,690	91			44.4
64 - 1	"	2.25	"	385	225	11,000		111		50.0
64 - 2	"	"	"	385	225	9,870			143	50.0
64 - 3	"	"	"	385	225	11,000	143			50.0
64 - 4	"	"	"	342	200	10,690		250		44.4
64 - 5	"	"	"	342	200	10,360			91	44.4
64 - 6	"	"	"	342	200	11,030	111			44.4
65 - 1	10.0	0.43	2.15	486	226	10,570		91		50.1
65 - 2	"	"	"	486	226	10,570			111	50.1
65 - 3	"	"	"	486	226	10,570	167			50.1
65 - 4	"	"	"	432	200	10,540		167		44.5
65 - 5	"	"	"	432	200	10,540			143	44.5
65 - 6	"	"	"	432	200	10,800	167			44.5
66 - 1	"	0.43	"	486	226	10,800		111		50.1
66 - 2	"	"	"	486	226	10,570			125	50.1
66 - 3	"	"	"	486	226	10,570	167			50.1
66 - 4	"	"	"	432	200	10,800		200		44.5
66 - 5	"	"	"	432	200	10,800			143	44.5
66 - 6	"	"	"	432	200	10,800	167			44.5
67 - 1	"	0.80	"	486	226	10,570		111		50.1
67 - 2	"	"	"	486	226	10,570			143	50.1
67 - 3	"	"	"	486	226	10,570	143			50.1
67 - 4	"	"	"	432	200	10,540		111		44.5
67 - 5	"	"	"	432	200	10,540			143	44.5
67 - 6	"	"	"	432	200	10,540	111			44.5
68 - 1	"	1.57	"	486	226	10,570		125		50.1
68 - 2	"	"	"	486	226	10,570			125	50.1
68 - 3	"	"	"	486	226	10,340	167			50.1
68 - 4	"	"	"	432	200	10,290		143		44.5
68 - 5	"	"	"	432	200	10,290			111	44.5
68 - 6	"	"	"	432	200	10,540	111			44.5
69 - 1	"	0.63	"	486	226	10,800				50.1
69 - 2	"	"	"	486	226	10,570				50.1
69 - 3	"	"	"	486	226	10,800				50.1
69 - 4	"	"	"	432	200	10,540				44.5
69 - 5	"	"	"	432	200	10,290				44.5
69 - 6	"	"	"	432	200	10,540				44.5
Atlas 60										
71 - 1	5.0	4.76	1.71	385	225	11,000		143		37.7
71 - 2	"	"	"	385	225	10,400			100	37.7
71 - 3	"	"	"	385	225	11,000	125			37.7
71 - 4	"	"	"	342	200	11,030		167		33.5
71 - 5	"	"	"	342	200	10,690			125	33.5
71 - 6	"	"	"	342	200	11,030	77			33.5
72 - 1	10.0	4.62	2.15	486	226	11,050		143		38.6
72 - 2	"	"	"	486	226	10,800			83	38.6
72 - 3	"	"	"	486	226	11,050	143			38.6
72 - 4	"	"	"	432	200	10,800		125		34.3
72 - 5	"	"	"	432	200	10,800			125	34.3
72 - 6	"	"	"	432	200	11,080	67			34.3
74 - 1	5.0	3.90	1.71	342	200	10,360		91		33.5
74 - 2	"	"	"	342	200	10,690			100	33.5
74 - 3	"	"	"	342	200	10,360	100			33.5

*Avg of first five pulses

Data Sheet D: (cont'd)

Blast and jug no.	W (lb)	λ_c Scaled charge depth	$\lambda = \sqrt[3]{W}$	R Jug distance (ft)	$\frac{R}{\lambda}$	Velocity to jug (ft/sec)	Frequency* (cps) L	V	T	$\frac{R}{\sqrt{W}}$
Atlas 60 (cont'd)										
74 - 4	5.0	3.90	1.71	385	225	10,405		200		37.7
74 - 5	"	"	"	385	225	10,130			77	37.7
74 - 6	"	"	"	385	225	10,690	100			37.7
75 - 1	2.5	6.33	1.36	272	200	10,070		100		33.6
75 - 2	"	"	"	272	200	9,710			111	33.6
75 - 3	"	"	"	272	200	9,710	125			33.6
75 - 4	"	"	"	306	225	10,200		200		37.8
75 - 5	"	"	"	306	225	9,870			111	37.8
75 - 6	"	"	"	306	225	10,200	143			37.8
Coalite 7S										
83 - 1	20.0	0.20	2.71	542	200	11,290		111		44.4
83 - 2	"	"	"	542	200	10,840			100	44.4
83 - 3	"	"	"	542	200	11,060	167			44.4
83 - 4	"	"	"	610	225	11,090		250		50.0
83 - 5	"	"	"	610	225	10,890			100	50.0
83 - 6	"	"	"	610	225	11,090	100			50.0
87 - 1	2.5	7.17	1.36	272	200	10,460		143		45.3
87 - 2	"	"	"	272	200	10,070			111	45.3
87 - 3	"	"	"	272	200	10,460	125			45.3
87 - 4	"	"	"	306	225	10,200		143		51.0
87 - 5		"	"	306	225	9,870			125	51.0
87 - 6	"	"	"	306	225	10,550	111			51.0
90 - 1	5.0	2.86	1.71	342	200	11,032		125		44.4
90 - 2	"	"	"	342	200	10,690			125	44.4
90 - 3	"	"	"	342	200	10,690	125			44.4
90 - 4	"	"	"	385	225	10,690		250		50.0
90 - 5	"	"	"	385	225	10,405			167	50.0
90 - 6	"	"	"	385	225	10,405	111			50.0
Atlas 60										
95 - 1	20.0	1.88	2.15	362	168					23.7
95 - 2	"	"	"	362	168					23.7
95 - 3	"	"	"	362	168					23.7
95 - 4	"	"	"	271	126					17.7
95 - 5	"	"	"	271	126					17.7
95 - 6	"	"	"	271	126					17.7
96 - 1	"	2.98	"	362	168	10,340		83		23.7
96 - 2	"	"	"	362	168	8,420			59	23.7
96 - 3	"	"	"	362	168		111			23.7
96 - 4	"	"	"	271	126	10,040		111		17.7
96 - 5	"	"	"	271	126	10,040			91	17.7
96 - 6	"	"	"	271	126	10,040				17.7
97 - 1	"	3.47	"	362	168	11,310				23.7
97 - 2	"	"	"	362	168	10,650				23.7
97 - 3	"	"	"	362	168	11,310				23.7
97 - 4	"	"	"	271	126	10,840				17.7
97 - 5	"	"	"	271	126	10,040				17.7
97 - 6	"	"	"	271	126	10,840				17.7
98 - 1	"	5.58	"	610	284	11,300		125		39.9
98 - 2	"	"	"	610	284	11,090			111	39.9
98 - 3	"	"	"	610	284	11,300	111			39.9
98 - 4	"	"	"	542	252	11,290		125		35.4
98 - 5	"	"	"	542	252	11,060			125	35.4
98 - 6	"	"	"	542	252	11,300	100			35.4
99 - 1	"	4.17	"	542	252	11,290		143		35.4
99 - 2	"	"	"	542	252	11,840			111	35.4
99 - 3	"	"	"	542	252	11,060	167			35.4
99 - 4	"	"	"	610	284	11,300		200		39.9
99 - 5	"	"	"	610	284	11,090			100	39.9
99 - 6	"	"	"	610	284	11,300	111			39.9
100 - 1	"	4.70	"	542	252	11,060				35.4
100 - 2	"	"	"	610	284	11,300				39.9
100 - 3	"	"	"	677	315	11,280				44.2
100 - 4	"	"	"	745	347	11,120				48.7
100 - 5	"	"	"	813	378	11,140				53.1
100 - 6	"	"	"	880	409	11,430				57.5

*Avg of first five pulses

Data Sheet D: (cont'd)

Blast and jug no.	W (lb)	λ_c Scaled charge depth	$\lambda = \sqrt[3]{W}$	R Jug distance (ft)	$\frac{R}{\lambda}$	Velocity to jug (ft/sec)	Frequency* (cps) L	V	T	$\frac{R}{N}$
Atlas 60 (cont'd)										
101 - 1	20.0	6.72	2.15	548	255	11,180				35.8
101 - 2	"	"	"	615	286	11,180				40.2
101 - 3	"	"	"	683	318	11,380				44.6
101 - 4	"	"	"	750	349	11,190				49.0
101 - 5	"	"	"	816	380	11,330				53.3
101 - 6	"	"	"	884	411	11,480				57.8
102 - 1	40.0	3.55	3.42	684	200	11,210		100		37.
102 - 2	"	"	"	684	200	11,030			[illegible]	37.0
102 - 3	"	"	"	684	200	11,210	250			37.0
102 - 4	"	"	"	770	225	11,490		250		41.6
102 - 5	"	"	"	770	225	11,320			250	41.6
102 - 6	"	"	"	770	225	11,490	250			41.6
103 - 1	"	5.46	"	684	200	11,210		91		37.0
103 - 2	"	"	"	684	200	10,860			83	37.0
103 - 3	"	"	"	684	200	11,030	500			37.0
103 - 4	"	"	"	770	225	11,320		333		41.6
103 - 5	"	"	"	770	225	11,160			125	41.6
103 - 6	"	"	"	770	225	11,320	83			41.6
104 - 1	"	2.37	"	684	200	11,030		111		37.0
104 - 2	"	"	"	684	200	10,690			91	37.0
104 - 3	"	"	"	684	200	11,030	250			37.0
104 - 4	"	"	"	770	225	11,160		250		41.6
104 - 5	"	"	"	770	225	11,000			200	41.6
104 - 6	"	"	"	770	225	11,160	167			41.6
Military explosive C-4										
154 - 1	20.0	4.34	2.15	542	252	11,290				40.8
154 - 2	"	"	"	610	284	11,300				45.9
154 - 3	"	"	"	677	315	11,280				50.9
154 - 4	"	"	"	745	347	11,290				56.0
154 - 5	"	"	"	813	378	11,450				61.1
154 - 6	"	"	"	880	409	11,580				66.2
154B - 1	10.0	1.25	1.71	432	253	14,400		125		41.9
154B - 2	"	"	"	432	253	10,050			167	41.9
154B - 3	"	"	"	432	253	14,400	200			41.9
154B - 4	"	"	"	486	284	11,300		143		47.2
154B - 5	"	"	"	486	284	9,530			250	47.2
154B - 6	"	"	"	486	284	11,300	125			47.2
154C - 1	"	"	"	432	253	11,370		125		34.3
154C - 2	"	"	"	432	253	10,290			125	34.3
154C - 3	"	"	"	432	253	11,080	200			34.3
154C - 4	"	"	"	486	284	11,300		143		47.2
154C - 5	"	"	"	486	284	9,530			167	47.2
154C - 6	"	"	"	486	284	11,300	125			47.2
	"									
Coalite 7S										
154D - 1	10.0	1.25	1.71	432	253	11,080				44.5
154D - 2	"	"	"	432	253	10,540				44.5
154D - 3	"	"	"	432	253	10,800				44.5
154D - 4	"	"	"	486	284	10,800				50.1
154D - 5	"	"	"	486	284	10,340				50.1
154D - 6	"	"	"	486	284	11,050				50.1
Coalite 5S										
154E - 1	10.0	1.25	1.71	432	253	11,080		250		47.0
154E - 2	"	"	"	432	253	9,820			143	47.0
154E - 3	"	"	"	432	253	10,800	250			47.0
154E - 4	"	"	"	486	284	10,570		250		52.8
154E - 5	"	"	"	486	284	9,920			250	52.8
154E - 6	"	"	"	486	284	11,300	333			52.8
Military explosive C-4										
156 - 1	40.0	4.96	3.42	684	200	11,210		143		40.0
156 - 2	"	"	"	684	200	11,030			111	40.0
156 - 3	"	"	"	684	200	11,210	167			40.0
156 - 4	"	"	"	770	225	11,320		250		45.0

* Avg of first five pulses

Blast and jug no.	W (lb)	λ_c Scaled charge depth	$\lambda = \sqrt[3]{W}$	R Jug distance (ft)	$\frac{R}{\lambda}$	Velocity to jug (ft/sec)	Frequency* (cps) L	V	T	$\frac{R}{N}$
Military explosive C-4 (cont'd)										
156 - 5	40.0	4.96	3.42	770	225	11,000			111	45.0
156 - 6	"	"	"	770	225	11,490	100			45.9
171 - 1	5.0	0.96	1.71	486	284	14,290		167		62.3
171 - 2	"	"	"	486	284	14,730				62.3
171 - 3	"	"	"	486	284	13,890	200			62.3
171 - 4	"	"	"	432	253	13,940		167		55.4
171 - 5	"	"	"	432	253	12,710			167	55.4
171 - 6	"	"	"	432	253	13,940	143			55.4

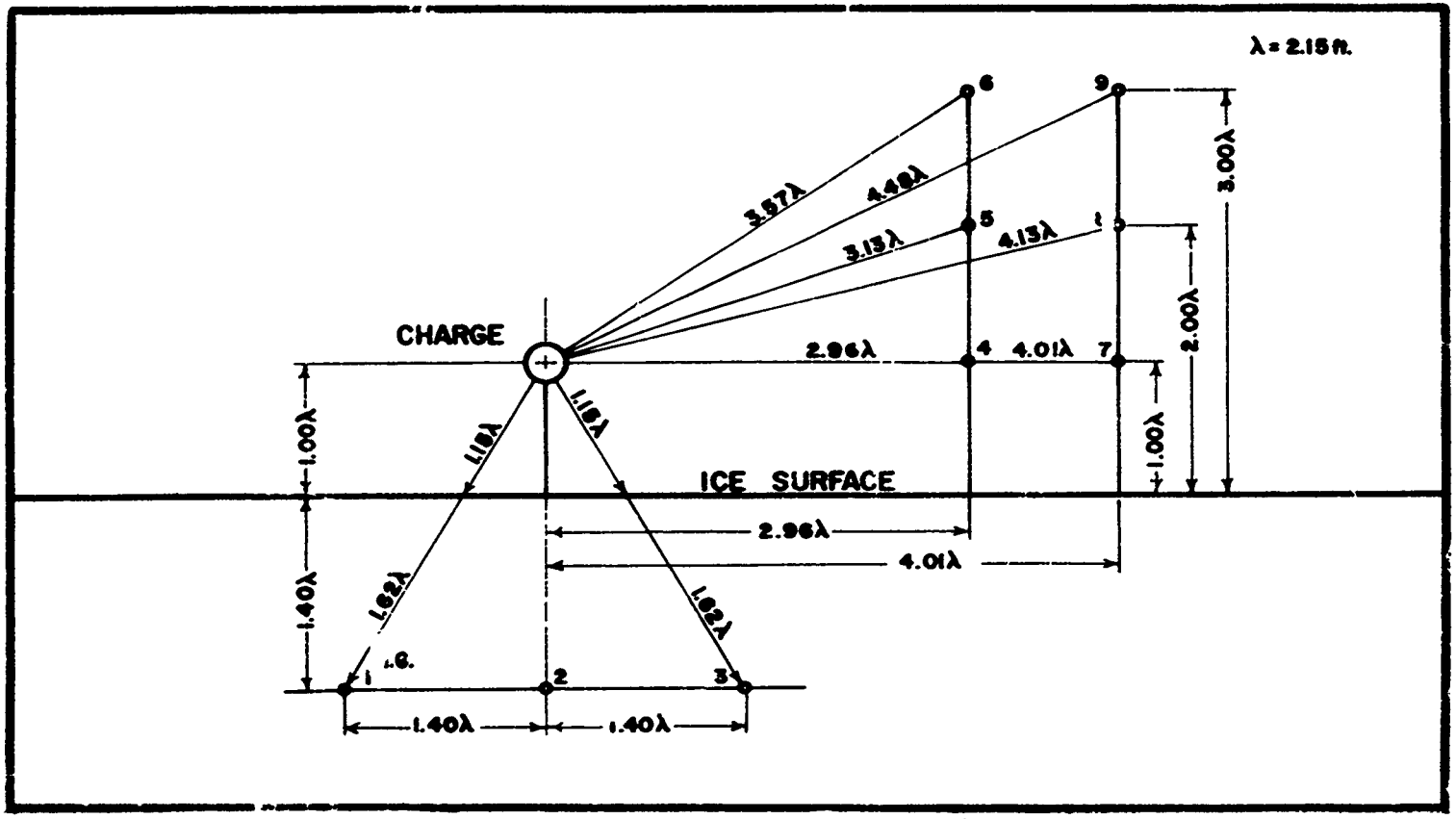

Figure A1. Blast no. 154F - 10 lb Atlas 60.

Gage	Shock velocity charge to gage (ft/sec)	Positive duration (ms)	Positive impulse (lb-ms/in)	Maximum pressure (psi)	Gage	Shock velocity charge to gage (ft/sec)	Positive duration (ms)	Positive impulse (lb-ms/in)	Maximum pressure (psi)
2					7	4,892	1.700	41	56
3	11,977	1.760	51	90	8	4,289	2.510	39	53
4	10,276	4.720	213	108	9	4,259	6.890	92	45
5	6,057	2.590	102	52	NG1	4,484	2.260	46	32
6	5,554	4.260	77	53					

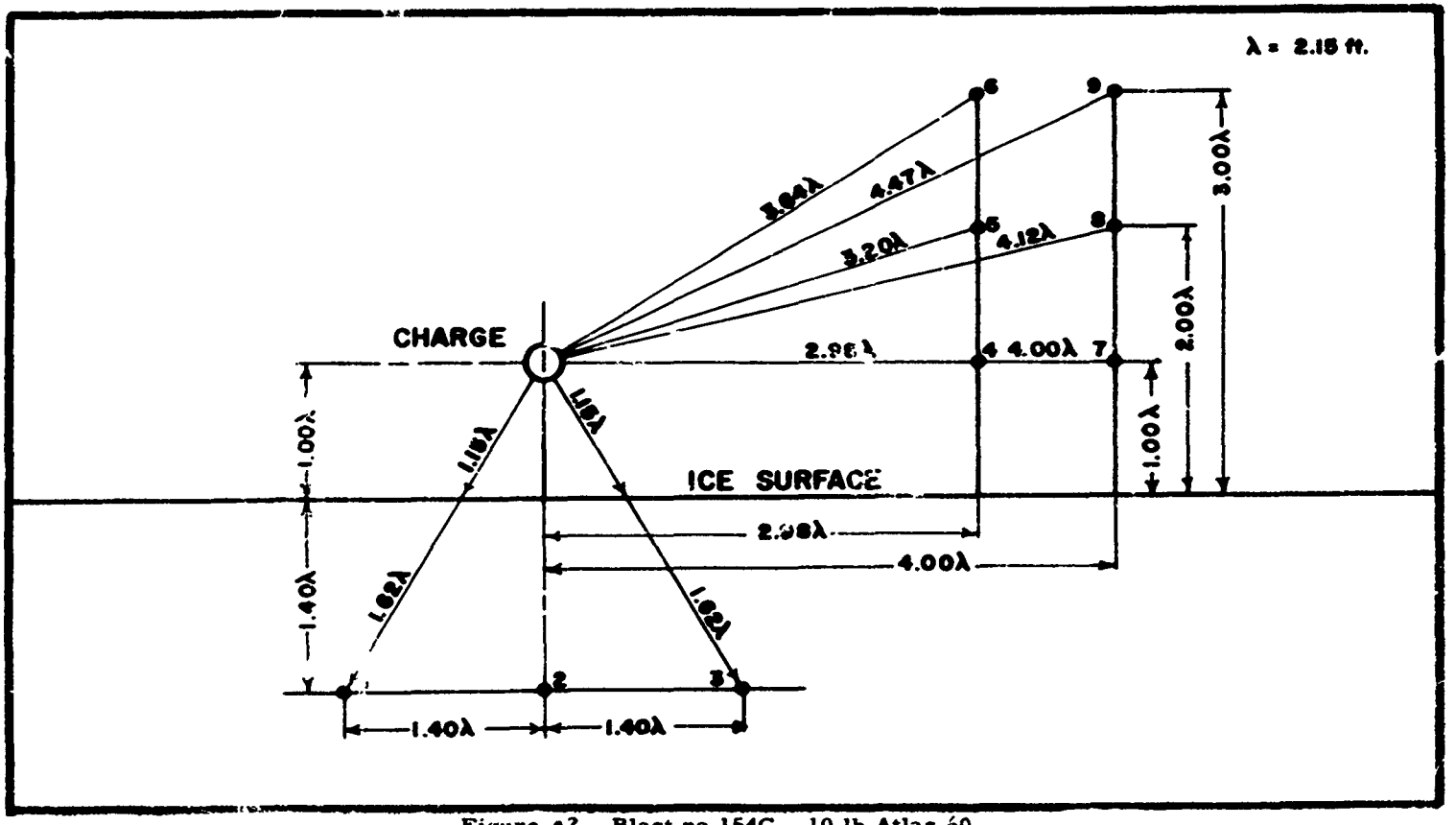

Figure A2. Blast no 154C - 10 lb Atlas 60.

Gage	Shock velocity charge to gage (ft/sec)	Positive duration (ms)	Positive impulse (lb-ms/in)	Maximum pressure (psi)	Gage	Shock velocity charge to gage (ft/sec)	Positive duration (ms)	Positive impulse (lb-ms/in)	Maximum pressure (psi)
1	11,686	5.100	204	142	6	4,099	2.050	41	24
2	10,239			155	7	3,568	1.660	26	47
3	10,456			78	8	3,903	1.890	20	21
4	5,190			76	9	3,258	2.420	60	56
5	4,785	1.840	22	38					

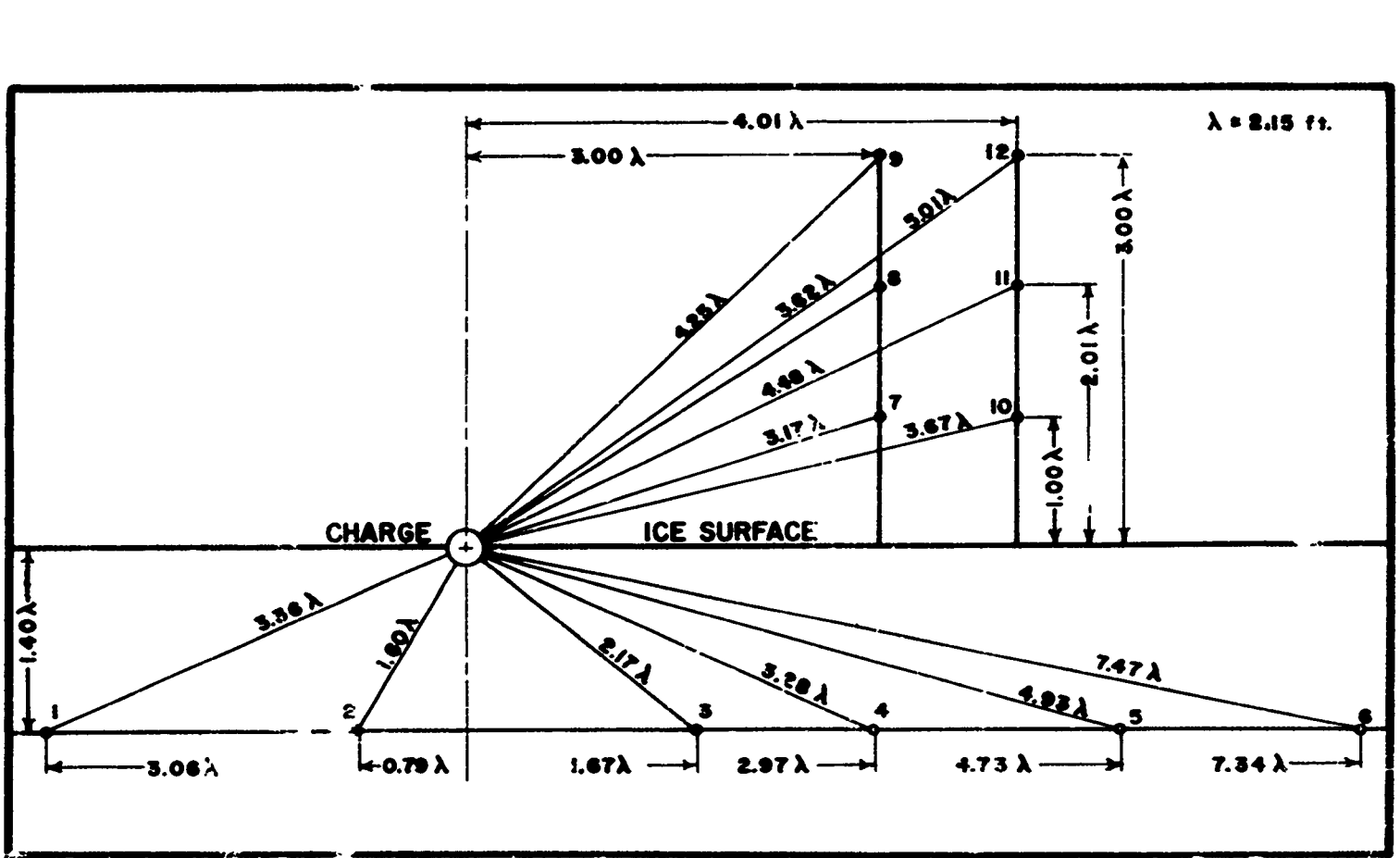

Figure A3. Blast no. 110 - 10 lb Atlas 60.

Gage	Shock velocity charge to gage (ft/sec)	Positive duration (ms)	Positive impulse (lb-ms/in)	Maximum pressure (psi)	Gage	Shock velocity charge to gage (ft/sec)	Positive duration (ms)	Positive impulse (lb-ms/in)	Maximum pressure (psi)
1	12,050	1.550	90	174	7	4,283	1.540	[illegible]	45
2	10,455	2.120	1257	2348	8	4,365	1.630	[illegible]	59
3	12,972	0.960	20	508	9	4,155	2.000	[illegible]	37
4	11,492	1.820	475	441	10				
5	11,398	1.950	108	81	11	3,394	1.700	17	24
6	11,730	1.130	48	53	12	3,578	2.370	22	20

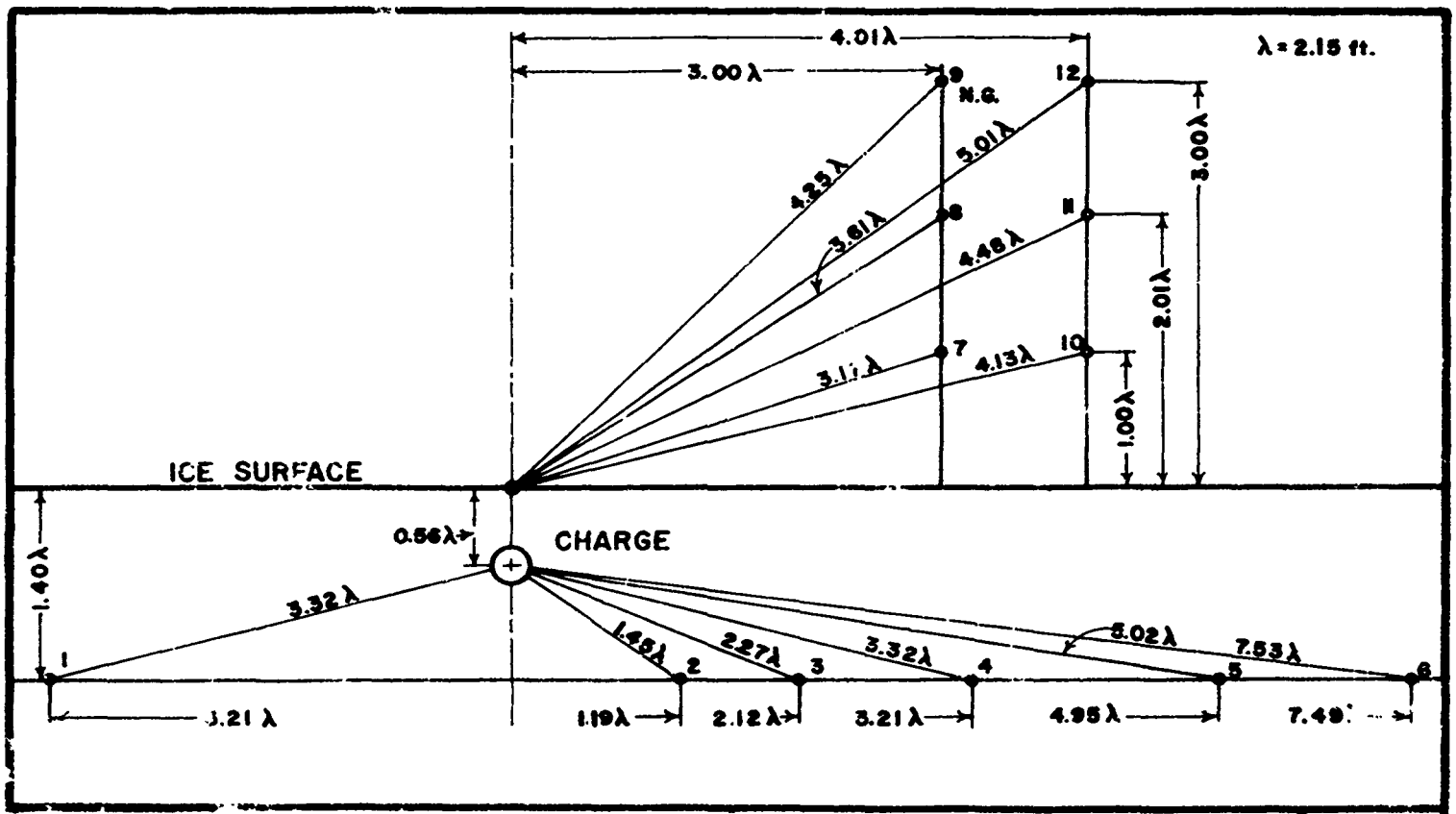

Figure A4. Blast no. 113 - 10 lb Atlas 60.

Gage	Shock velocity charge to gage (ft/sec)	Positive duration (ms)	Positive impulse (lb-ms/in)	Maximum pressure (psi)	Gage	Shock velocity charge to gage (ft/sec)	Positive duration (ms)	Positive impulse (lb-ms/in)	Maximum pressure (psi)
1	10,642	2.25	316	160	7				2.1
2	10,541	2.22	2227	5700	8				2.6
3					10				
4	10,902	9.380	2463	783	11	1,140	6.270	3	0.987
5	11,514	1.400	178	234	12	1,622	6.460	490	155
6	11,714	3.650	527	271	NG9	1,385	7.230		

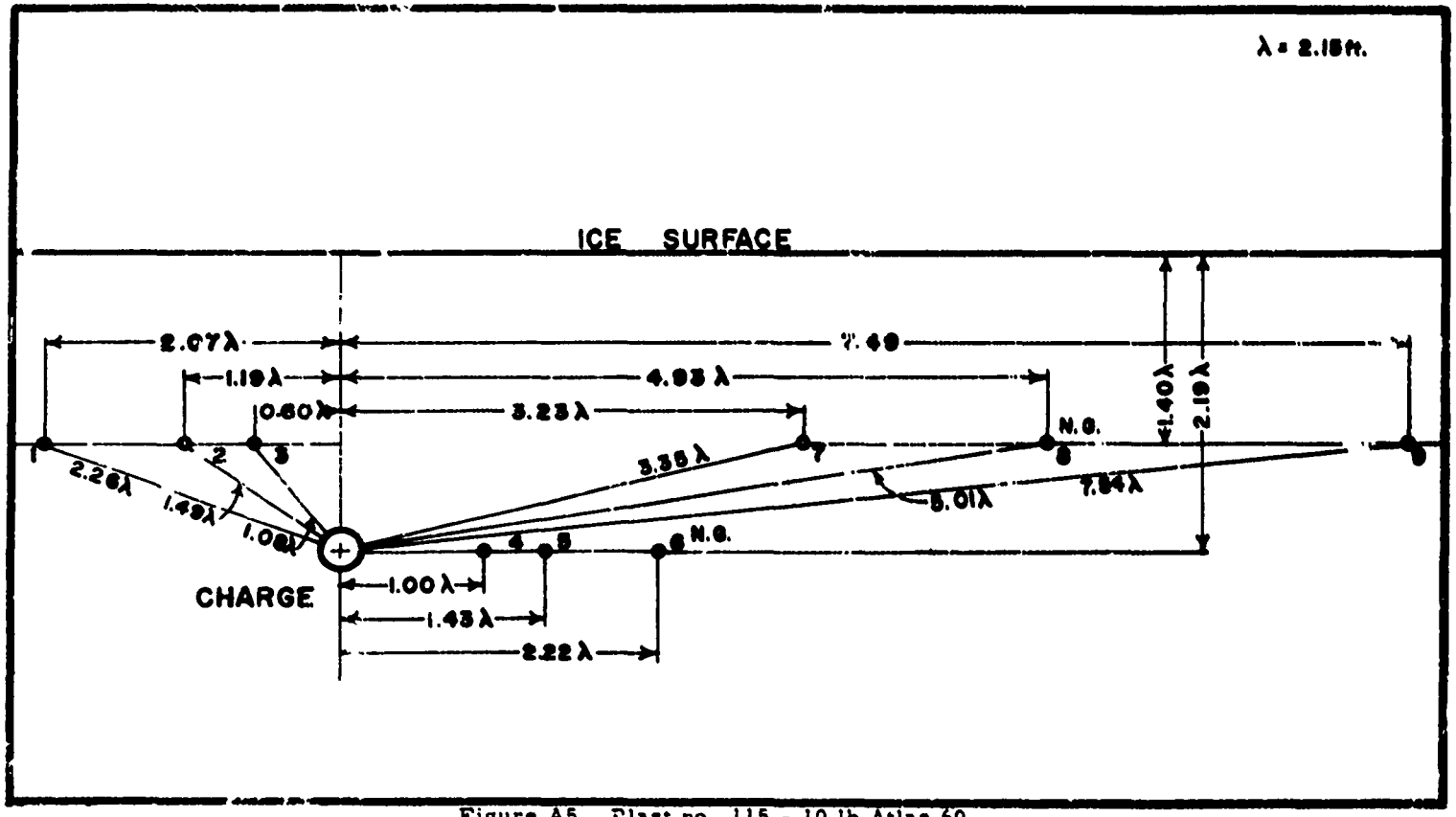

Figure A5. Blast no. 115 - 10 lb Atlas 60.

Gage	Shock velocity charge to gage (ft/sec)	Positive duration (ms)	Positive impulse (lb-ms/in)	Maximum pressure (psi)	Gage	Shock velocity charge to gage (ft/sec)	Positive duration (ms)	Positive impulse (lb-ms/in)	Maximum pressure (psi)
1	10,319	2.42	3786	2385	7				
2	9,302	2.160	1926	2620	9	10,403	1.270	104	151
3	11,422	2.020	5298	8900	NG6				
4	10,550		3231	9500	NG8				
5	8,720	2.420	2040	2570					

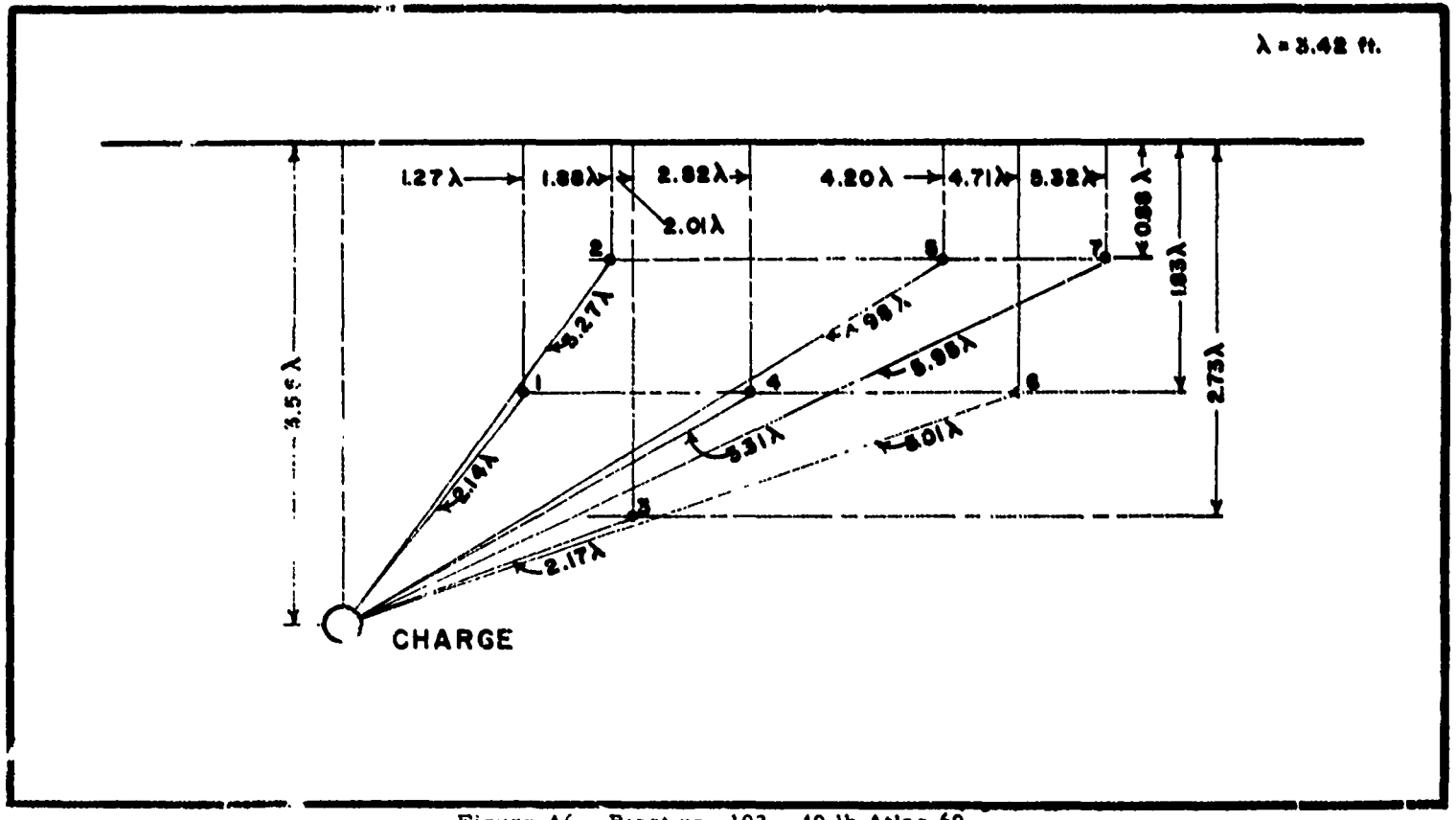

Figure A6. Blast no. 102 - 40 lb Atlas 60.

Gage	Shock velocity charge to gage (ft/sec)	Positive duration (ms)	Positive impulse (lb-ms/in)	Maximum pressure (psi)	Gage	Shock velocity charge to gage (ft/sec)	Positive duration (ms)	Positive impulse (lb-ms/in)	Maximum pressure (psi)
1	7,595	2.98	1496	1100	5	9,737	4.38	683	343
2	11,047	2.36	367	260	6	9,744	8.15		239
3	7,906	8.40	2106	567	7	10,080	4.08	683	209
4	8,633	8.47	1865	518					

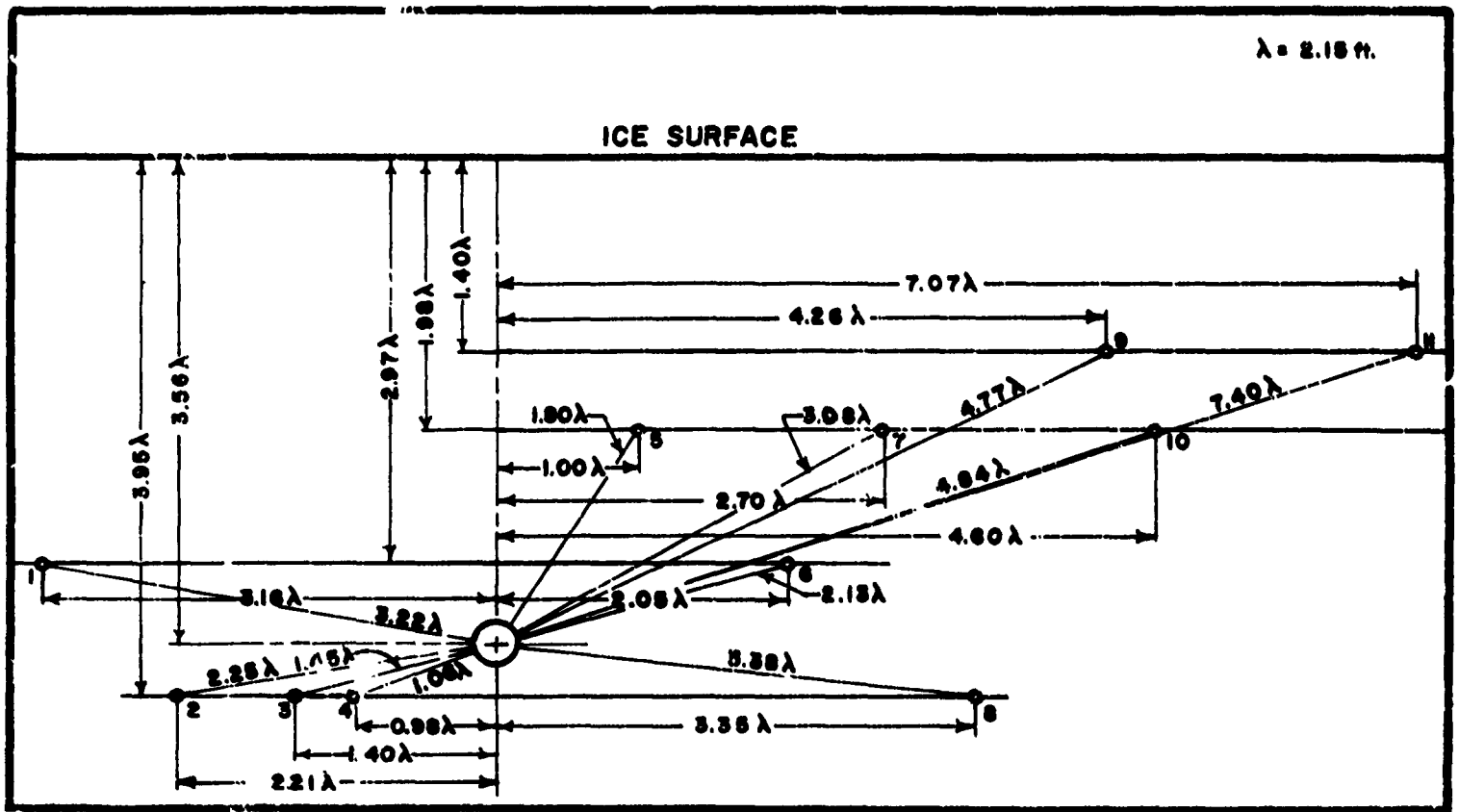

Figure A7. Blast no. 116 - 10 lb Atlas 60.

Gage	Shock velocity charge to gage (ft/sec)	Positive duration (ms)	Positive impulse (lb-ms/in)	Maximum pressure (psi)	Gage	Shock velocity charge to gage (ft/sec)	Positive duration (ms)	Positive impulse (lb-ms/in)	Maximum pressure (psi)
1	7,864				7	8,380	0.650	[illegible]	172
2	7,000				8	6,713	1.470	94	125
3					9	9,080	1.860	170	186
4				5988	10	9,212		835	339
5	6,772				11	10,192	3.180	213	159
6	7,763								

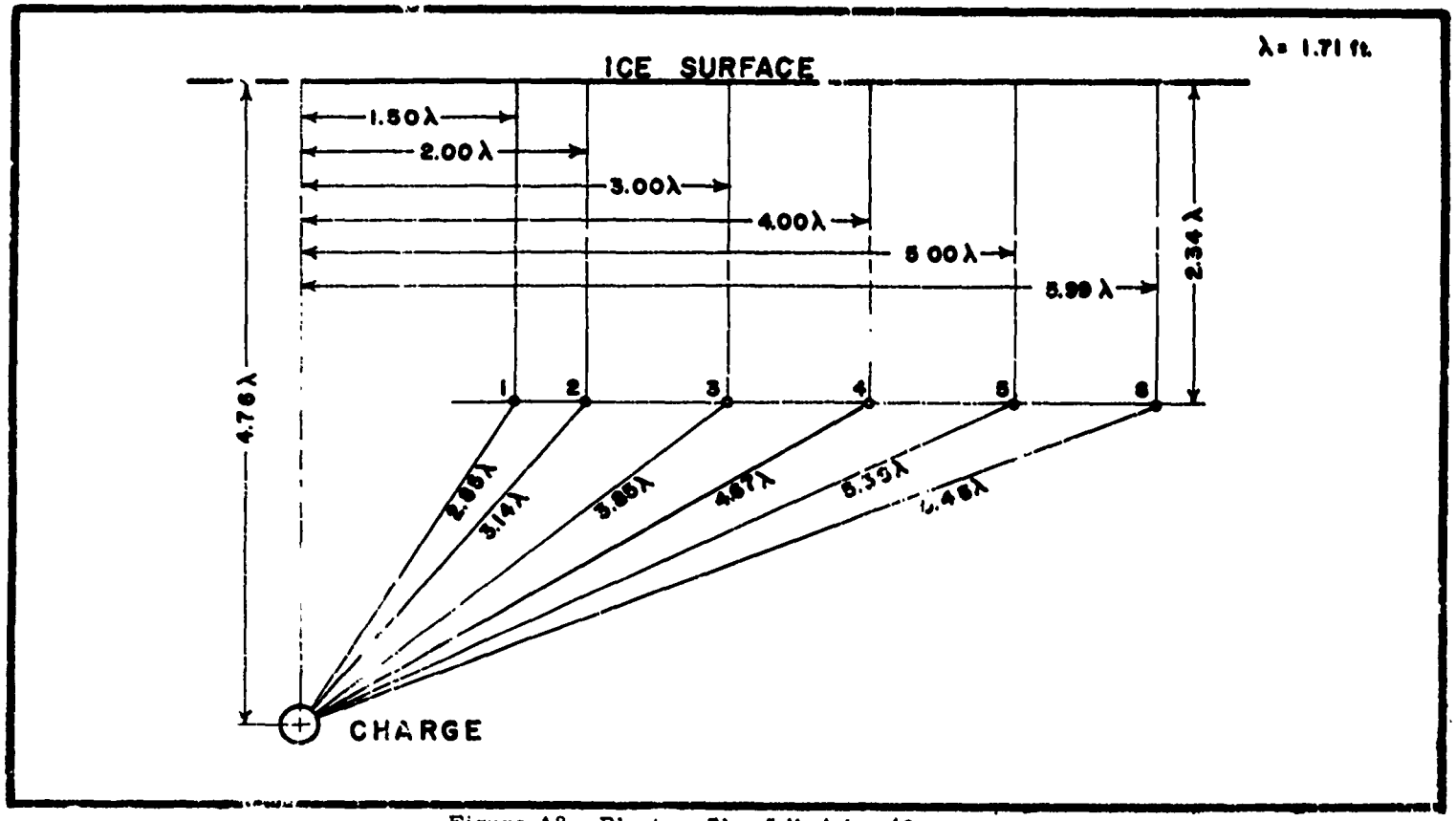

Figure A8. Blast no 71 - 5 lb Atlas 60.

Gage	Shock velocity charge to gage (ft/sec)	Positive duration (ms)	Positive impulse (lb-ms/in)	Maximum pressure (psi)	Gage	Shock velocity charge to gage (ft/sec)	Positive duration (ms)	Positive impulse (lb-ms/in)	Maximum pressure (psi)
1	11,513	1.41	92	156	5	12,820	2.09	65	104
2	10,870	1.67	345	195	6	12,514			50+
3	11,705	1.38	118	200	7	11,660			207
4	12,124	5.02	379	329					

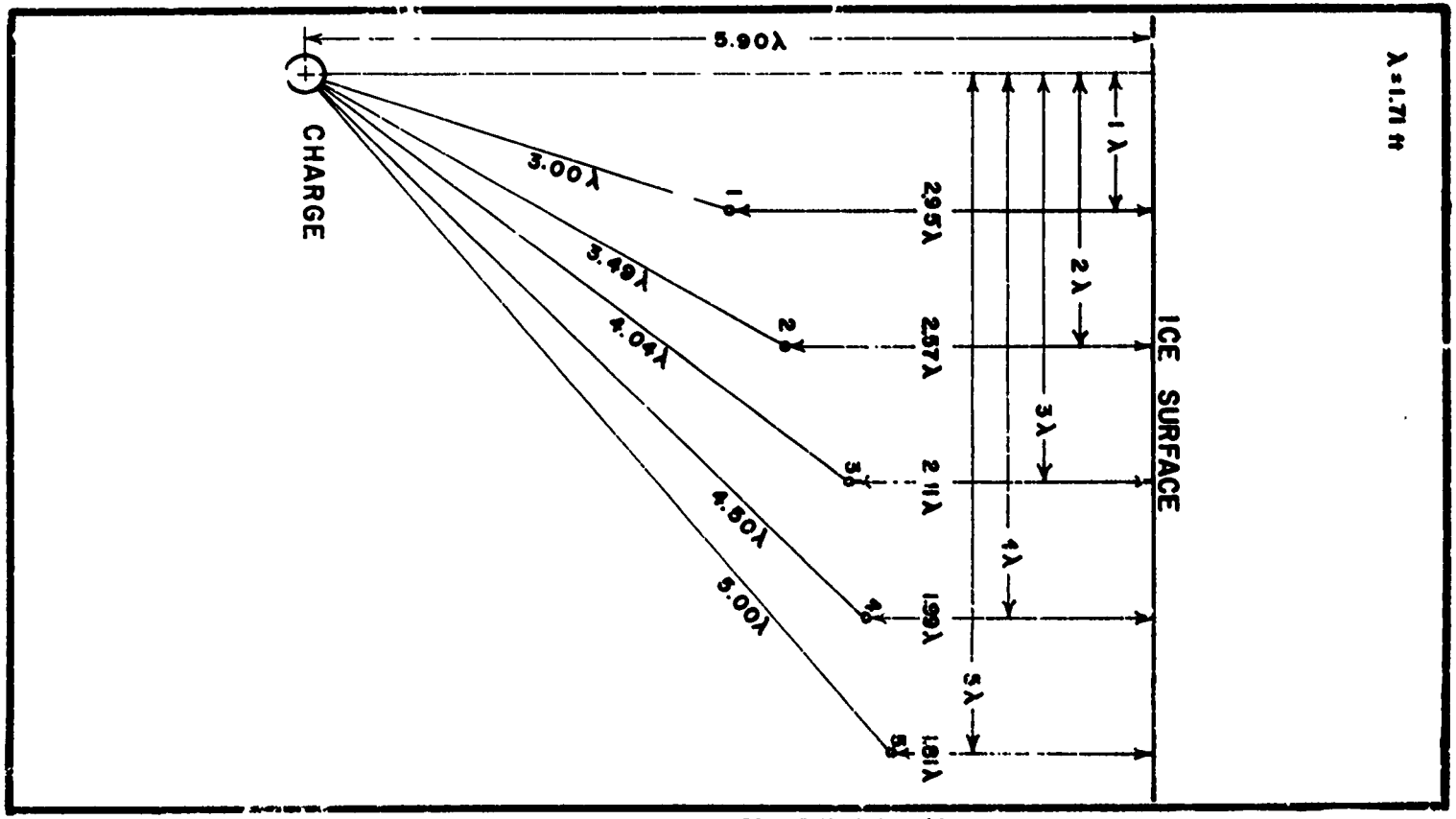

Figure A9. Blast no. 70 - 5 lb Atlas 60

Gage	Shock velocity charge to gage (ft/sec)	Positive duration (ms)	Positive impulse (lb-ms/in)	Maximum pressure (psi)	Gage	Shock velocity charge to gage (ft/sec)	Positive duration (ms)	Positive impulse (lb-ms/in)	Maximum pressure (psi)
1	11,690	1.62	293	579	4	12,150	0.48	913	292
2	12,100	3.65	348	254	5	12,240	1.44	17	104
3	12,000	0.29	153	153					

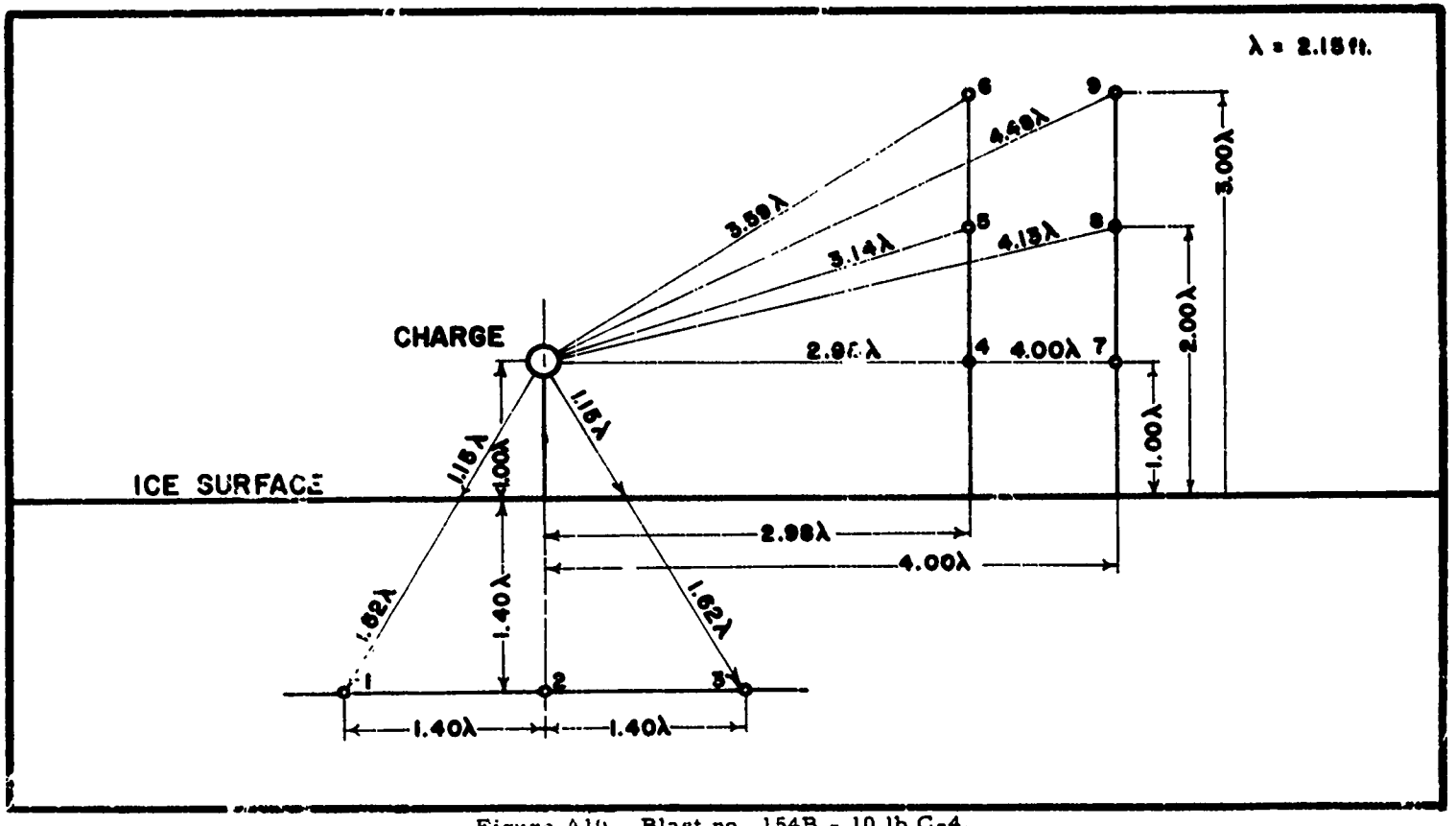

Figure A10. Blast no. 154B - 10 lb C-4.

Gage	Shock velocity charge to gage (ft/sec)	Positive duration (ms)	Positive impulse (lb-ms/in)	Maximum pressure (psi)	Gage	Shock velocity charge to gage (ft/sec)	Positive duration (ms)	Positive impulse (lb-ms/in)	Maximum pressure (psi)
1	11,666	0.410	182	161	6	4,886	1.820	44	60
2	11,454	2.360	125	123	7				
3	11,92.	0.570	116	246	8	4,327	2.270	·	62
4	6,41'	1.630	62	117	9				
5	5,878	2.930	28	102					

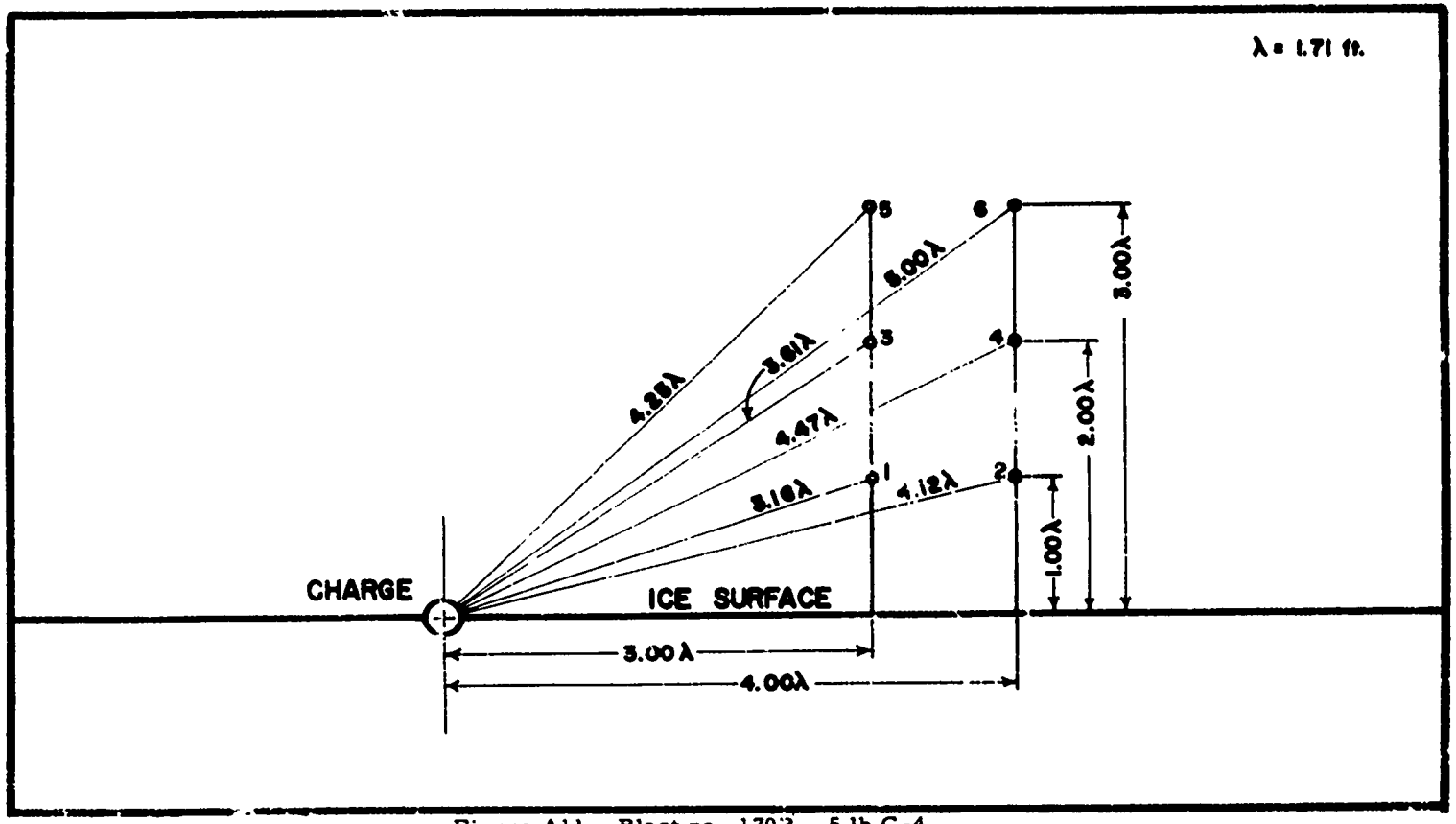

Figure A11. Blast no. 1703 - 5 lb C-4.

Gage	Shock velocity charge to gage (ft/sec)	Positive duration (ms)	Positive impulse (lb-ms/in)	Maximum pressure (psi)	Gage	Shock velocity charge to gage (ft/sec)	Positive duration (ms)	Positive impulse (lb-ms/in)	Maximum pressure (psi)
1	5,037	1.260	61	108	4	3,825	0.855	49	49
2	3,860	0.955	30	56	5	4,167	1.460	23	85
3	4.866	1.180	50	131	6				

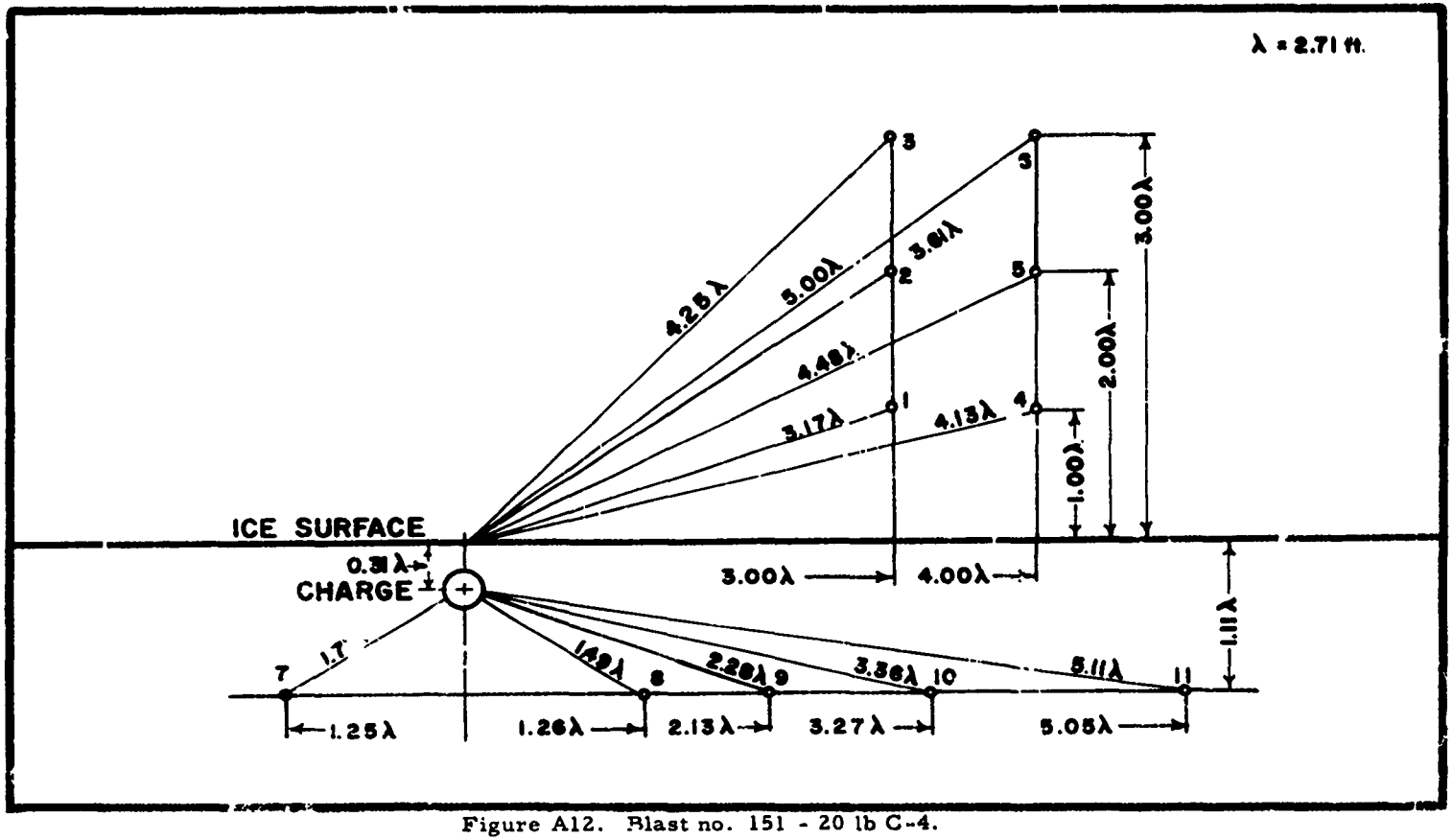

Figure A12. Blast no. 151 - 20 lb C-4.

Gage	Shock velocity charge to gage (ft/sec)	Positive duration (ms)	Positive impulse (lb-ms/in)	Maximum pressure (psi)	Gage	Shock velocity charge to gage (ft/sec)	Positive duration (ms)	Positive impulse (lb-ms/in)	Maximum pressure (psi)
1					8	12,089	3.140	1706	2,215
2	1,970	6.28	48	15.5	9	12,748	2.110	213	371
4					10	12,670	0.786	1[illegible]	61
5					11	12,591	3.300	584	77
6					NG3				
					NG7				

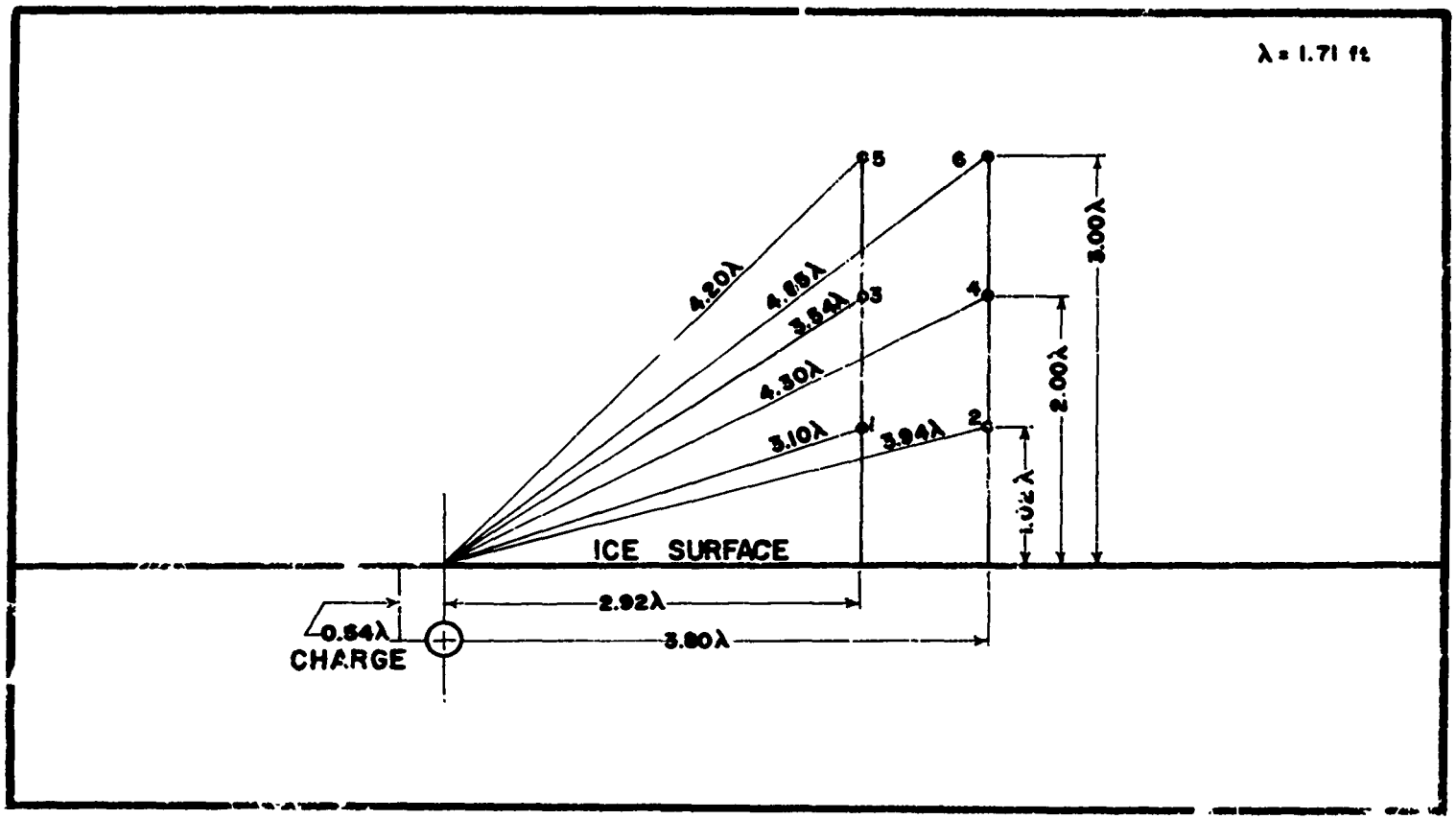

Figure A13. Blast no. $170\frac{3}{4}$ - 5 lb C-4.
No pressure recorded at gages.

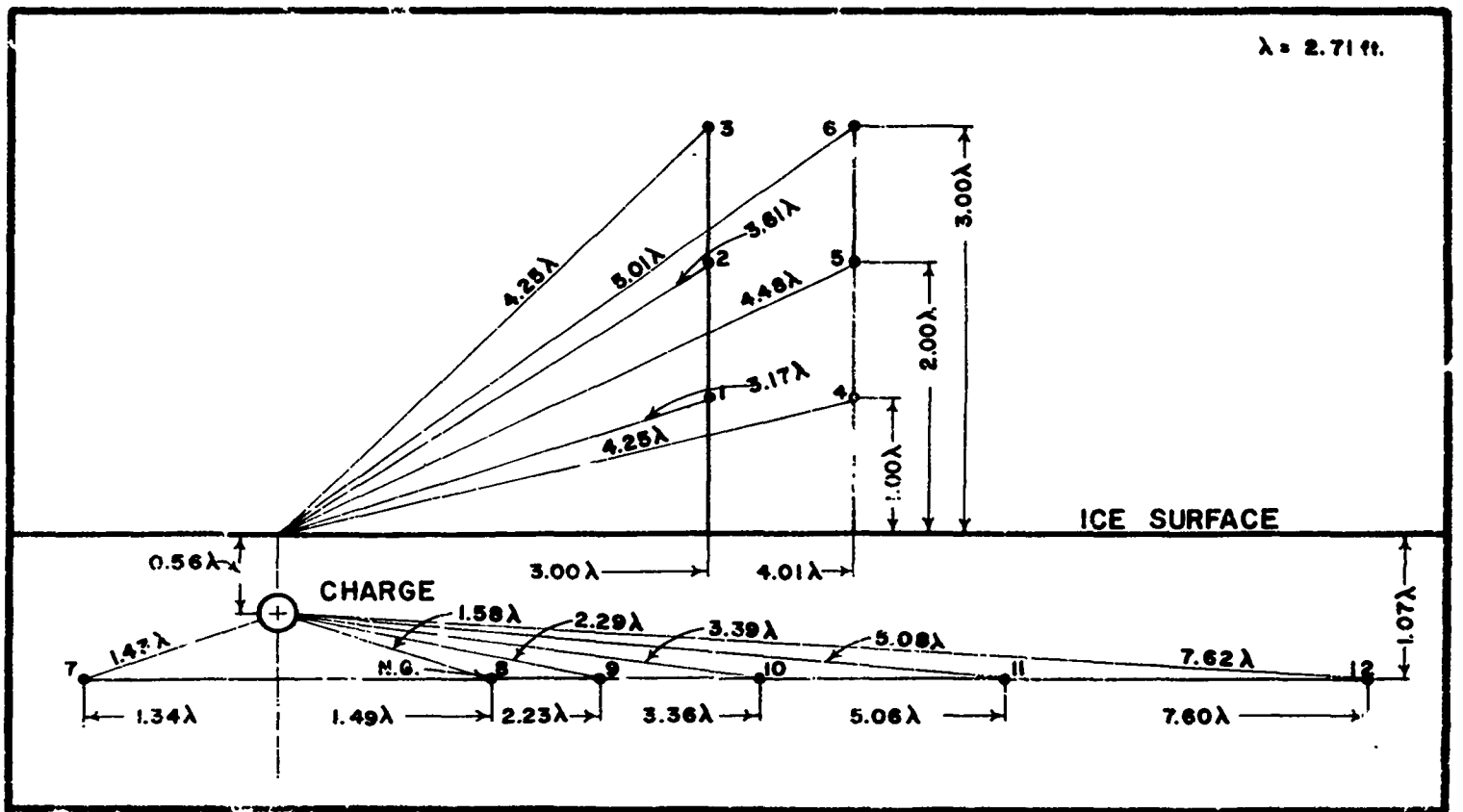

Figure A14. Blast no. 152 - 20 lb C-4.

Gage	Shock velocity charge to gage (ft/sec)	Positive duration (ms)	Positive impulse (lb-ms/in)	Maximum pressure (psi)	Gage	Shock velocity charge to gage (ft/sec)	Positive duration (ms)	Positive impulse (lb- s/in)	Maximum pressure (psi)
1					7				
2					9	11,923	2.00	143	1402
3	2,465	14.57	60	7.98	10	11,900	1.605	24[illegible]	311
4					11	11,980	2.680	129	128
5					12	12,200	2.660	220	136
6					NG8				

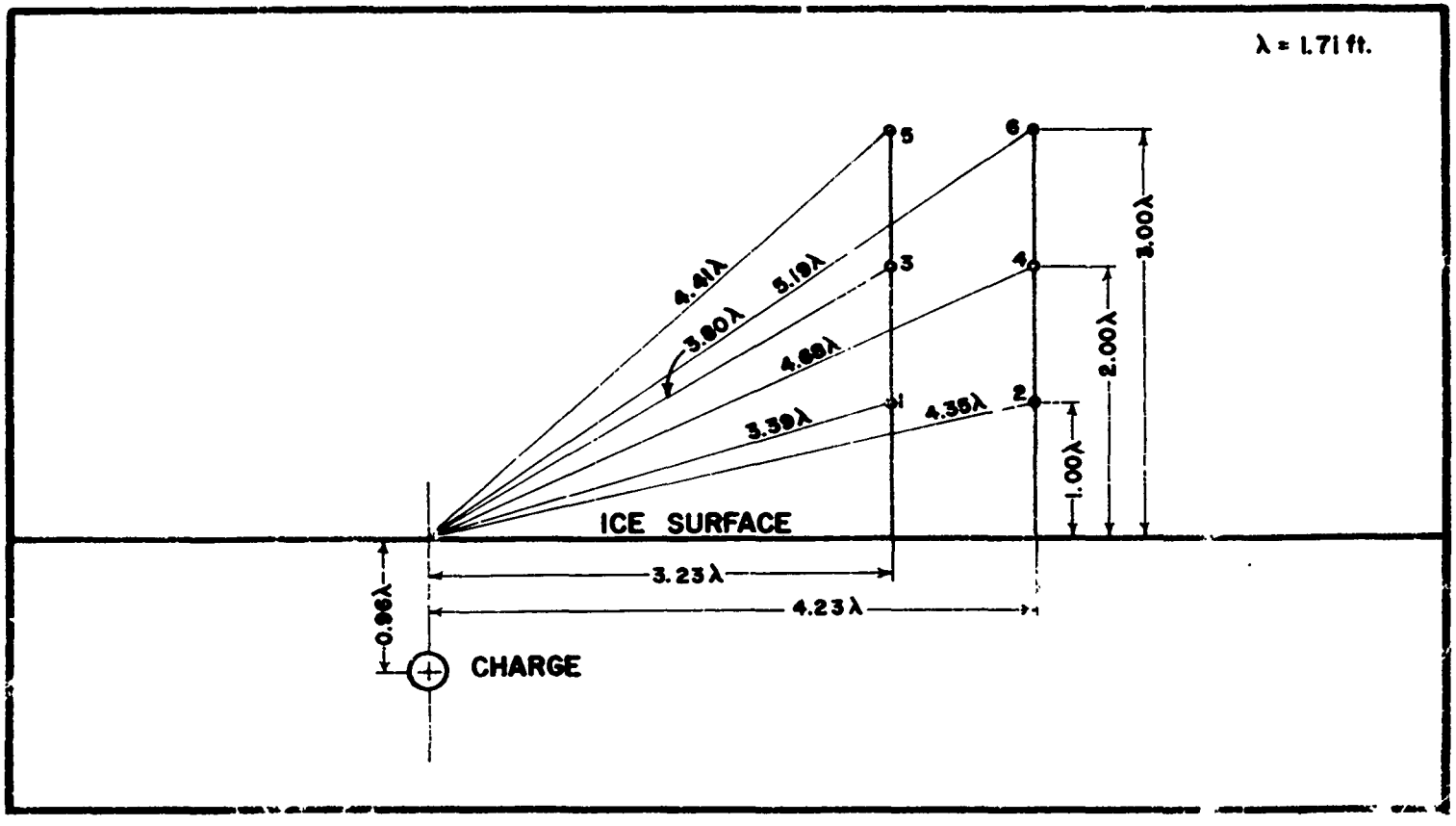

Figure A15. Blast no. 171 - 5 lb C-4.
No pressure recorded at gages.

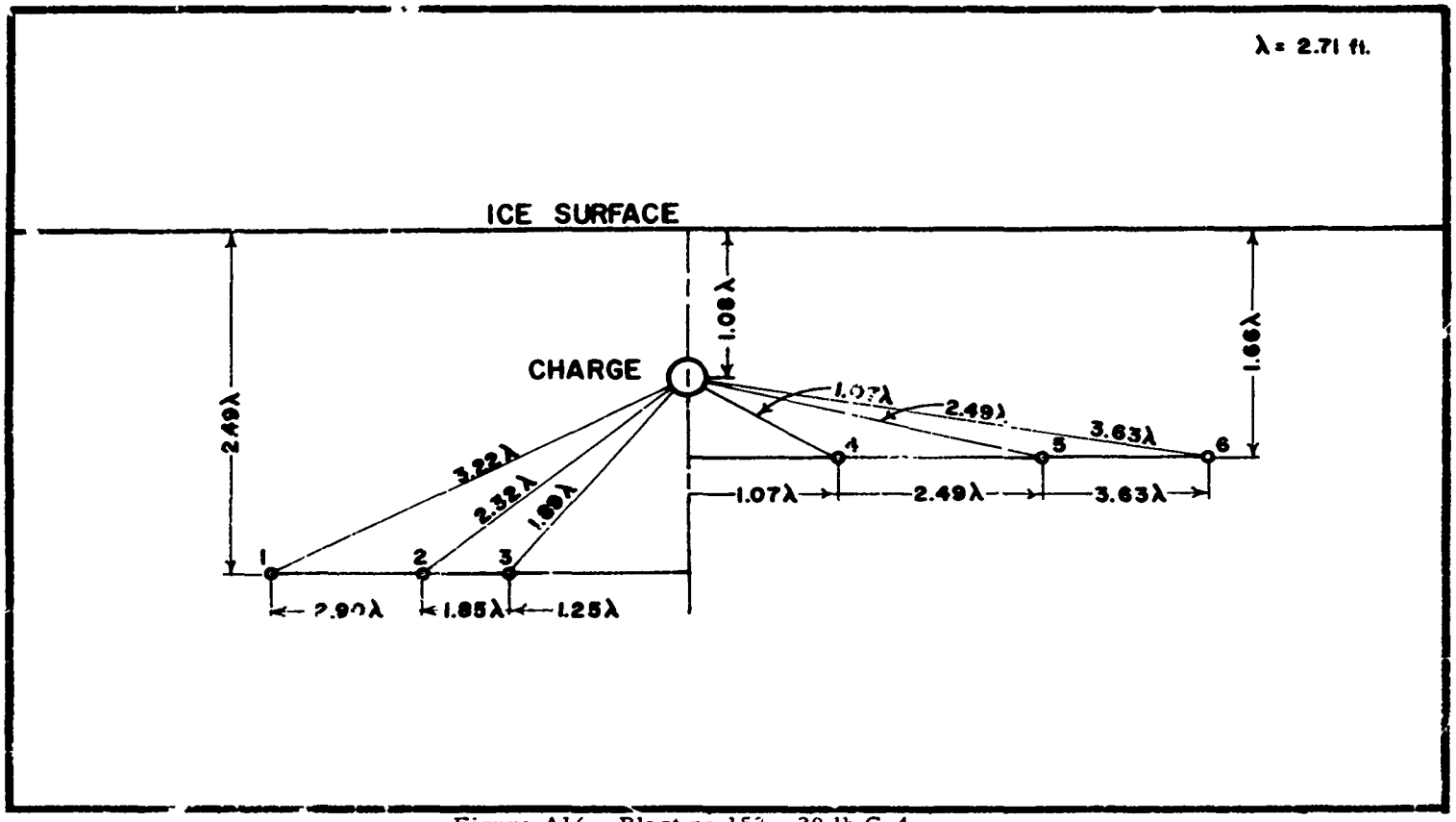

Figure A16. Blast no. 153 - 20 lb C-4.

Gage	Shock velocity charge to gage (ft/sec)	Positive duration (ms)	Positive impulse (lb-ms/in)	Maximum pressure (psi)	Gage	Shock velocity charge to gage (ft/sec)	Positive duration (ms)	Positive impulse (lb-ms/in)	Maximum pressure (psi)
1	3,410	1.620	118	178	4	1,475	2.360	2826	3,757
2					5				
3	1,805	2.780	1369	2,411	6	3,734	1.360		

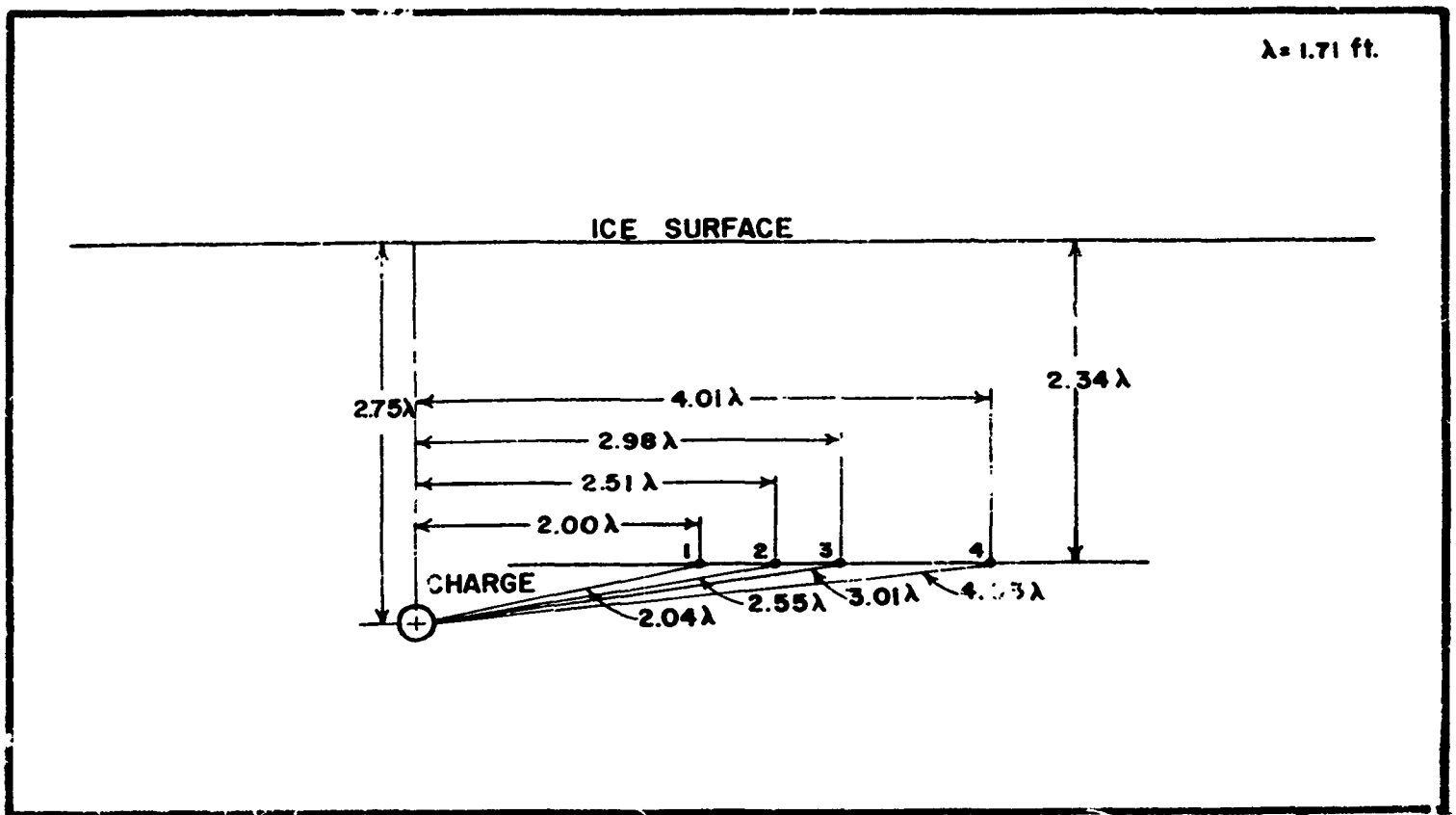

Figure A17. Blast no. 5R - 5 lb C-4.

Gage	Shock velocity charge to gage (ft/sec)	Positive duration (ms)	Positive impulse (lb-ms/in)	Maximum pressure (psi)	Gage	Shock velocity charge to gage (ft/sec)	Positive duration (ms)	Positive impulse (lb-ms/in)	Maximum pressure (psi)
1					3	11,320	1.41	185	235
2	11,580			792	4	11,590			67

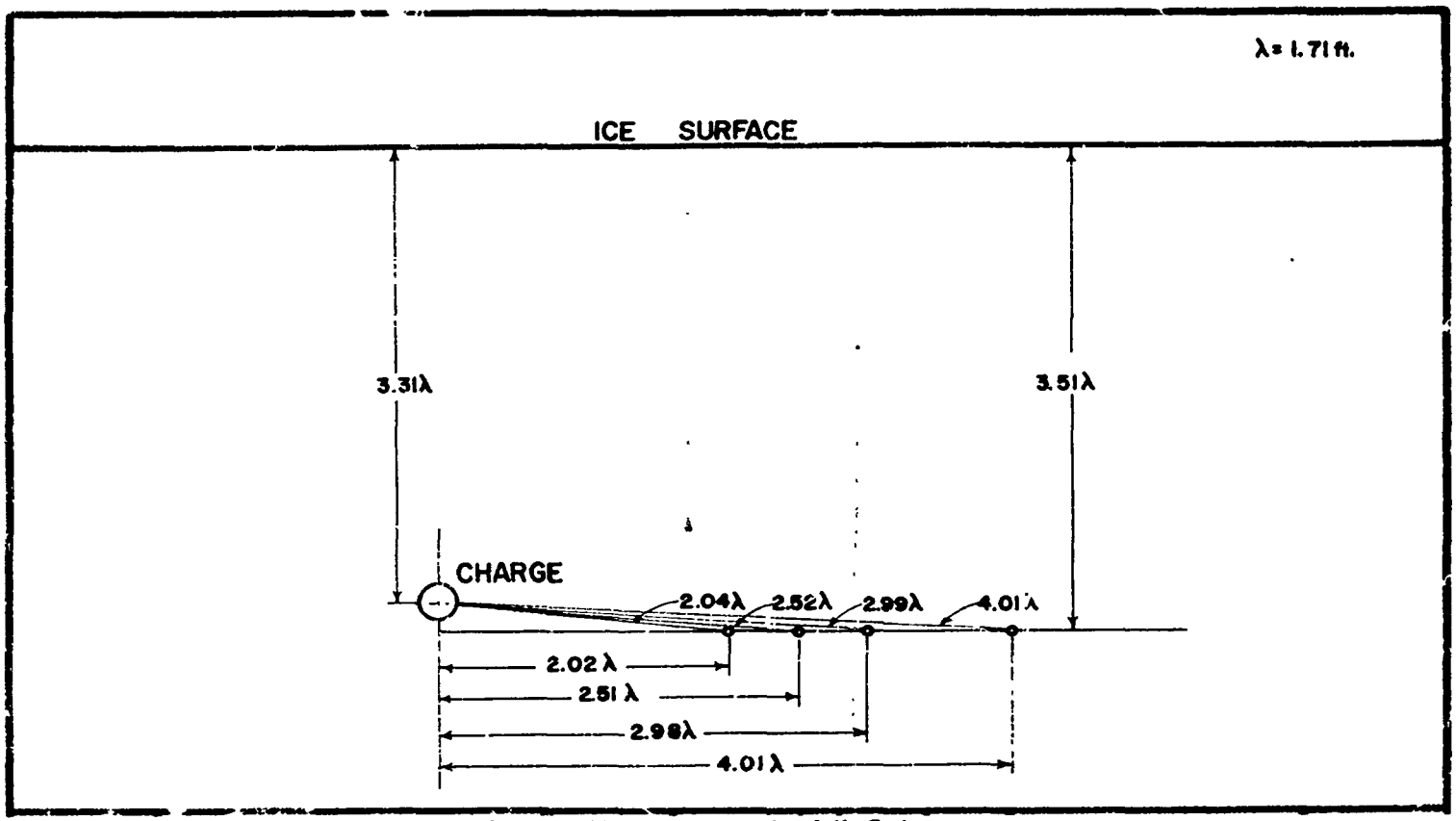

Figure A18. Blast no. 4 - 5 lb C-4.

Gage	Shock velocity charge to gage (ft/sec)	Positive duration (ms)	Positive impulse (lb-ms/in)	Maximum pressure (psi)	Gage	Shock velocity charge to gage (ft/sec)	Positive duration (ms)	Positive impulse (lb-ms/in)	Maximum pressure (psi)
1	13,385	1.65	743	1295	3	11,614	0.95	357	281
2				264	4	12,925	1.96	160	238

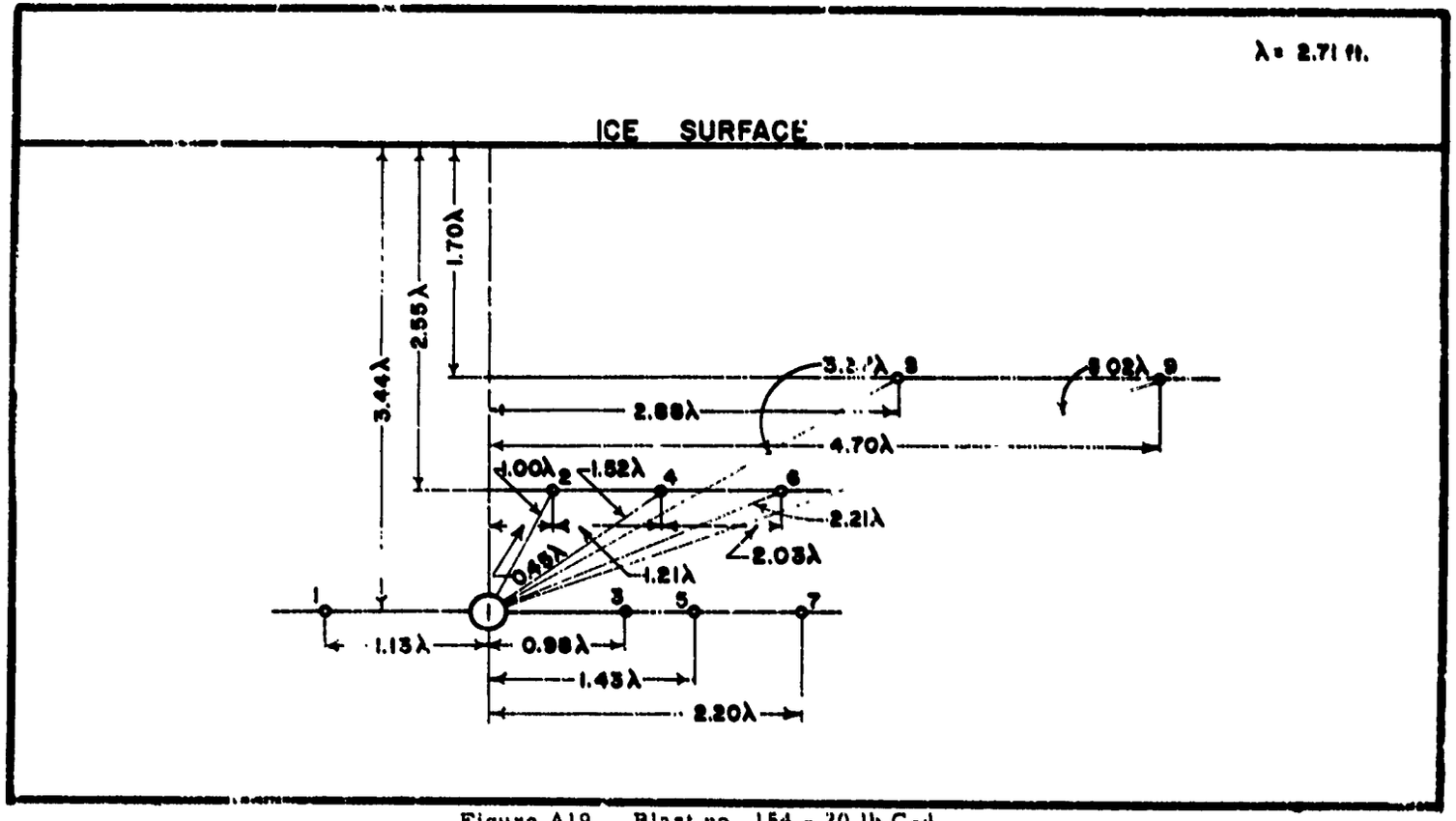

Figure A1c. Blast no. 154 - 20 lb C-4.

Gage	Shock velocity charge to gage (ft/sec)	Positive duration (ms)	Positive impulse (lb-ms/in)	Maximum pressure (psi)	Gage	Shock velocity charge to gage (ft/sec)	Positive duration (ms)	Positive impulse (lb-ms/in)	Maximum pressure (psi)
1	8,472	1.290	2558	8474	8	9,806	2.780		
2	6,634			5909	9	10,382	2.120	951	1058
5	6,559	2.370	231	3458	RRL				
6	5,825	1.830	590	737	NG3				
7					NG4				

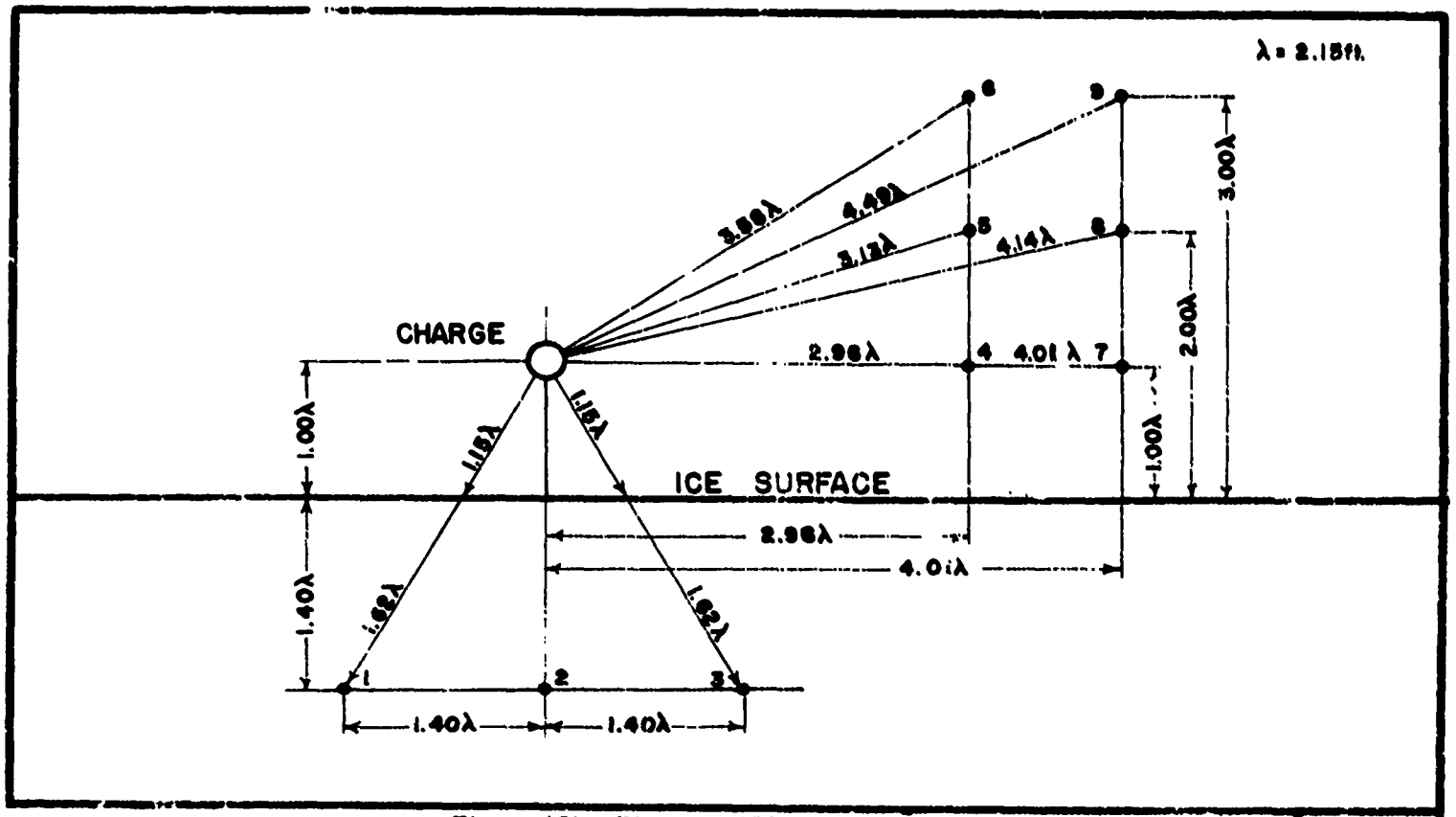

Figure A20. Blast no. 154D - 10 lb Coalite 7S.

Gage	Shock velocity charge to gage (ft/sec)	Positive duration (ms)	Positive impulse (lb-ms/in)	Maximum pressure (psi)	Gage	Shock velocity charge to gage (ft/sec)	Positive duration (ms)	Positive impulse (lb-ms/in)	Maximum pressure (psi)
1	9,613	0.250	16	92	6	3,807	1.020	15	34
2	13,919	2.170	203	206	7	3.626	2.110	14	21
3	7,770	0.280	11	91	8	2,926			16
4	4,650	1.465	31	46	9	3,063	2.480	31	42
5	4,314	1.110	20	61					

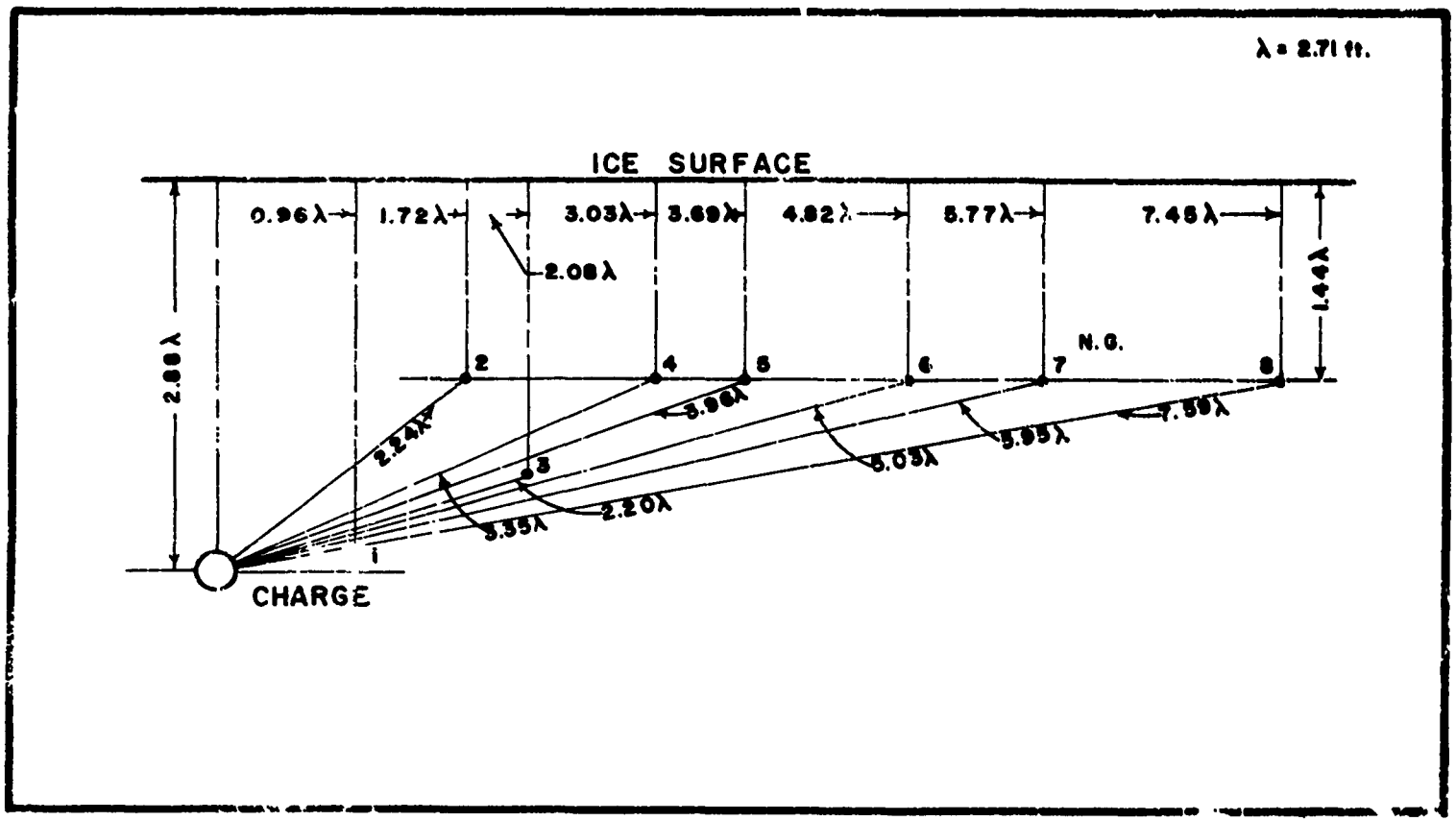

Figure A21. Blast no. 84 - 20 lb Coalite 7S.
No pressure recorded at gages.

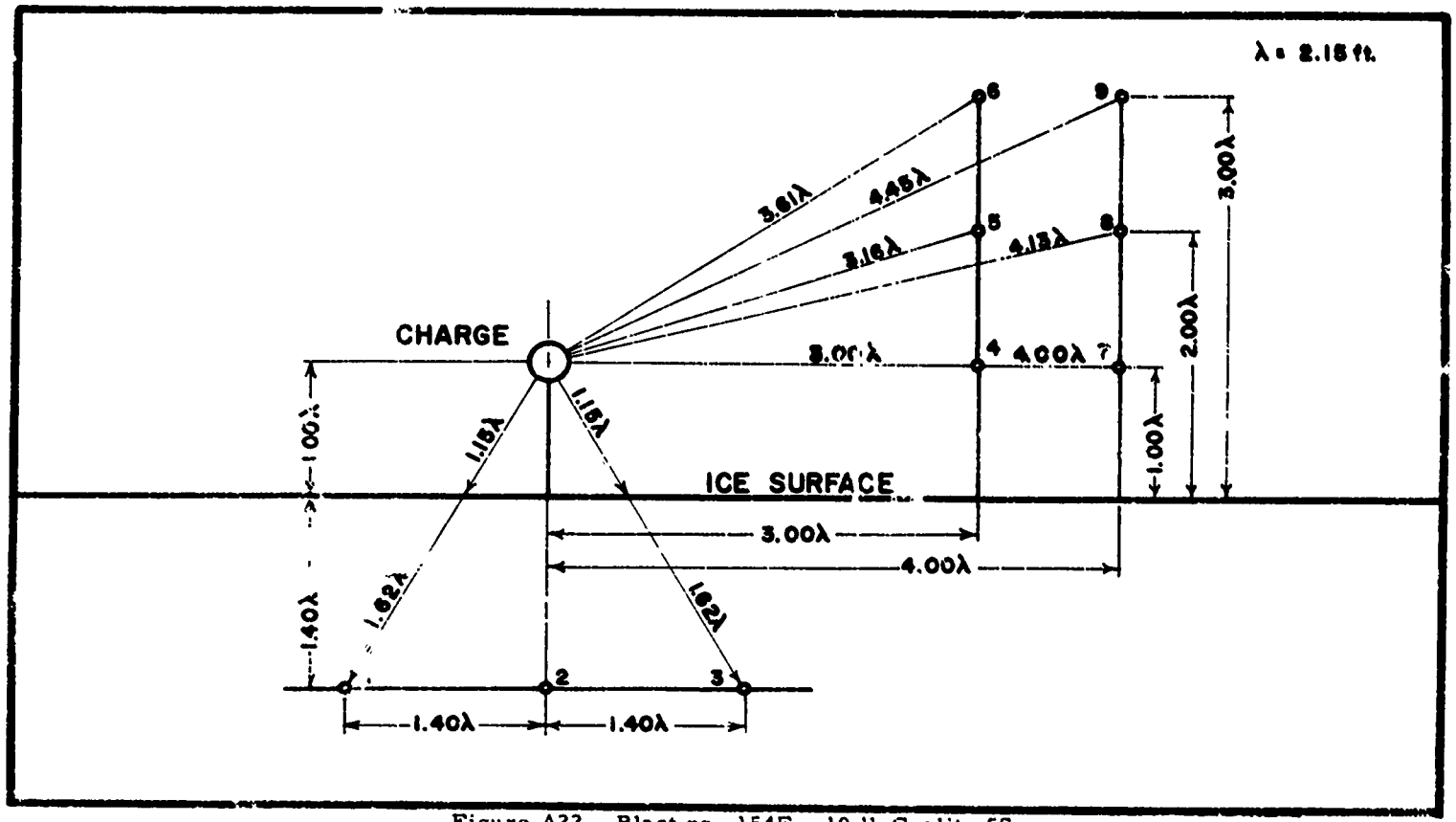

Figure A22. Blast no. 154E - 10 lb Coalite 5S.

Gage	Shock velocity charge to gage (ft/sec)	Positive duration (ms)	Positive impulse (lb-ms/in)	Maximum pressure (psi)	Gage	Shock velocity charge to gage (ft/sec)	Positive duration (ms)	Positive impulse (lb-ms/in)	Maximum pressure (psi)
1	10,643	0.660	58	97	6	3,660	1.110	...	21.3
2	22,391				7	3,282	2.410	29	27
3	10,102	1.510	15	104	8				
4	4,358	1.500	20	31	9	2,883	1.840	21	34
5	4,198	1.310	15	39					

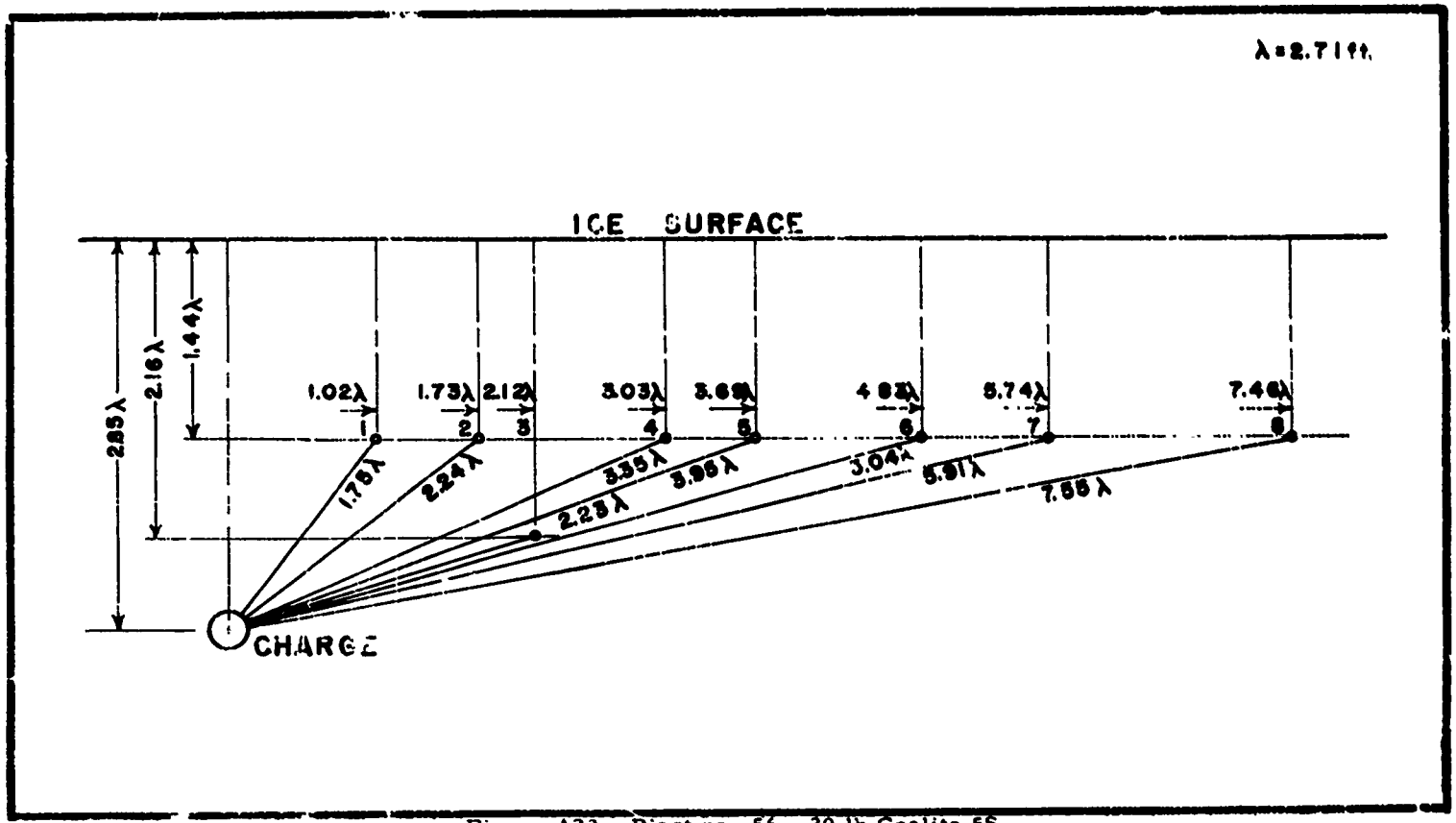

Figure A23. Blast no. 56 - 20 lb Coalite 5S.

Gage	Shock velocity charge to gage (ft/sec)	Positive duration (ms)	Positive impulse (lb-ms/in)	Maximum pressure (psi)	Gage	Shock velocity charge to gage (ft/sec)	Positive duration (ms)	Positive impulse (lb-ms/in)	Maximum pressure (psi)
1	5,513	3.36	36	2800	5	11,600	2.44	52*	454
2	11,420	2.24	1456	944	6	11,550	1.94	26*	225
3					7	11,520	2.18	366	292
4	11,350	2.61	427	333					

* and estimated

damage distance containing coefficients measurable at critical depth, and equations involving volume measurements and containing coefficients measurable at optimum depth. The results for all explosives and weights tested indicate that explosives in glacier ice deviate from cube-root scaling. Comparisons of the relations between crater volume and depth ratio, and between fly-rock travel height and depth ratio indicate that: the energy used in deforming the ice without loss of cohesion is not available to the fracture process; the energy used to deform without loss of cohesion and to fracture the ice is not available to accelerate the isolated fragments; and events subsequent to the breakage process depend on the manner in which energy is partitioned to the breakage process and on all parameters affecting cratering in ice. The depth of the crater is the sum of the depth to the center of gravity of the charge and the vertical radius of the explosion cavity, which is larger for a contact burst than a charge at optimum depth, larger at critical than at optimum depth, larger at critical depth than at optimum weight, and is affected both by charge shape and type of explosive.

damage distance containing coefficients measurable at critical depth, and equations involving volume measurements and containing coefficients measurable at optimum depth. The results for all explosives and weights tested indicate that explosives in glacier ice deviate from cube-root scaling. Comparisons of the relations between crater volume and depth ratio, and between fly-rock travel height and depth ratio indicate that: the energy used in deforming the ice without loss of cohesion is not available to the fracture process; the energy used to deform without loss of cohesion and to fracture the ice is not available to accelerate the isolated fragments; and events subsequent to the breakage process depend on the manner in which energy is partitioned to the breakage process and on all parameters affecting cratering in ice. The depth of the crater is the sum of the depth to the center of gravity of the charge and the vertical radius of the explosion cavity, which is larger for a contact burst than a charge at optimum depth, larger at critical than at optimum depth, larger at critical depth than at optimum weight, and is affected both by charge shape and type of explosive.

damage distance containing coefficients measurable at critical depth, and equations involving volume measurements and containing coefficients measurable at optimum depth. The results for all explosives and weights tested indicate that explosives in glacier ice deviate from cube-root scaling. Comparisons of the relations between crater volume and depth ratio, and between fly-rock travel height and depth ratio indicate that: the energy used in deforming the ice without loss of cohesion is not available to the fracture process; the energy used to deform without loss of cohesion and to fracture the ice is not available to accelerate the isolated fragments; and events subsequent to the breakage process depend on the manner in which energy is partitioned to the breakage process and on all parameters affecting cratering in ice. The depth of the crater is the sum of the depth to the center of gravity of the charge and the vertical radius of the explosion cavity, which is larger for a contact burst than a charge at optimum depth, larger at critical than at optimum depth, larger at critical depth than at optimum weight, and is affected both by charge shape and type of explosive.

damage distance containing coefficients measurable at critical depth, and equations involving volume measurements and containing coefficients measurable at optimum depth. The results for all explosives and weights tested indicate that explosives in glacier ice deviate from cube-root scaling. Comparisons of the relations between crater volume and depth ratio, and between fly-rock travel height and depth ratio indicate that: the energy used in deforming the ice without loss of cohesion is not available to the fracture process; the energy used to deform without loss of cohesion and to fracture the ice is not available to accelerate the isolated fragments; and events subsequent to the breakage process depend on the manner in which energy is partitioned to the breakage process and on all parameters affecting cratering in ice. The depth of the crater is the sum of the depth to the center of gravity of the charge and the vertical radius of the explosion cavity, which is larger for a contact burst than a charge at optimum depth, larger at critical than at optimum depth, larger at critical depth than at optimum weight, and is affected both by charge shape and type of explosive.